Università degli Studi di Napoli "Federico II"

Scuola Politecnica delle Scienze di Base

Ph.D. School in Chemical Sciences

Wavelet Analysis for Non-Equilibrium Processes in Chemistry

Supervisor:
Prof. Nadia Rega

Ph.D. Candidate:
Greta Donati

2013-2016

Contents

Introduction

The charm of the unknown is actually the greatest boost for Science to grow.

The Research in Chemical field must be focused on overcoming limits and frontiers of what is already known day by day in order to get closer and closer to the truth that molecules want to tell us.

Nowadays a huge number of research areas in Chemistry are open, thanks also the important progresses in the technological field. Spanning from the medical, farmaceutical, biological, biotechnological, industrial, energetic fileds to the basis research, Chemistry is everywhere and it is assuming an always more complex and fascinating aspect.

My research during these three years, was forged by a spirit of curiosity toward molecules and their (and our) world. The capability to explore some challenging fields of Chemistry drived my daily work and strengthened the desire to say somenthing different, something new and, possibly, something mine.

The approach of my chemical research was based on a theoretical-computational approach, aimed to disentangle the chemical events under study at the most possible accurate and atomistic level. This approach could be considered relatively

new if compared with the *classical* experimental one based on an activity almost centered in the laboratories, indeed the first has reached an important push thanks the technological progresses especially in terms of always more performing computers. The arrival of computers of course allowed to easily perfom calculations and translate into algorithms the theories and models proposed by the Scientists reducing in a substantial way the huge gap between theory and experiments and so allowing to directly observe and verify the goodness of the hypothesized models. This innovation is of course a fundamental support to the experimental results. The theoretical-computational approach in Chemistry is the essential ring conjugating the physical models that try to rationalize in a physical-mathematical way the Chemistry of atoms and molecules with the complex world of practical experiments. Another great advantage of this approach is that it is possible to simulate experiments that are difficult to realize practically, and so also to make previsions on possible chemical scenario. The computer simulations, indeed, have been able to elucidate a multiplicity of experimental spectra and to reveal detailed dynamics at molecular level [1].

It must be underlined that an important part of the chemical research is based on spectroscopy. Spectroscopic techniques represent another important piece in the composition of the puzzle of a chemical event. The fingerprint of a molecule is obtained through its spectra and it is an essential information in disentangling a chemical problem. Many spectroscopic techniques exist and they provide of course infor-

mation that are different and often complementary. Nowadays thanks to the huge developments in technological field, more advanced and sophisticated spectroscopies are born and these ones allow to investigate the complex world of non-equilibrium processes such as the photo-induced ones. During the last decades ultrafast lasers have been of fundamental importance in the development of modern spectroscopic techniques, these allow time-resolved experiments in which transient species can be observed. A their important property is that with modest energy they can have huge powers. Today femtosecond pulses have changed the concept of what *fast* means in Chemistry, allowing the spectroscopic investigation to reach the attosecond time-scale: in other words we are entering in the molecular time-scale. Femtosecond pulses are suitable for a huge number of applications, also the ones that we can believe are not time-resolved, such as multi-phonon absorption (for imaging of biological materials), fragmentation (of DNA into fragments), production of pulses of electrons or even neutrons [2]. Fig. 1 is a simple and clear view of the progresses in Chemistry during the time in terms of an always more short time scale that today can be investigated [3].

In femtochemistry, studies of physical, chemical, or biological changes are at the fundamental time scale of molecular vibrations: the actual nuclear motions [3]. Understanding the mechanism of a complex chemical reaction, for example, requires determining the locations of all the relevant nuclei as a function of time, and with such knowledge we can understand *how* and *why* a chemical reaction takes place.
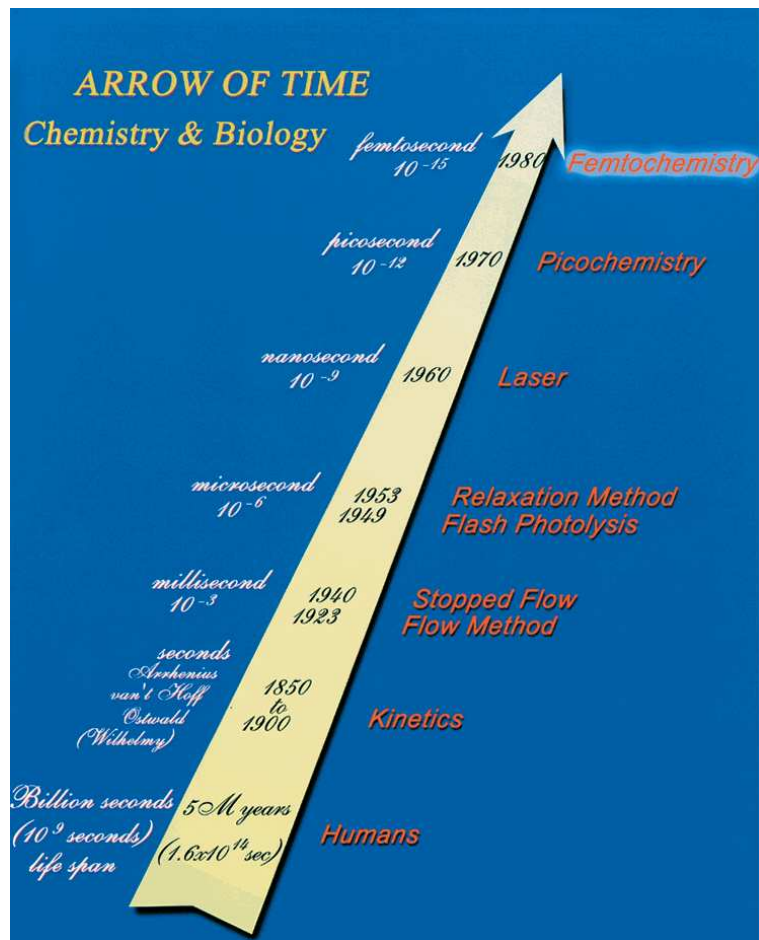
Fig. 1: Improvements during the time of the time-scale accessible in Chemistry and Biology. [3]

In this contest, among the most advanced spectroscopies, optical spectroscopy is a powerful technique to study a chemical reaction dynamics, commonly by monitoring electronic transitions in pump-probe experiments. However, in this way the structural information and interpretation can be made difficult by overlapping absorption and emission bands and ambiguous assignments [4]. Vibrational spectroscopy is a powerful tool to investigate structural dynamics and today, through advanced and time-resolved techniques, it is possible to follow a chemical reaction in the real time

and obtain information about nuclear dynamics in a wide range of frequencies spanning from the low ones (characteristic of collective and backbone motions), to the high frequencies involving atomic motions on a time scale of 10 fs (such as intra-molecular stretchings). Among the most performing vibrational spectroscopies, the Femtosecond Stimulated Raman Spectroscopy (FSRS) [5–10] is the excellent and maybe the most powerful technique to obtain a complete vibrational spectrum on the timescale that is most valuable for understanding reaction dynamics.

So often the knowledge just based on spectroscopic results is not enough, and for this reason a theoretical-computational approach is necessary to obtain the atomistic detail of the process of interest. This Ph.D. Project was focused on this important aspect with the main aim to build a general and innovative theoretical-computational protocol to study chemical processes. In this contest, the field of the non-equilibrium Chemistry is still a frontier argument for both experimentalists and theoreticians. The exploration of solvent dynamics and reorganization around a solute in either the electronic ground or excited state, the photo-induced reactivity in a molecule, proton and/or electron transfer reactions, or the charge separation taking place after the excitation [11], are the main arguments that drive the scientific research to break the existing horizons. The time scale of such processes is often fast (from fs to ps) and on a spectroscopic point of view, although the high performances, it is still challenging to reach a femtosecond time resolution. The building of a robust theoretical-computational protocol is also very complex. The treatment of

excited states needs accurate theory-level and often several approximations have to be done especially because of the huge computational cost of the calculations. For this reason the theory level is often a compromise between a satisfactory accuracy and a reasonable computational cost, especially when dealing with molecules of medium or large sizes (from a few to hundred or thousand atoms).

Especially in the field of non-equilibrium Chemistry, the knowledge of characteristic properties of a molecule in terms of their temporal evolution is of crucial importance and the perfect strategy to obtain such information is represented by an approach based on the Ab-Initio Molecular Dynamics (AIMD) simulations [12–18]. In this way the temporal information related to all the desired molecular properties can be achieved, such as, for example, the structural dynamics. The great potentiality of such approach is represented by the fact that the ad-hoc treatment of these quantities allows to obtain properties that can be connected with spectroscopic parameters, and so a direct comparison with these ones can be achieved. All the results presented in this work are obtained in this way, however this approach is not enough to have a complete picture of a chemical process. A robust analysis method must support the AIMD results: here it is proposed for the first time the Wavelet Analysis [19–22] as an innovative protocol of analysis in the chemical field and more in general in the field of non-equilibrium processes. The last frontiers of the Science, in terms of time-resolved spectroscopy, from the picosecond transient Raman Spectroscopy, time-resolved fluorescence [23], femtosecond stimulated Raman

Spectroscopy [7], to the femtosecond UV spectroscopy [2], give us the possibility to explore time scales on the limits of the measurable and we want to extend the overcome of such limits to the theoretical-computational approach.

So for the first time a novel vibrational analysis can be performed by a non-conventional protocol based on the analysis of ab-initio dynamics trajectories at both ground and excited states. At equilibrium conditions, the linear response approach [24] is invoked to use the time-dependent information for calculating the infrared spectrum [25]. In this case the method originally proposed by Strachan [26] can be used to perform normal-modes-like analysis from the ab-initio molecular dynamics. The dynamical method can go beyond the standard analysis that is based on the solution of the ro-vibrational Hamiltonian Hro-vib [27, 28]. Standard analysis includes all the the so-called *Hessian-based* methods that have the limitations of giving a statical picture of the system and being computationally prohibitive for large systems such as molecules in condensed phase or biomolecules [29]. The complex dynamics of many body systems at thermal equilibrium can be characterized by time correlation functions [30] and Fourier analysis in the frequency domain. From a theoretical viewpoint, such representation provides a great simplification by replacing a detailed dynamical knowledge of all the particle positions and velocities with an approximate statistical description based on modeling dynamical quantities as stochastic variables [31]. In this view, time evolution of the system is characterized by a set of appropriate correlation functions. Important physical quantities such as

7

spectral densities and transport coefficients can be derived by Fourier transforma-
tions (FT) of these correlation functions [30].

However, performance of the standard Fourier analysis involves the loss of the
instantaneous temporal information provided from ab-initio molecular dynamics,
retaining *only* an average information over the time, and causing a loss of the in-
stantaneous time-frequency correlation. In this contest the Wavelet Analysis is the
solution. Apart the processes at equilibrium conditions, such as solvation dynamics
of complex systems, this analysis is fundamental for far-from-equilibrium investiga-
tions. The Wavelet Analysis is already employed in many fields: from economy to
mathematics, from music to image processing [21]. This relatively novel method
is indeed largely used with excellent results to perform frequency analysis of time-
dependent signals in meteorology [22], engineering [32], medicine [33], music [34],
image processing [35], economy [36], while applications in chemical field are still not
widespread.

In our work we present this alternative analysis applied to two case studies
in non-equilibrium conditions. The basic concept of Wavelet Transform (WT) is
not so different from the FT: the principal difference is that different functions are
employed to transform the signal, moreover the WT allows to catch the different
frequency content of the signal in a more accurate way by an ad-hoc modulation of
the analysing function performed during the analysis. This fact allows to perform
a so-called *multiresolution* analysis that cannot be achieved by the FT or other

8

techniques such as the Short Time Fourier Transform (STFT), although it is based like the WT on localized basis functions. The other peculiarity of this analysis is the fact that the *evolution during the time* of the frequencies is retained, so the instantaneous frequency position is catched and no average is performed. This fact is of fundamental importance especially when dealing with non-equilibrium signals for which the concept of average frequency content makes no sense. In Fig. 2 we show a scheme describing the *multiresolution* feature of the WT.
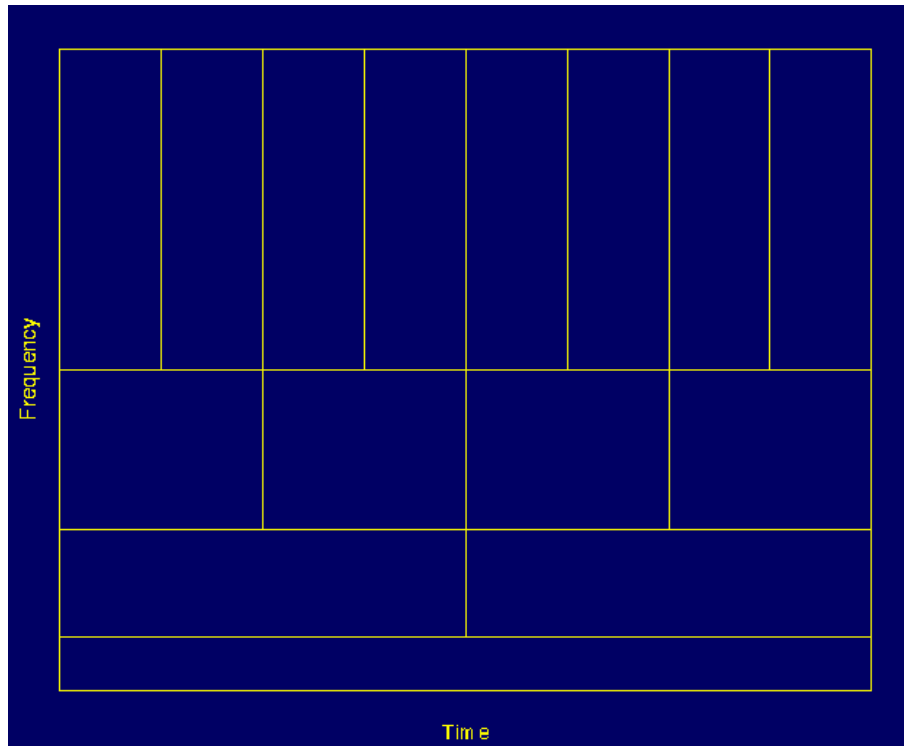
Fig. 2: The characteristic time-frequency plane of the Wavelet Transform. Every box corresponds to a value of the wavelet transform. Every box has a certain non-zero area, which implies that the value of a particular point in the time-frequency plane cannot be known. All the points in the time-frequency plane that falls into a box is represented by one value of the WT. (This image is taken from *the Wavelet Tutorial* by Robert Polikar http://users.rowan.edu/ polikar/WAVELETS/WTpart3.html)

The different size boxes presented in the Figure are a graphical picture of the

fact that the WT adapts to the different frequencies and for each kind of frequency the resolution is not the same, these boxes represent an equal portion of the time-frequency plane (they have a constant area). The low frequencies present a better frequency resolution and a poorer time resolution, since there is less ambiguity regarding the value of the exact frequency, but they show a worse temporal evolution because there is more ambiguity regarding the value of the exact time. At higher frequencies the time resolution becomes better while the frequency resolution becomes poorer. The feature described for this time-frequency plane is peculiar of the WT, on the contrary the STFT (although has some elements in common with the WT), presents a plane equally divided in boxes of the same size: in other words once decided the basis functions, the resolution is fixed and cannot be modulated anymore, on the contrary of the WT.

The field of non-equilibrium processes is accessible by the time-resolved spectroscopy. An interesting phenomenon to study is the polar solvent relaxation after an instantaneous alteration of a solute charge distribution, initially in equilibrium. The system relaxation to a different state of equilibrium, appropriated to the new solute charge distribution, can be followed by time-resolved spectroscopy [37]. Molecular probes are widely used to study polar solvation dynamics, usually they are solvatochromic dyes whose color strongly depends strongly on the surrounding because the ground and excited state differently interact with the solvent. Among these dyes the N-methyl-6-oxyquinolinium-betain (MQ) represents a suitable probe for

femtosecond solvation experiments. The time resolved fluorescence of MQ provides the dynamics of the Stokes shift and a linear image of the solvation relaxation [38].

Dealing with a non stationary signal, the *mean* description provided by the Fourier analysis is not representative of the temporal evolution. The idea of performing the Fourier analysis is misleading, and only a description in terms of the frequency function of the time can be realistic. We studied the Stokes shift dynamics of N-methyl-6-oxyquinolinium-betain by means of Wavelet Analysis, employing for the first time this analysis in the non-equilibrium Chemistry. This experiment had excellent results [39]. Our result was absolutely innovative because we extracted from a time-resolved optical signal the main motions ruling the signal dynamics: in other words we disentangled the signal relaxation in terms of the molecular motions ruling it through the Wavelet Analysis that allowed us to unvail the frequencies hidden behind the time-resolved fluorescence signal. We discovered that the solvent collective motions ruled the signal relaxation dynamics. In Fig. 3 the Wavelet transform performed on the simulated Time Dependent Stokes shift (TDSS) ($S(t)$) signal is shown.

The 3D Wavelet spectrum clearly shows the time axis, allowing the visualization of the frequencies temporal evolution. The major part of the vibrational bands is found under 1000 cm^{-1}, and these are assigned to water collective motions. On the basis of such promising result our main goal was to generalize the Wavelet Analysis, employing this one to study a very challenging problem of chemical interest:
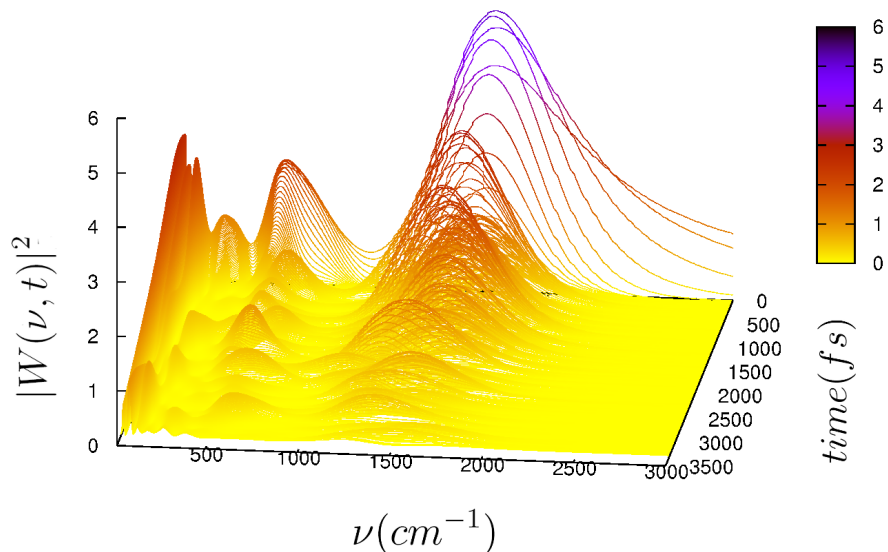
Fig. 3: Wavelet power spectra of the simulated S(t) for MQ in aqueous solution. Time and frequency are reported in fs and cm^{-1}, respectively. Wavelet power spectrum values $|W(\nu, t)|^2$ are expressed in arbitrary units. [39]

the photo-induced Excited State Proton Transfer (ESPT) of the Green Fluorescent Protein (GFP).

GFP is deeply studied since many years first of all for its huge number of applications such as, for example, as a reporter gene, fluorescent marker in cell biology [40], fungal biology, bacterial protein localization, real-time molecular and cellular analysis [41], but also for the complex nature of its photophysics and photochemistry that makes this protein, for the first time isolated from the jellyfish *Aequorea Victoria* (wtGFP), a very interesting chemical system on both an experimental and theoretical point of view. The always growing number of GFP applications has driven toward an increasing interest for the whole class of fluorescent proteins that are nowadays deeply investigated [42–44].

The complex photophysics of the caged GFP chromophore, *p*-hydroxybenzylideneimidazolinone (HBDI), is firstly related to its different forms. In the ground state both its neutral (so-called A form, or reactant form) and anionic (B form) are present although the neutral population is six time higher that the anionic one under physiological conditions [45], so the absorption spectrum is almost composed by a band around 395 nm due to the A form, and a minor one around 480 nm due to the B form. The optical behavior of GFP chromophore and the assignment of the absorption and emission bands are deeply confirmed by both experimental and theoretical investigations. The wtGFP experimental absorption and emission bands are shown in Fig. 4.
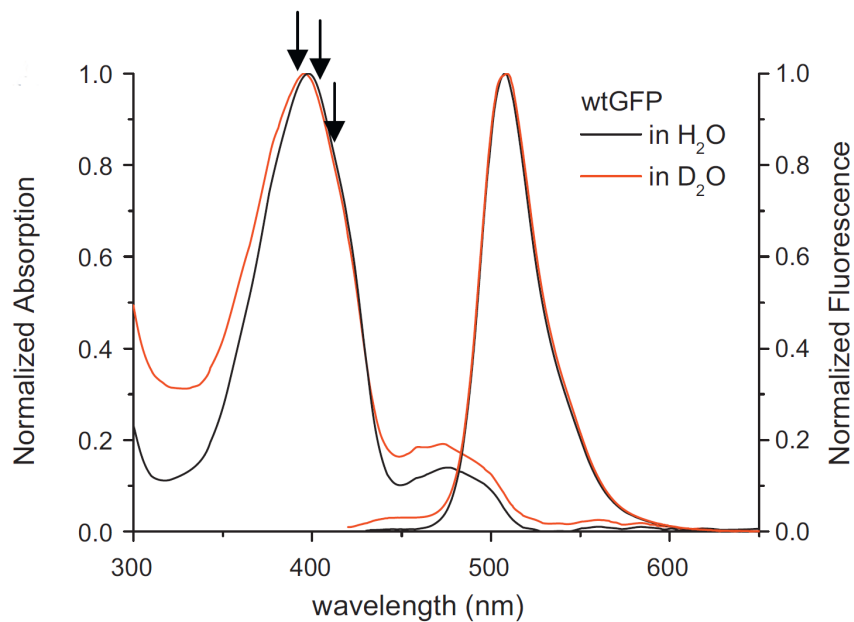
Fig. 4: The absorption and emission spectra of GFP in H_2O and D_2O. [46]

After the excitation an excited state proton transfer reaction takes place, lead-

ing to the formation of an anionic form denoted as I* responsible of the emission around 508 nm [45]. The reaction consists of three proton transfers involving the chromophore and residues engaging an hydrogen bond network with it: a crystallographic water molecule, Ser205 and Glu222 as final acceptor, as firstly suggested by Brejc and co-workers [47]. A schematic picture of the GFP active site and of the ESPT reaction is shown in Fig. 5 [48].
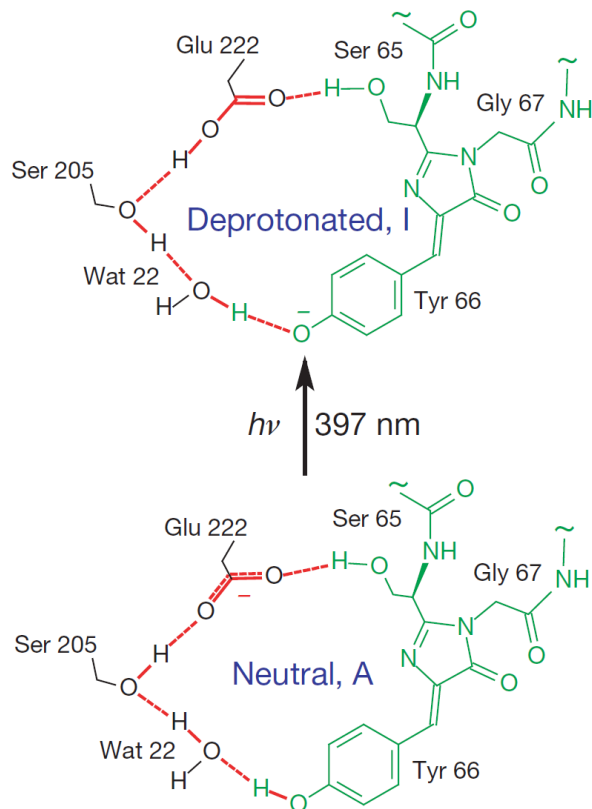
Fig. 5: The hydrogen-bonding network linking the two ends of the chromophore in the protein pocket before (neutral, A) and after (deprotonated, I) proton transfer. The tildes indicate the omission of the protein residues not directly involved in the ESPT chain. [48]

Crystallographic and site-directed mutagenesis experiments confirmed the con-

nection among these residues, and the role of the Glu222 as final acceptor that was also proved by Stoner-Ma and co-workers through site specific mutagenesis (E222D) and ultrafast time-resolved infrared spectroscopy [49].

Boxer and co-workers [45] estabilished a biphasic kinetics for the ESPT reaction with time scales of 3 and 10 ps that has been confirmed by pump-probe infrared measurements [49–51] for GFP in H_2O buffer.

The molecular reasons underlying the ESPT biphasic kinetics are still unclear. In this contest a crucial question is related to the number of intermediate species, that is still under debate. Indeed some experiments suggest only one intermediate specie (I^*) formed from A^* [46,52] while more than one intermediate is proposed by Di Donato and co-workers [53].

Beyond different interpretations, structural arrangements of the chromophore and the nearest residues seem to be important to understand the proton transfer reaction and its kinetics suggesting a complex nature of the ESPT involving the whole hydrogen bond network, and that it should be not only driven by the chromophore photo-acidity. In this contest, the importance for the chromophore to reach the right conformation for the proton transfer is underlined by Prof. Mathies and co-workers [48] through their femtosecond stimulated Raman spectra. Prof. Mathies and co-workers [48] through their femtosecond stimulated Raman spectra, suggest that structural rearrangements happen before the PT and in particular a low frequency mode, the wagging of the phenolic ring at 120 cm^{-1}, drives the PT kinetics

because it allows to the chromophore to reach the right conformation for the proton transfer.

Concerning this biphasic behavior, a *parallel* kinetics scheme is proposed by Van Thor and co-workers [52], in which only one intermediate (I^*) is hypothesized to be formed from A^*. Di Donato and co-workers [53] instead suggest a *sequential* scheme in which the intermediate I_0^* is directly formed from A^* and dominates the faster part of the dynamics (3 ps), then it evolves to I^* on the slower time scale (10 ps). The hypothesis of only one intermediate specie directly formed from A^* is supported by Meech and co-workers [46] that, on the basis of their experiments, suggest that no other forms are present apart A^* and I^*. Recent experimental works underline the importance of low-frequency motions role in the ESPT reaction [54].

Theoretical-computational investigations of the different chromophore forms, driving forces and ESPT mechanism are grown during these years. Helms and co-workers, on the basis of their classical molecular mechanics simulations, proposed a sequential mechanism for the reaction in which the first step is the proton transfer from the chromophore to the water molecule [55]. Further studies on the PT mechanism in the ground and in the excitd states were performed by Zhang and co-workers [56] and by Vendrell and co-workers [57], respectively, on quite simple models of GFP. These studies suggested a substantially concerted mechanism for the reaction. A recent work of Krylov and co-workers [58] was performed on the whole protein employing a combined QM/MM approach. They deeply investigated

16

the main chromophore species and examined the stabilizing factors for the anionic ones. Lluch and coworkers also worked on the GFP ESPT [59].

The disentanglement of the complex photo-reactivity of GFP in terms of driving forces, reaction mechanism and kinetics is a huge challenge on a theoretical point of view. High accuracy of the theory level is required to simulate the GFP reactivity while on the other side the whole protein matrix has to be taken into account in order to accurately reproduce the chromophore environment. We decided to employ an high-level computational strategy based on ab-initio molecular dynamics simulations on the whole protein in both the ground and the excited state for the first time to unveil the ESPT mechanism and to investigate with a molecular detail the main events happening before the proton transfer event (we found that these were significantly more important than the ESPT alone). We catched the crucial rearrangements involving both the chromophore and the protein environment that represent necessary conditions to allow the reaction event beside the increased acidity of the chromophore after the excitation. Our calculations were performed on the whole protein matrix in order to retain the environment structural influence on the reaction. Because of the system complexity, and so the huge computational cost, we perfomed a study almost focused on both the important events preceeding the reaction and on its mechanism, this last also discussed in detail. We found important differences in structural rearrangements related to the chromophore and to residues directly and indirectly involved in the reaction in the ground and in the excited

17

state simulations. The crucial role of residues not directly involved in the reaction, such as His148, is also highlighted for the first time. Our results suggest an almost structural-controlled ESPT reaction more than a chromophore photoacidity driven process.

In order to analyse the huge number of data collected from the molecular dynamics simulations we needed a robust protocol of time-resolved vibrational analysis: the Wavelet transform, to deeply investigate the main interesting physical quantities obtained from the trajectories. This promising analysis allowed us to follow during the time the non-equilibrium vibrational spectra of ad-hoc quantities chosen to investigate the ESPT main promoting molecular events: the fundamental role of the protein matrix and the importance of a structural optimization of the active site, taking place after the excitation, are the key instruments to understand the GFP photo-reactivity.

The chromophore and network residues necessity to find the right geometry promoting the ESPT was observed in high-level experiments such as femtosecond stimulated Raman spectroscopy [48], in accordance with our hypotheses. In these experiments emerges the crucial role of low frequency modes activated after the excitation, and the peculiar trends of some marker bands (C-O and C=N stretching modes) that are confirmed and well-reproduced in our time-resolved vibrational analysis.

The capability to make the Wavelet Analysis a general instrument in Chemistry was the main aim of my Ph.D. Project. We tested this analysis also in another chal-

lenging problem of chemical interest: the investigation of transient charged species formation and dynamics on organic molecules interesting for photovoltaic applications.

In this field semiconducting organic polymers have a rich history in the development of alternative photovoltaics. [60–63] While advances in organic photovoltaic material's quantum efficiencies lag behind those of modern inorganic and mixed organic/inorganic materials, organic semiconductors are nonetheless an important class of materials that have unique advantages for certain applications due to their mechanical properties. Another important advantage of such molecules is that these can be easily monitored through spectroscopic techniques such as Raman spectroscopy that is able to give an important insight of the processes happening at a molecular level [64]. The functionality and performance of organic materials strongly depend on molecular scale features that can be chemically modified to improve macroscopic properties and capabilities. Perhaps the most important process in determining the material's characteristic charge carrier mobilities and transfer rates is the coupled, non-equilibrium electron-nuclear dynamics that follow photoexcitation. This process intimately correlates exciton dissociative (or charge separation) dynamics with structural skeletal changes induced in the molecule along particular vibrational modes. Therefore, the exciton diffusion and dissociation rates can be modulated by excitonic coupling to intrinsic vibrational modes and the presence of photon-induced self-trapped [65] states (i.e. polarons). [66–76] A fundamen-

tal understanding of these coupled exciton-nuclear dynamics is crucial to improving the performance of semiconducting organic polymers. However, the detailed physical processes and consequential observations arising from the coupled excited-electron-nuclear dynamics lack accurate theoretical descriptions. In Fig. 6 a schematic representation of polaron and exciton formation in co-polymers in shown [77].
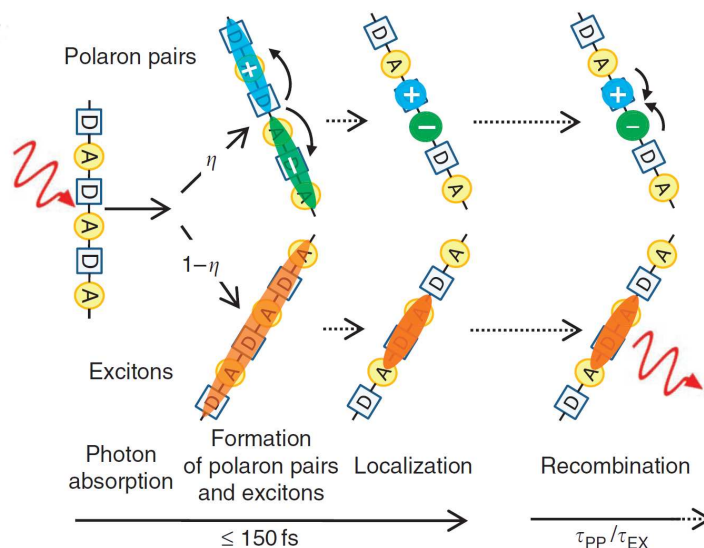
Fig. 6: Illustration of the photo-induced processes in co-polymers; on light absorption a delocalized exciton or polaron pair is formed with a yield η, this occurs within 150 fs. The polaron pairs decay by recombination on a longer time scale. D and A indicate donor and acceptor moieties.

The formation of polaron pairs is one of the possible photophysical processes that can take place after the excitation. Recent work suggests that polaron formation plays a significant role in photovoltaic action and that polaron dynamics are considered to be as important as those of 'bare' excitons. [77–79] Moreover, an important feature of both excitons and polarons is the strong dependence of their dynamical properties on the structural dynamics of the polymers. [80] This feature permits

these pseudo-particles' study by techniques such as Raman spectroscopy, because structural information can be probed to deduce the polaron pairs' formation and dynamics. [64,80,81] In fact, the role played by the dynamics of polaron pairs in the poly(3-hexylthiophene), one of the most performing polymers, has been studied by various time-resolved excited state spectroscopies, confirming the importance of the structural feature for the polaron pairs dynamics. [77,80–83]

Even with advanced time-resolved spectroscopic techniques, the mechanistic underpinnings of the experimental observations are still difficult to resolve without cross-correlating spectroscopic signals of electronic and vibrational degrees of freedom. From the theoretical modeling standpoint, the main challenge is presented by the complex multi-scaled time-evolution of a fast-evolving electronic wave function coupled to (and perturbed by) the slower non-equilibrium nuclear dynamics. [84] Our work wanted to propose for the first time a novel approach to treat such kind of processes based on the first-principles Ehrenfest dynamics [85–88] combined, for the first time, with multiresolution Wavelet Analysis to simulate and characterize the chemical dynamics following photoexcitation of a regioregular alkylthiophene oligomer. Our results demonstrate the great potentiality of this combined approach, indeed this coupled electronic-nuclear dynamics approach accurately reproduced the non-equilibrium chemical dynamics to properly simulate polaron pair formation, and at the same time also permitted analysis of the molecular dynamics in terms of both the charge carrier evolution and structural rearrangements. The importance of the

temporal evolution of the analysed frequencies is crucial in allowing the identification of important structural rearrangements with both spatial and temporal resolution.

The proposed strategy and the results collected during these years are deeply discussed in this thesis.

Chapter 1

Theoretical-Computational Protocol

A huge part of my Ph.D. Project was devoted to the development of an innovative theoretical-computational protocol aimed to the building of a robust methodology to study a big class of chemical phenomena. Such class involves both complex systems at their electronic ground state (such as solute-solvents) and far-from-equilibrium chemical processes such as photo-induced reactivity, time-resolved spectroscopic signals, formation of transient charged species after the excitation. This methodology was employed for the first time to study ground state processes in a previous work before starting the Ph.D. Project. Moreover we also employed for the first time this protocol to analyse a simulated time-resolved spectroscopic signal with excellent results [39]. Its extention on non-equilibrium processes, especially focusing on photo-induced reactivity of complex systems was the principal theme of this work.

The scheme proposed by us is composed by ab-initio molecular dynamics simulations, employed to investigate the ground and excited state potential energy

surfaces and to extract information of the system under study, and by the Continuous Wavelet Transform, adapted for the first time to the field of excited state reactivity, in order to perform a non-conventional analysis in the frequency domain of non-equilibrium signals extracted from the trajectories. This combined approach allowed to disentangle complex chemical phenomena and to give a molecular picture of such processes by extraction of the frequency content from the ad-hoc chosen molecular properties.

All the elements constituting this protocol are explained in this Chapter. We start discussing the novel vibrational analysis protocol introducing the Wavelet Transform and then the ab-initio molecular dynamics technique. The Computational Details are then discussed.

1.1 Equilibrium and Non-Equilibrium Vibrational Analysis

Molecular dynamics simulations represent a key tool to investigate many processes of chemical interest, going from molecules reactivity and photo-reactivity to the investigation of molecules in condensed phase and the simulation of spectroscopic signals. Nowadays the limits in the field of theoretical-computational chemistry are always more restricted, indeed the exploration of excited states is allowed, and so it is possible to study phenomena such as photo-induced reactivity, simulate time-dependent spectroscopic signals, investigate non-equilibrium photo-induced transient species. However these simulations are so expensive on a computational point of view and

still represent a frontier approach in treating such arguments, requiring a fine and meticulous work in terms of choice of the theoretical description of the system, that has to be highly accurate, and also affordable in terms of computational cost.

Ab-initio molecular dynamics simulations allow to perform descriptions of molecular systems in which the forces acting on the nuclei are computed from electronic structure calculations, on the contrary of classical molecular dynamics simulations where predefined force fields are employed. Although a good investigation of chemical systems can be performed by classical dynamics, an of course better molecular picture of the phenomena under study can be achieved by ab-initio simulations, and also problems "chemically complex" can be handled easily through this approach such as, for example, those where the electronic density changes drastically during the dynamics.

Several physical quantities can be obtained together with their temporal evolution and can be ad-hoc treated to gain spectroscopic quantities that can be directly connected with experiments. Among several spectroscopic techniques, the vibrational one is among the best ones, allowing for a molecular picture of chemical processes. Indeed in the vibrational spectra the molecular motions can be monitored and the chemical event can be followed with a molecular resolution. The appearance of vibrational bands, couplings among these ones, and frequency shifts are crucial information that today, thanks to time-resolved advanced techniques, can be achieved with a great detail. Excited state vibrational spectra and their tempo-

ral evolution can be recorded, and so non-equilibrium processes can be investigated after the excitation and followed during the time, in this way transient structural rearrangements are monitored.

Anyway, so often a picture of a chemical event only based on a spectroscopic point of view is not enough to have a complete understanding with a molecular resolution of the problem under study, and for this reason a theoretical-computational study is necessary. In this field, statistical mechanics provides the appropriate theoretical foundation for condensed phase systems at equilibrium [30]. Analysis of molecular dynamics simulations allows for the calculation of thermodynamic or statistical mechanics quantities such as temperature, correlation functions, transport coefficients [31]. Generally, physical quantities of interest can be obtained from the Fourier transform of suitable correlation functions. This statistical approach is usually valid for systems in stationary states and allows also to perform a vibrational analysis from equilibrium molecular dynamics simulations.

Dynamical processes in many-body systems that are far-from-equilibrium present further challenges. In this case correlation functions and spectra change with time as energy redistribution occurs. The conventional signal processing based on Fourier transform is not able to capture this evolution, instead a non-stationary time series analysis is required. Furthermore, modern ultrafast spectroscopy is today able to provide a detailed dynamics of a far-from-equilibrium system in condensed phase. Also in this case, a non conventional analysis should be invoked [31]. This field

represents the great challenge for this Ph.D. Project: the building of a general and

stable protocol of analysis for non-equilibrium molecular dynamics simulation of

complex systems. The work was based on the developing of the Wavelet Analysis in

theoretical-computational chemistry for studying excited states. The choice of this

technique was based on many key reasons that make it a precious instrument in this

contest.

The many differences between the more common Fourier transform and Wavelet

transform are discussed in detail in the next paragraphs, however the main one re-

sides in the fact that Wavelet Analysis is the most natural and ad-hoc choice to

treat non-stationary signals. In general, in equilibrium conditions a satisfactory

analysis could be performed by the Fourier protocol obtaining its frequency content

as an *average* of all the different frequencies contained in it, but for non-equilibrium

conditions the idea of an *average* analysis applied on a non-stationary signal is un-

correct because transient frequencies, instantaneous couplings and shifts could exist

and it is the information connected to their *temporal* evolution to be fundamental.

In other words, the intrinsic time-dependent nature of the frequencies is lost in an

irreversible way. This Ph.D. Project is focused on the demonstration of the Wavelet

transform potentiality in chemistry and, more in detail, in the complex world of

non-equilibrium chemistry.

1.2 From Fourier to Wavelet Analysis

The Fourier transform is ubiquitous for extracting the frequency components of a system's response to a time-dependent perturbation [89]. Spectral information can be calculated by the FT of the time correlation function $C(t)$ of a given physical property.

$$F(\omega) = \int C(t)e^{-i\omega t}dt \qquad (1.1)$$

where ω is the angular frequency. For example, the C(t) of the ith normal mode velocity $\dot{Q}_i$ extracted from an equilibrium simulation, leads to the corresponding spectrum $F_i(\omega)$. However the C(t) quantity can be any useful molecular parameter whose frequency content can be employed for the investigation of the system under study.

The information provided by the FT yields an average description of a *stationary* signal, i.e. a signal whose frequencies do not change with time. The frequency content of a signal is indeed achieved, but it is not possible to establish *when* such frequencies appear during the time, or *where* these are localized. For example, we cannot know if a sampled frequency in the spectrum is present in the signal for all its length or if it appears just for a limited period of time. This fact can be of crucial importance to understand if that frequency as a ruling importance in the spectrum or if it is just an instantaneous contribution. However in equilibrium conditions this aspect should not be important because it is not supposed to have frequencies

changing during the time, and so in these cases we can conclude with a good degree of accuracy that the Wavalet Analysis could be in principle avoided.

A very different situation is found in the case of non-stationary signals belonging to systems in far-from-equilibrium conditions. In these cases a different analysis is necessary to investigate time-varying spectral properties. As matter of fact, the Fourier series is composed of oscillatory trigonometric functions that are not adequate to capture signals not resulting from the superposition of harmonic oscillators [31]. A straightforward alternative is to split the signal into equal length sections in the time domain in which the stationary assumption can be locally applied and such pieces are analysed individually for their frequency content. The Short Time Fourier Transform (STFT) is commonly used to perform this decomposition. In this approach a window function $g(t)$ of limited extent and centered at a time location τ is introduced in the standard Fourier Transform to obtain the local frequency of the signal that is assumed to be stationary within this window. However the crucial point of this procedure is the strong dependence on the choice of the window $g(t)$ [21] because it ensures that the local signal is sufficiently stationary. The selection of the window width involves a tradeoff, indeed narrowing the time window improves time/localization resolution but reduces clarity of the frequency information. However, although the STFT procedure manages to garner some signal position information via the location of the windows, it is still fundamentally hindered by the stationary nature of the sinusoidal basis of the FT method. A

transformation method that uses basis functions that are simultaneously localized in both the time and the frequency domains would neatly avoid this tradeoff.

A powerful alternative to the traditional FT or STFT in the field of non-stationary signals is represented by the Wavelet Analysis [19,20]. The Wavelet Transform (WT) seems to represent the *natural* analysis for signals extracted from molecular dynamics simulations, especially in non-equilibrium cases such as the investigation of excited states. The intrinsic time dependence of all the properties of a system is a problem that the Fourier Analysis cannot handle because of the intrinsic lack of the temporal information after the transform. In these cases the knowledge of the frequencies temporal evolution is necessary, the appearance of a frequency during the time, suggesting for example the activation of a specific motion, can be necessary to study a chemical process, or the presence of couplings during the time among vibrational bands, or frequency shifts that could be due to localized molecular events. All these information intrinsic in the dynamics of a vibrational spectrum at non-equilibrium conditions have to be necessarily taken into account in the study and the Wavelet Analysis can be the right answer for this problem.

The Wavelet transform allows for the localization of a signal both in time and frequency domain [22], and this feature is particularly appealing for the simulation of time-resolved spectroscopic signals [90]. One of the advantages of the Wavelet Analysis is that the temporal information is retained and so the instantaneous frequencies are catched, in this way we have not an *average* frequency content but we

localize them at every instant. Another advantage is that the resolution at which the signal is analysed is not fixed, but changes and is adapted to the underlying frequency. In this way a *multiresolution* analysis is performed and the different frequencies are analysed with an ad-hoc resolution.

In the Wavelet Analysis the decomposition of the signal is carried out by means of the wavelets functions that are employed as basis functions instead of the sinusoidal ones that are employed both in the FT and in the STFT analyses. This is the first great advantage because the basis set is composed by functions localized both in the time and frequency domain. The analysis is performed by employing a special function ψ called wavelet "mother" that can be localized in time by a translation ruled by the index b. Furthermore ψ can be 'dilated' or 'contracted' by using the *scale* parameter a in order to focus on a given range of oscillations [91]. The Wavelets are derived from the mother and constitute a family, they represent translated and scaled versions of ψ, obtained by changing the a and b parameters of the mother prototype.

The Wavelet transform is also used as an efficient method to filter specific frequencies of a signal. In this regard the WT (called *discrete* [20, 21] in this case), permits to filter out the high-frequency noise without completely omitting the high-frequency phenomena [92]. Applications of this kind of analysis have been published in many fields [31, 92].

Our analyses have been performed using the so-called *continuous* WT, which is

the appropriate one for our time series analysis. The mathematical expression for the continuous Wavelet Transform simply replaces the Fourier basis function with a Wavelet one:

$$W(a,b) = \int C(t)\psi_{a,b}(t)dt \tag{1.2}$$

where the wavelet function $\psi_{a,b}(t)$ is defined by dilation and translation of a "mother wavelet" $\psi(t)$ expressed as

$$\psi_{a,b}(t) = |a|^{-\frac{1}{2}}\psi\left(\frac{t\text{-}b}{a}\right)(a, b \in R; a \neq 0) \tag{1.3}$$

where a is the scale (dilation) proportional to the inverse of frequency and b is the position (translation) parameter. The b parameter allows the analysing functions to shift along the temporal axis, in this way the frequencies can be localized during the time, while the a parameter causes the dilation or compression of the analysing functions so that the frequencies are analysed with different and appropriate resolutions.

We recall here that in the STFT the time and frequency resolution are bound to the choice of the window function, characterized by a fixed bandwidth. On the contrary, the Wavelet analysis allows for a *multiresolution analysis* where the bandwidth is variable and can be adapted to the signal. However, the time and frequency resolution is limited by the uncertainty principle (or Heisenberg inequality): the time and frequency resolution cannot be arbitrarily small because their product is lower

bounded according to

$$\Delta t \Delta f \geq 1/4\pi \qquad\qquad (1.4)$$

where Δt and Δf are root mean square measures of the duration and the bandwidth of an analysis function, respectively.

Many wavelet families exist (someones are shown in Fig. 1.1), and the choice of one of these is related to the nature of the signal to process.
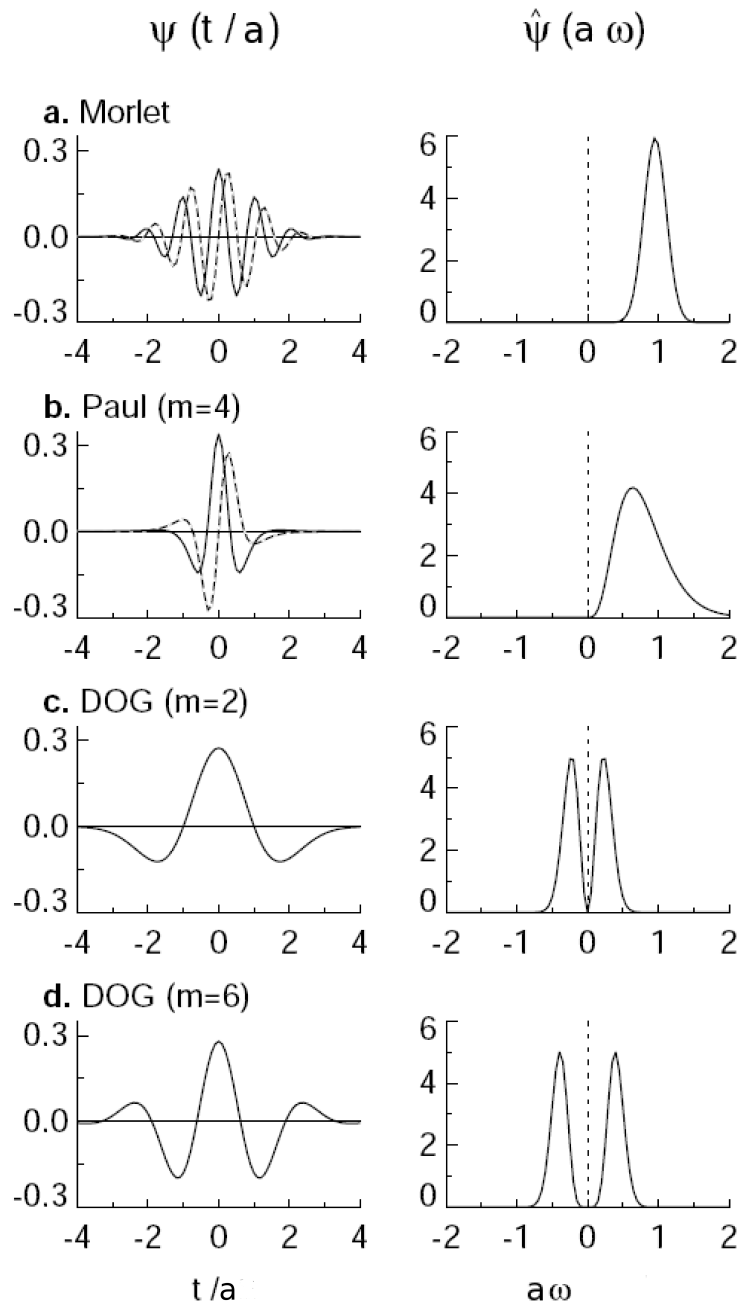
Fig. 1.1: For different wavelet bases. The plots on the left give the real part (solid) and imaginary part (dashed) for the wavelets in the time domain. The plots on the right give the corresponding wavelets in the frequency domain. The m values are typical mother wavelet parameters, see ref. [22]. According with ref. [22] the a value represents the scale.

The Morlet and Paul wavelets are both complex, while the DOGs are real valued.

Such differences can have obviously repercussions on the analysis performance. A complex wavelet function will return information about both amplitude and phase and is better adapted for capturing oscillatory behaviour. A real wavelet function returns only a single component and is suitable to isolate peaks or discontinuities [22].

We have chosen to work with the Morlet wavelet, a plane wave modulated by a Gaussian-type function. The choice has been based on preliminary tests, moreover it is the most used in chemical applications [90, 93–95]. The Morlet wavelet can be expressed as

$$\psi(t) = \pi^{-1/4} e^{i\omega_0 t} e^{-t^2/2} \tag{1.5}$$

where ω_0 is the nondimentional frequency, whose value is usually set to be ≥ 6 to satisfy the so called admissibility condition [20]. A large ω_0 value allows for a good frequency resolution at the cost of poor time resolution [93].

To reduce the computational time required to calculate the wavelet transforms, the equation 1.2 is often solved in the reciprocal space [22]. By the convolution theorem the wavelet transform is the inverse Fourier transform of the product:

$$W(a,b) = \sum_{k=0}^{N-1} \hat{x}_k \hat{\psi}^*(a\omega_k) e^{i\omega_k b \delta t} \tag{1.6}$$

where N is the number of points in the time series, $k = 0 \ldots N-1$ is the frequency index, $\hat{x}_k$ is the discrete Fourier transform of the general time series, $\hat{\psi}$ is the Fourier transform of the wavelet function, (*) indicates the complex conjugate, δt is the

sampling time, and ω_k is the angular frequency.

The resolution of a wavelet function is determined by the balance between the width in the real space and the width in the Fourier space. For example, a broad function of time will have poor time resolution, yet a good frequency resolution [22].

The wavelet function should reflect the features present in the time series. Therefore, a different shape should be chosen when the signal occurs with sharp jumps or steps, or when it is a smoothly varying one.

The choice of values for a can be arbitrary and must be done in order to obtain a complete picture of the frequencies. We remember that for short scales $\psi_{a,b}(t)$ is a very highly concentrated ("shrunken") version of $\psi(t)$, with a frequency content mostly in the high frequency range. Conversely, for greater values of the scale the wavelet $\psi_{a,b}(t)$ is spread out and contains mainly low frequencies [20].

It is convenient, for computational efficiency, to express the scales as fractional powers of two:

$$a_j = a_0 2^{j\delta j}, j = 0, 1, ..., J \tag{1.7}$$

with

$$J = \delta j^{-1} log_2(N\delta t/a_0) \tag{1.8}$$

where δt is the sampling time, and s_0 is the smaller resolvable scale whose typically value is $2\delta t$. Moreover, J determines the largest scale, while δj is the scale

spacing. The choice of a sufficiently small δj gives a finer scale resolution. In the case of the Morlet wavelet, a δj of about 0.5 is the largest value that still gives an adequate sampling of scale values [22].

Although wavelets are characterized by a definite scale, they do not bear any resemblance to Fourier modes (sines and cosines). Therefore, a relation between the wavelet scale and the common Fourier wavelength is not necessarily straightforward. However, a correspondence between wavelength and the scale a sometimes can be achieved. For example, in the case of the Morlet wavelet, which is a periodic function enveloped by a Gaussian, this correspondence is possible. For a Morlet wavelet with $\omega_0 = 6$, the relation is $\lambda = 1.03s$ where λ is Fourier wavelength, indicating that the scale is almost equal to the Fourier frequency [96].

1.3   Ab-initio Molecular Dynamics Simulations

The preparation of a rational GFP model characterized the first phase of this study. It involved many steps and an ad-hoc strategy in order to be able to reproduce not only the active site at a huge theoretical level, but also the protein environmemt with good accuracy.

The procedure for the model preparation started from the crystallographic structure of wild type GFP of jellyfish *Aequorea Victoria* (PDB code 1GFL) [97]. The protein model preparation and preliminar calculations performed before running the molecular dynamics simulations are discussed in detail in Computational Details Paragraph. The employed multilayer quantum mechanics/molecular mechan-

ics (QM/MM) description of the system, according with the ONIOM partition scheme [98–101] is presented elsewhere [102]. According to this scheme, the high theory level part included the chromophore completed by Ser65 side chain and the residues directly involved in the hydrogen bond network and in the ESPT event (a crystallographic water molecule, Ser205 and Glu222) while the remaining part of the protein was treated at molecular mechanics theory level.

The studied model, consisting in the whole protein is presented in Fig. 1.2 employing two different representations in order to distinguish the active site from the rest of the protein matrix. In Fig. 1.3 just the active site, treated at quantum mechanics theory level, is shown. In Fig. 1.4 the active site is presented again but enlarged with the His148 residue that is involved in an hydrogen bond with the chromophore phenolic ring and is treated at MM theory level in our study. This picture is introduced because, as will be deeply discussed in the Results Chapter, the His148 residue has a crucial role as one of the ESPT driving forces.

The protocol of study consisted in a combined approach of molecular dynamics simulations in the ground and excited states to obtain several information concerning the chromophore, and Wavelet transform to analyse the obtained quantities.

In particular, ab-initio molecular dynamics (AIMD) simulations within the Born-Oppenheimer (BO) approximation [103, 104] were performed to characterize the system in both the ground and the excited states. The ground state simulation was performed at B3LYP [105]/6-31+G(d,p) level of theory. The trajectory on the S_0
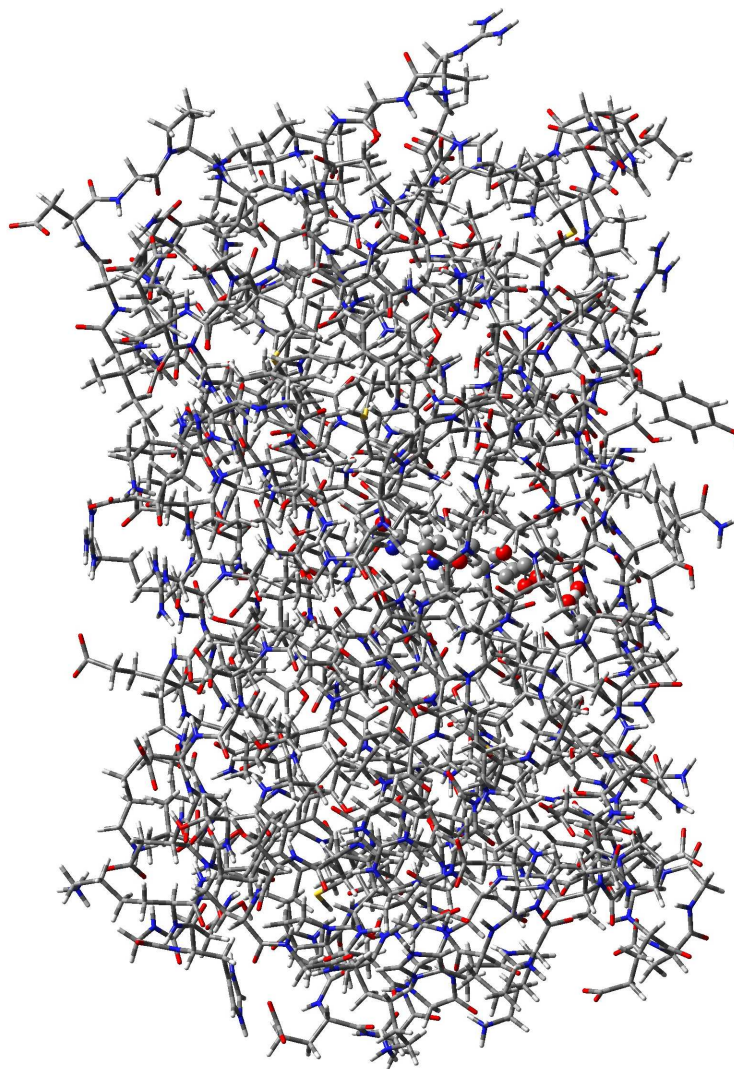
Fig. 1.2: The GFP protein model. The whole protein is shown. Two representations are employed to distinguish the active site treated at QM theory level and the rest of the protein treated at MM theory level.

potential energy surface was collected for 5 ps employing a time step of 0.5 fs. Several

singlet excited state AIMDs were collected, excited state energies and gradients were

calculated on-the-fly by the linear response TD-DFT [106–109] formalism at CAM-

B3LYP [110]/6-31+G(d,p) theory level. These trajectories were collected for less
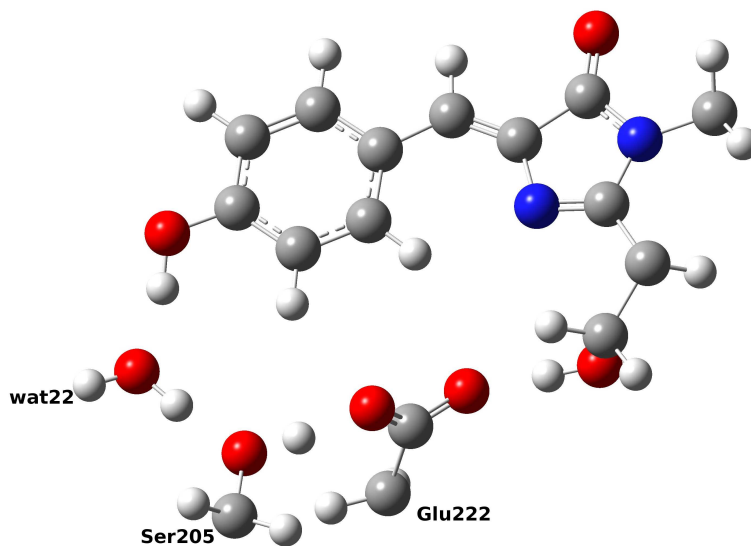
Fig. 1.3: The GFP active site model treated at QM theory level in our study.
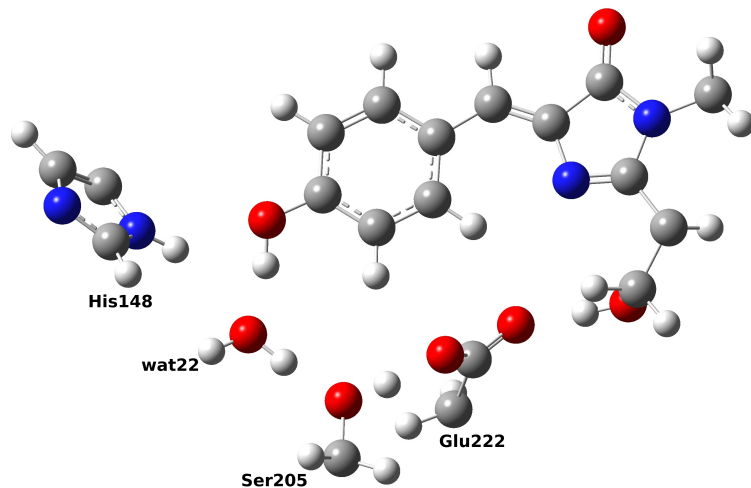
Fig. 1.4: The GFP active site model treated at QM theory level in our study and His148 residue, treated at MM theory level.

then 1 ps with a time step of 0.5 fs. In all the cases the excited state simulations were long enough to observe an ESPT event.

1.3.1 Anharmonic and Energetic Analysis

Anharmonic frequency calculations were performed on a minimal GFP model. This study was performed to support the choice of two different functionals for the ground and excited state AIMD. The frequency trends obtained with B3LYP and CAM-B3LYP were consistent, suggesting that a very similar description of the ground state potential energy surface curvature is obtained with both the functionals, reinforcing our choice.

In order to build the model, GFP structures optimized by the ONIOM scheme at DFT and linear response TD-DFT have been employed to characterize both the S_0 and S_1 electronic state, respectively. From these structures a minimal model has been extracted including the chromophore, the crystallographic water surrounding the chromophore tyrosine and the residues Ser205 and Glu222. Also chromophore tail (Ser65) has been included.

An energetic analysis was performed on the GFP chromophore in its anionic form at both the ground and excited states. In particular an investigation on a range of possible chromophore N-C-C-C dihedral angle values was performed by employing the same theory level used in the molecular dynamics simulations. This energetic analysis was performed in order to energetically quantify which are the more favored dihrdral angle values assumed by the chromophore in the ground and the excited states.

1.4 Non-Adiabatic Ehrenfest Dynamics

Part of the third year has been also focused on the investigation of systems interesting for photovoltaic applications. In particular in the field of organic photovoltaic devices. In order to study the chemical processes characterizing such systems, an ad-hoc theoretical-computational strategy was adopted. In order to build our oligomer model, we started from the regioregular poly(3-hexyl)thiophene and prepared a thiophene oligomer in order to study the formation and dynamics of transient charged species after the excitation. The oligomer was studied by employing the Ehrenfest dynamics technique, in this way we could follow the electronic dynamics and its couplings with nuclear dynamics.

The Ehrenfest dynamics is a non standard technique that is mandatory for this kind of challenging phenomena and has been implemented and tested in previous works [85,86,111], here we just provide a brief descriprion. The electronic degrees of freedom are propagated with real−time Time Dependent Density Functional Theory (TDDFT) while the electron-nuclear non adiabatic interactions are modeled with the Ehrenfest technique, which propagates the nuclei on the mean−field electronic potential.

The Ehrenfest dynamics scheme employs a three time step integrator. These time steps are implemented with three different integrators: nuclear velocity-Verlet [112], a nuclear position coupled midpoint Kohn−Sham integrator and a a modified midpoint and unitary transformation (MMUT) TDDFT employed to propagate the

electronic degrees of freedom [86, 111, 113]. The unitary trasformation matrix is a time-evolution operator constructed from the eigenvectors $\mathbf{C}(t_k)$ and eigenvalues $\epsilon(t_k)$ of the Kohn−Sham matrix ($\mathbf{K}$):

$$\mathbf{C}^\dagger(t_k) \cdot \mathbf{K}(t_k) \cdot \mathbf{C}(t_k) = \epsilon(t_k) \tag{1.9}$$

$$\mathbf{U}(t_k) = \exp[i \cdot 2\Delta t_e \cdot \mathbf{K}(t_k)] = \mathbf{C}(t_k) \cdot \exp[i \cdot 2\Delta t_e \cdot \epsilon(t_k)] \cdot \mathbf{C}^\dagger(t_k) \tag{1.10}$$

In the second equation Δt_e represents the time step for the MMUT integrator. The density matrix $\mathbf{P}$ is then propagated from time t_{k-1} to t_{k+1} with a fixed nuclear position:

$$\mathbf{P}(t_{k+1}) = \mathbf{U}(t_k) \cdot \mathbf{P}(t_{k-1}) \cdot \mathbf{U}^\dagger(t_k) \tag{1.11}$$

Because the electronic wave function changes significantly faster than the nuclear motion, the integrals required in the Kohn−Sham matrix are updated with a second time step Δt_{Ne} that includes $m\Delta t_e$ iterations, by the nuclear position coupled mid-point Kohn−Sham integrator. The nuclear positions are updated for $n\Delta t_{Ne}$ steps before recalculating the gradient, using a third time step $\Delta t_N = n\Delta t_{Ne}$, and the Velocity Verlet algorithm is employed to propagate nuclear coordinates.

The non-adiabatic Ehrenfest dynamics represented the natural choice for the study of transient charged species formation such as the polaron formation. The

propagation of the electronic density directly allowed to follow the evolution of such species, moreover through the nuclear dynamics the coupling and the effects of the nuclear degrees of freedom on the polarons could be investigated.

1.5 Computational Details

1.5.1 Modeling the GFP Protein

A reliable model for the neutral GFP form (reactant form) was chosen in order to characterize the system in both the ground and excited state and, in this last case, to follow the ESPT reaction. A crystallographic structure of wild type GFP of jellyfish *Aequorea Victoria* (PDB code 1GFL) [97] was chosen for the modeling.

As first step the coordinates of 1GFL were augmented with hydrogen atoms using the program MolProbity from Richardson group [114]. Residues such as Arg and Lis, and Asp and Glu, were considered with positive and negative charge, respectively. Concerning the fine equilibrium of histidine residues we decided to protonate six histidines in both δ and ϵ positions, while of the remaining three, two were protonated in δ (one of these is His148) and the other one in ϵ. All the internal crystallographic water molecules were protonated and retained.

Once obtained the structure, a partitioning of the whole protein according with the ONIOM scheme [98–101] was performed. On the basis of this multi-layer approach, a QM description of the chromophore, (including the residue Ser65), and of the residues directly involved in the reaction (a crystallographic water molecule, Ser205 and Glu222) was performed, in order to be sure of obtaining a fine description

CHAPTER 1. THEORETICAL-COMPUTATIONAL PROTOCOL

of the active site and in accordance with the partition presented in [102]. All the other residues were treated at MM level of theory by employing the AMBER force field [115] and including the parameters specifically developed for the chromophore by Reuter. [116].

The cuts at the interface between the QM/MM layers were performed on single bonds of non-polar or slightly polar bonds and in the most of cases C-C bonds were involved. The electronic embedding [99, 117] scheme has been employed to account the interaction between the two layers.

Structure optimizations were performed at the ONIOM CAM-B3LYP [110]/6-31+g(d,p)/Amber level including the aqueous solvent that was treated implicitly by the so-called ONIOM/CPCM-X [118, 119] scheme. Then the system was relaxed by neglecting the implicit solvation effects in order to save time for the subsequently MD study. This approximation is still valid because we ensure that the implicit solvation does not affect too much the vertical excitation energy, moreover our MD simulations are not long enough to be needed the inclusion of the volume preserving effects of implicit solvation.

Ab-initio molecular dynamics (AIMD) simulations within the Born-Oppenheimer (BO) approximation [103, 104] were performed to characterize the system in both the ground and the excited states.

The ground state simulation was performed at B3LYP [105]/6-31+G(d,p) level of theory. We collected a trajectory on the S_0 potential energy surface for 5 ps

employing a time step of 0.5 fs. Several singlet excited state AIMDs were collected where excited state energies and gradients were calculated on-the-fly by the linear response TD-DFT [106–109] formalism at CAM-B3LYP [110]/6-31+G(d,p) theory level. These trajectories were collected for less then 1 ps with a time step of 0.5 fs. In all the cases the excited state simulations were long enough to observe an ESPT event.

Concerning the choice of the potential for the molecular dynamics simulations, preliminar tests were performed in order to find the more suitable in terms of both reproducing GFP optical properties and exploring the excited state potential energy surface. In particular excited state AIMD simulations employing the B3LYP functional were performed but, unfortunately, it was not robust and also very unstable for such calculations, not allowing the excited state potential energy surface exploration. On the basis of the performed tests, the CAM-B3LYP functional was found to be more robust for excited state dynamics calculations, allowing us to collect trajectories almost 1 ps long. The choice of two different functionals for the ground and excited state AIMD was supported by anharmonic frequency calculations by employing both B3LYP and CAM-B3LYP on a reduced GFP model. The consistent frequency trends obtained with both the functionals suggested that a very similar description of the ground state potential energy surface curvature is obtained with both the functionals, reinforcing our choice.

We extracted the starting configuration for the ground state molecular dynamics

while only one of the excited state ones, (called TrjIV), started from the optimization calculations. Randomly chosen momenta coherent with a starting average temperature of 298 K were assigned to this configuration. This choice is in agreement with our aim to investigate the PT mechanism and the network structural re-organizations in the two electronic states. A kinetics study of the reaction is prevented because it would request a larger number of excited state trajectories, that are so expensive on a computational point of view, however we were able to perform a deep investigation of the structural re-organization after the excitation and to follow the reaction event.

The starting points for the other three excited state ab-initio MD hereafter called TrjI, TrjII and TrjIII, were extracted from the ground state simulation and both the starting coordinates and momenta were taken. Of course we had completely different input structures compared to the previous one (extracted from the optimization calculation), in order to monitor some peculiar trends and be sure that they were not random trends but that could be reproduced, so representing a characteristic behavior of the protein after the excitation.

1.5.2   Modeling GFP Minimal Models

Vibrational and energetic analyses were performed on ad-hoc chosen models of both the GFP chromophore and hydrogen bond network. These analyses, although performed on minimal models, gave important support to the molecular dynamics study.

The anharmonic vibrational analysis was performed on the GFP minimal model in which the chromophore is in its neutral form (the reactant form), in both the

ground and excited states. All the discussed calculations were performed at DFT level of theory employing the B3LYP/6-31+G(d,p) potential in both the time-indipendent and time-dependent formalism (although the same calculations were performed also at CAM-B3LYP/6-31+G(d,p) theory level). Concerning the energetic analysis, consisting in rigid scans of the chromophore N-C-C-C dihedral angle, it was performed on the chromophore in its anionic form in both the ground and the excited states at DFT and LR TD-DFT [106–109] level of theory employing both B3LYP and CAM-B3LYP functionals with 6-31+G(d,p) basis set for S_0 and S_1, respectively. All the calculations were performed by employing a development version of the Gaussian suite of programs.

1.5.3   The Thiophene Oligomer Modeling

All the calculations, including geometry optimizations and excitation energies, were performed employing the CAM-B3LYP [120]/6-31g(d) theory level. Several theoretical computational studies have demonstrated that the CAM-B3LYP functional is one of the most appropriate to study of polythiophene molecules [121, 122]. A development version of the Gaussian suite of progams [123] was employed for all the calculations. As a preliminar step, we compared our model with its analogue substituted with hexyl side chains instead of methyls, in order to be sure that we were not losing potential information with a shorter side chain. Fig. 1.5 shows the molecular model, the 3-methylthiophene heptamer, used in this work, which is a slightly simplified model of the heavily studied poly(3-hexylthiophene) [80, 124, 125]

structure. From a comparison of both frequency and optical properties, we were confident that the methyl substitution of the hexyl chains would not cause discrepancies in the excited state electronic structure. The role of side chains is not trivial in the optimization of these systems, especially in terms of optimization of π-stacking, polymer crystallinity, material miscibility [126]. In this case we deal with a monolayer oligothiophene in which, to a first approximation, it is the its length and its conformation to play a much more important role in tuning its properties.
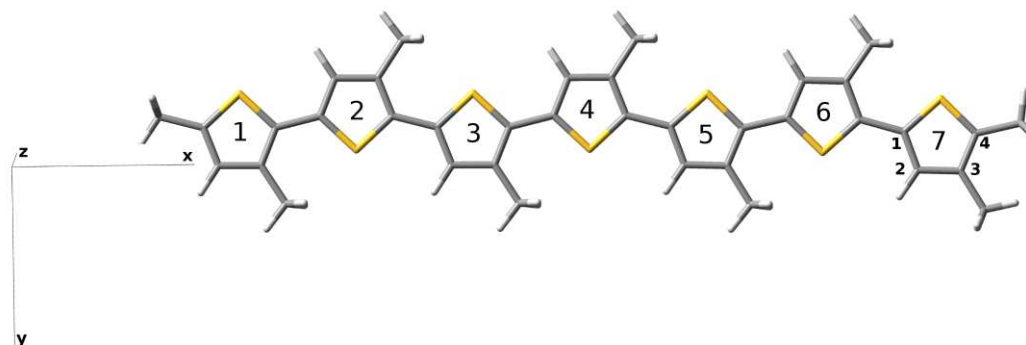
Fig. 1.5: The 3-methylthiophene heptamer model. The labels on the seven rings will be employed in the results discussion to recognize the different rings. The labels on come C atoms will also be employed in the results discussion. The cartesian axes are also shown.

In order to generate initial conditions (both coordinates and momenta) for the nuclei, we simulated a Boltzmann ensemble of 3-methylthiophene heptamer molecules at room temperature (298 K). For a specific vibrational mode with a given Boltzmann-sampled vibrational energy, the initial phase was chosen randomly and classically [127, 128]. Note that the motivation of this work is to illustrate the formation of a polaron pair and its spectroscopic consequence, rather than to investigate the statistical thermodynamics of a particular excited state ensemble. Therefore, we chose

a single initial condition with the most planar arrangement, which gives rise to the most delocalized electronic distribution, to "track" the polaron formation dynamics.

The initial excited state electronic density was prepared by promoting one electron from the highest occupied molecular orbital (HOMO) to the lowest unoccupied molecular orbital (LUMO) (see Fig. 1.6). These are the dominant orbital pairs in the $S_0 \rightarrow S_1$ excitation, as revealed by linear-response TDDFT calculations. The three time steps in the Ehrenfest dynamics simulation were $\Delta t_N = 0.1$ fs, $\Delta t_{Ne} = 0.01$ fs, $\Delta t_e = 0.001$ fs. The total energy conservation was within 0.022 kcal/mol. The Ehrenfest trajectory presented in this work is 89 fs long. The three time steps employed during the simulation were accurately chosen after a preliminar phase in which the most appropriate conditions for the dynamics were calibrated on the basis of both good total energy conservation and reasonable computational cost criteria.
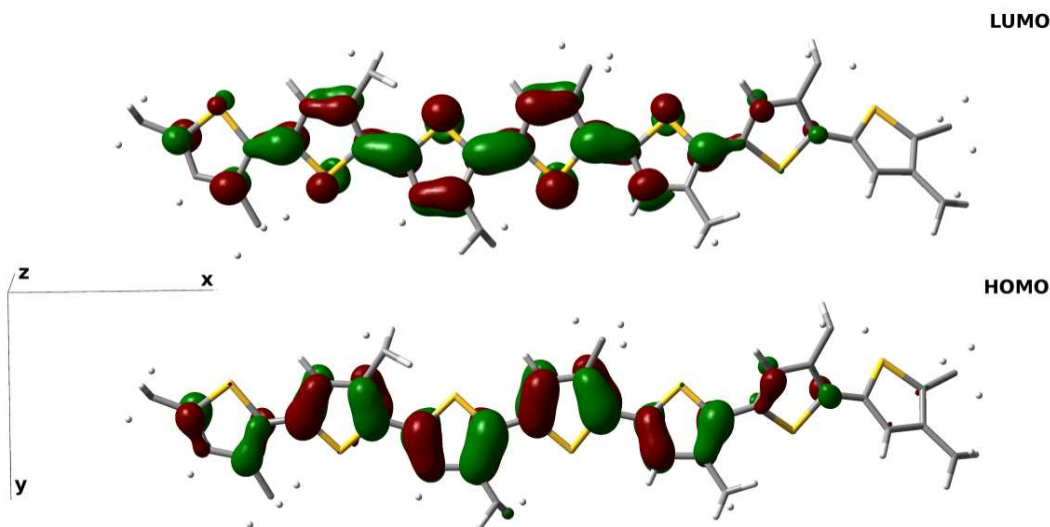
Fig. 1.6: The 3-methylthiophene heptamer model orbitals most relevant in the $S_0 \rightarrow S_1$ excitation evaluated at the nuclear geometry chosen for the Ehrenfest dynamics: LUMO (upper) and HOMO (lower). The cartesian axes are also shown.

We also performed an ab-initio Born-Oppenheimer molecular dynamics (BOMD) [129] simulation in order to compare the polaron formation dynamics to the structural dynamics of the system in the ground electronic state. The initial nuclear coordinates and momenta of the BOMD dynamics were the same used for the Ehrenfest dynamics. As in the excited state trajectory, the CAM-B3LYP/6-31g(d) theory level was employed and a nuclear time step of 0.1 fs was used. We collected a trajectory on the S_0 potential energy surface for 1.5 ps, however just the first 90 fs will be discussed in order to have a more clear comparison with the results obtained in the excited state.

Chapter 2

The GFP Photo-Induced Reactivity Investigation

The main results obtained in my Ph.D. Project are discussed in the present and the following Chapter. The Results presented in this Chapter represent a sort of "journey" aimed to the exploration of the GFP photo-reactivity. Our work started by a deep characterization of the GFP reactant form (in which the chromophore phenolic ring is protonated) in its ground state in order to describe the chromophore microsolvation in equilibrium conditions by ab-initio molecular dynamics simulation. The exploration of the excited electronic state was then performed. Several excited state trajectories were collected in order to follow the proton transfer reaction and give an insight on its mechanism. Surprisingly, our main goal was not to simulate the reaction event, as we supposed at the beginning, but to discover that it was an ensamble of molecular events in terms of structural reorganization of the active site (and not only of this one) to be important and crucial in promoting the proton transfer. For the first time a more complex view is given to this event, and other

residues not directly involved in the reaction were observed to play a key role, even if not directly involved in the reaction. We strongly underlined that the reasons favoring the reaction are several and not only one (such as, for example, the photo-acidity) as was sometimes supposed. Moreover we discovered that it is not enough that only one promoting condition was satisfied in order to observe the ESPT, but it was the simultaneous occurence of all these together to allow the reaction event. We demonstrated that it is not only the chromophore rearrangement to be important, but also the hydrogen bond network must optimize its arrangement and, more interestingly, *spectator* residues partecipate to the optimization of the reaction conditions.

All the results were obtained by means of our proposed innovative theoretical-computational approach. We performed ground and excited electronic state ab-initio molecular dynamics simulations to characterize the system and to simulate the ESPT. This approach is not so common because of its huge computational cost, especially because we simulated the whole protein and not only the active site.

The results analysis was performed in the frequency domain through the Wavelet Analysis approach, employing this technique for the first time to study the GFP ESPT, and more generally to investigate excited state photo-reactivity. The frequency domain based analysis gave the possibility to understand which were the main motions activated during the ESPT event and so to identify who was ruling the reaction. We could observe the activation or the shifts of vibrational bands dur-

ing the time and their differences with the ground state ones, in this way catching the instantaneous events that happen before and during the ESPT. This methodology was precious to disentangle this problem, showing its great potentialities in the chemical field and in the study of complex events.

2.1 Ab-initio Molecular Dynamics based ESPT Study

2.1.1 Ground State AIMD on GFP

A 5 ps long ground state BOMD trajectory of the GFP reactant form was collected. During this simulation no proton transfer reaction was observed, in agreement with the fact that in the ground state the reaction is not favored. We investigated the chromophore microsolvation in equilibrium conditions in order to characterize the whole active site. In particular this structural analysis in the ground state should be considered as a preliminar phase to the study of the ESPT, indeed in this way we investigated the behavior of the active site and of the protein matrix at equilibrium conditions, and more in detail we could catch the main structural changes on the active site after the excitation.

In Fig. 2.1 the normalized pair distribution functions of the monitored distances involving all the atoms belonging to the hydrogen bond network extracted from the ground state ab-initio molecular dynamics simulation are shown. In spite of the short time of sampling, we saw that the monitored distances adopt periodic oscillations around well defined minima along the simulation. The intermolec-

ular oxygen pair distances (left panels: Otyr-Owat(top), Owat-Oser205(middle), Oser205-Oglu222(bottom)), inter-molecular hydrogen-oxygen (middle panels: Htyr-Owat(top), Hwat-Oser205(middle), Hser205-Oglu222(bottom)), intra-molecular hydrogen-oxygen (right panels: Otyr-Htyr(top), Owat-Hwat(middle), Oser205-Hser205(bottom)) distributions are shown along with the relative averages made every 50 points (colored curves).
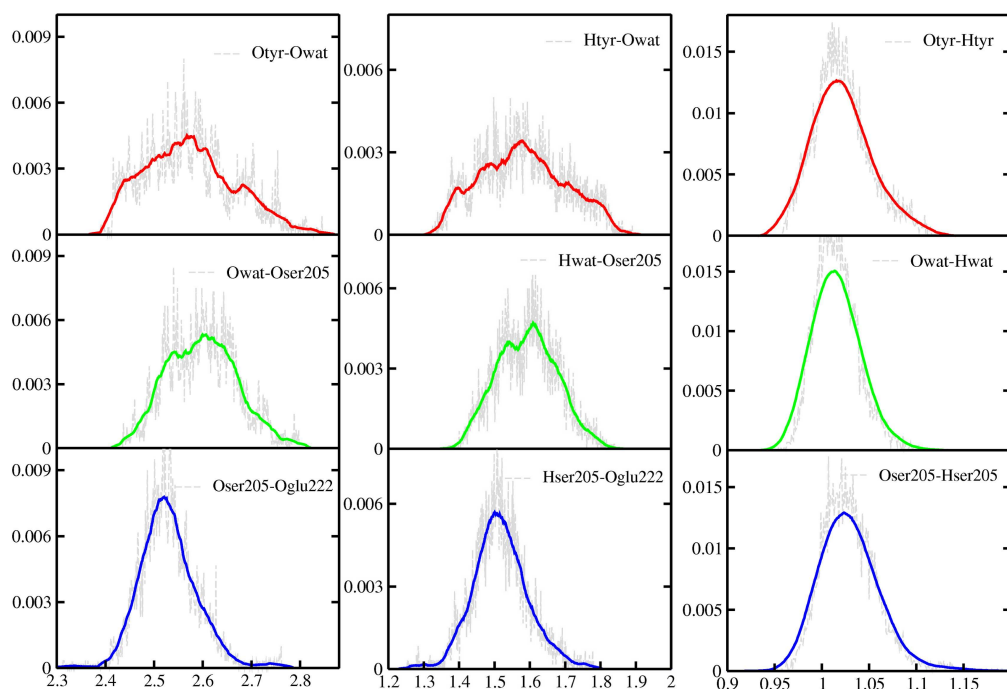
Fig. 2.1: Normalized distributions of network distances (Å) involved in the PT network obtained from S_0 AIMD simulation at B3LYP/6-31+g(d,p) level of theory. Left, Oxygen-Oxygen distances:Otyr-Owat (top), Owat-Oser205 (middle), Oser-Oglu(bottom). Middle, Proton-Acceptor units distances: Htyr-Owat (top), Hwat-Oser205 (middle), Hser-Oglu(bottom). Right, Proton-Donor units distances: Otyr-Htyr (top), Owat-Hwat (middle), Oser205-Hser205 (bottom). The relative average values, made every 50 points, are shown by different colored curves.

By an inspection of the left panel distributions, it is evident that the Oser205-Oglu222 pair distance presents the most regular shape. During the simulation

Oser205-Oglu222 distance oscillations explore a range of values extending from a minimum of 2.313 Å to a maximum of 2.761 Å, reached only once in the whole simulation, while this distribution is peaked around 2.522 Å. The average distance value is around 2.530 Å with a standard deviation of 0.059. This average distance value extracted from the simulation is so close to the maximum value of the distribution that is indeed peaked around 2.522 Å. The distribution in terms of both shape and maximum peak confirms a regular oscillation trend. A more complex behavior is observed for Otyr66-Owat, indeed these oxygens explore wider distance ranges and also less regular, compared to the Oser205-Oglu222 pair. Oscillations reach distances ranging from 2.391 to 2.845 Å, the average distance value is 2.574 Å with a standard deviation of 0.092. The trend observed along the trajectory is also supported by a corresponding wide shape and the absence of an actual main peak. This behavior can be attributed to the major mobility freedom of the water molecule. The average distance value reached by the Owat-Oser205 is around 2.599 Å with a standard deviation of 0.071. As observed in the Otyr66-Owat distribution, an irregular shape is found, although it explores a shorter range of values. The peculiar differences shown in the distributions are in perfect agreement with the relative distance oscillation trends. These ones reflect a major rigidity of the Oser205-Oglu222 interaction that is not observed in the other two cases, and this fact could be related to the major mobility that of course characterizes the water molecule in both the Otyr66-Owat and Owat-Oser205 pairs (the temporal evolution

of such discussed pair distances will be also analysed later in comparison with the excited state corresponding ones).

In Fig. 2.1 (middle panel) the proton acceptor distance distributions obtained from the 5 ps ground state simulation are presented. The acceptor pairs include Htyr-Owat, Hwat-Oser205 and Hser205-Oglu222 distances. Observing the distributions it is evident a similarity with the oxygens distributions shown before. From our analysis, we see that Htyr66-Owat ground state oscillations show an average distance value of 1.581 Å, with a standard deviation of 0.120. The distribution reflects a trend with no regular oscillations and with a wide range of explored values, indeed it appears spread and without a well-defined maximum peak reflecting an irregular behavior of this couple. A similar trend is observed in the Hwat-Oser205 case although it appears generally more regular during the simulation, with oscillations on average around 1.593 Å during the dynamics and a standard deviation of 0.084. The maximum distance value is 1.840 Å, while the minimum one is 1.370 Å. The relative distribution appears narrower than the previous one confirming a more regular oscillation trend, although also this time it is not trivial to define a main peak in the distribution. The last monitored distance, Hser205-Oglu222, confirms the stiff nature of these residues interaction with oscillations on average around 1.518 Å, and a standard deviation of 0.078. The distribution is well-centered around one distance value (1.507 Å) that is not so different from the calculated average value from the simulation. Moreover the shape is the most regular among the three distributions.

From these results it is evident that the residues Ser205 and Glu222 are closer than the other two pairs, as shown by the shift toward shorter distances of their distribution in respect to the others. The well-defined structural arrangement of Ser205 and Glu222 is almost preserved during the simulation, confirming in this way a retained rigidity between these residues that is not present in the other two cases, as already observed from the oxygens analysis.

In Fig. 2.1 (right), we report the distributions of the proton donor distances from the 5 ps ground state simulation. The investigated intra-molecular distances are: Otyr66-Htyr66, Owat-Hwat and Oser205-Hser205. Really tight oscillations and values typical of bond distances are observed in the ground state. These regular trends suggest a strong nature of the bond and no driving forces to react. The intra-molecular bond distance Otyr66-Htyr66 oscillates around an average distance value of 1.021 Å with a standard deviation of 0.030. The bonded nature is confirmed by a regular shape of the distribution with a maximum peak around 1.015 Å. Regarding the Owat-Hwat, distance oscillations show an average value of 1.016 Å with a standard deviation of 0.022. Also this time the distribution reflects an almost regular oscillation trend. It shows a regular gaussian shape with a maximum at about 1.012 Å, so really close to the average distance value. The pair Oser205-Hser205 shows an average distance value of 1.029 Å with a standard deviation of 0.030. A regular distribution is observed also this time in agreement with the bond nature of the examined distances.

Table 2.1: Average values, standard deviation and maximum values for the normalized distributions of distances (Å) involved in the PT network obtained from S_0 AIMD simulation at B3LYP/6-31+g(d,p) level of theory.

	Average distance	Standard deviation	Maximum value
Otyr-Owat	2.574	0.092	2.572
Owat-Oser205	2.599	0.071	2.604
Oser205-Oglu222	2.530	0.059	2.522
Htyr-Owat	1.581	0.120	1.581
Hwat-Oser205	1.593	0.084	1.161
Hser-Oglu222	1.518	0.078	1.507
Otyr-Htyr	1.021	0.030	1.015
Owat-Hwat	1.016	0.022	1.012
Oser205-Hser205	1.029	0.030	1.025

These evidences extracted from the ground state simulation suggest a crucial role of the protein matrix in modulating the conformation of the atoms in the network belonging or not to the protein skeleton.

In Table 2.1 are shown the main parameters for the pair distances distributions obtained from the S_0 AIMD trajectory. The average values, standard deviations and maximum values of the distributions are shown for the inter-molecular pair distances (Otyr-Owat, Owat-Oser205, Oser205-Oglu222, Htyr-Owat, Hwat-Oser205, Hser-Oglu222) and the intra-molecular ones (Otyr-Htyr, Owat-Hwat, Oser205-Hser205).

Other structural parameters involving the chromophore, the hydrogen bond network and *spectator* residues were considered. These ones help to understand and clarify the role of the protein environment on photo-reactivity. Hence the chromophore N-C-C-C dihedral angle, the dihedral angle involving the oxyen atoms belonging to the hydrogen bond network (Otyr-Owat-Oser205-Oglu222), and the

Hhis148-Otyr distance distributions relative to the previous mentioned S_0 MD are

shown in Fig. 2.2 and Fig. 2.3.
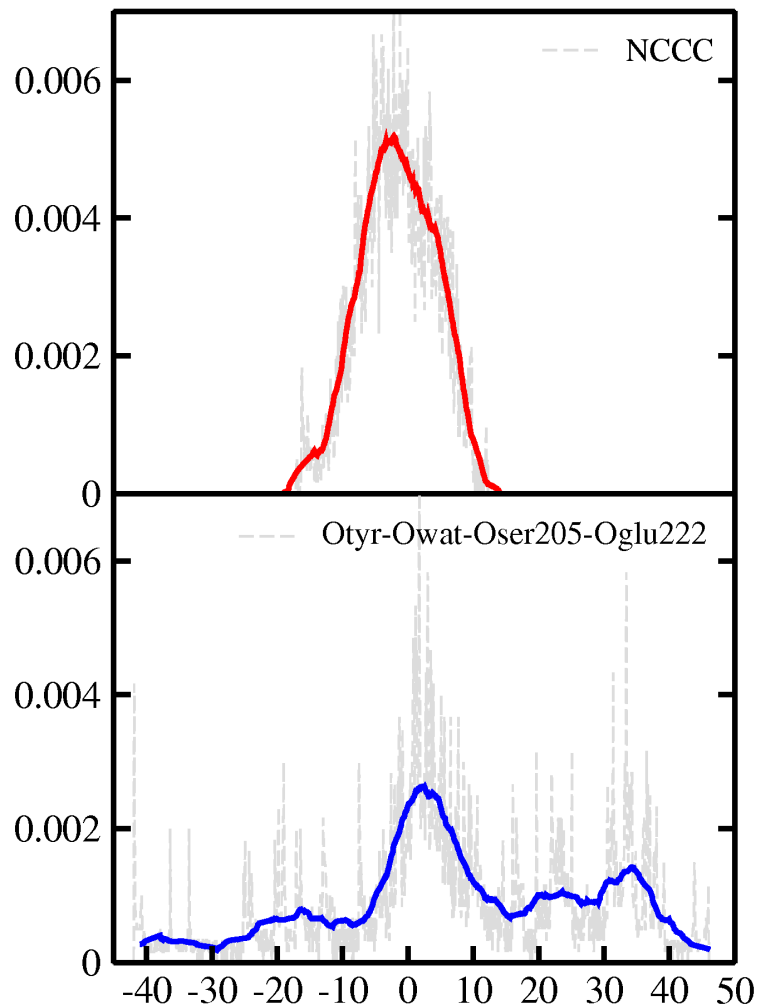
Fig. 2.2: Normalized distributions of dihedral (degree) angles obtained from S_0 AIMD simulation at B3LYP/6-31+g(d,p) level of theory. The chromophore N-C-C-C dihedral angle (upper left) and the dihedral angle of oxygen atoms involved in the hydrogen bond network Otyr-Owat-Oser205-Oglu222 (lower left) are shown, respectively. The relative average values, made every 50 points (and every 100 for the oxigens dihedral angle), are shown by different colored curves.

The chromophore dihedral angle shows a very tight distribution centered around

-2 degrees, suggesting that the chromophore prefers a planar conformation in its
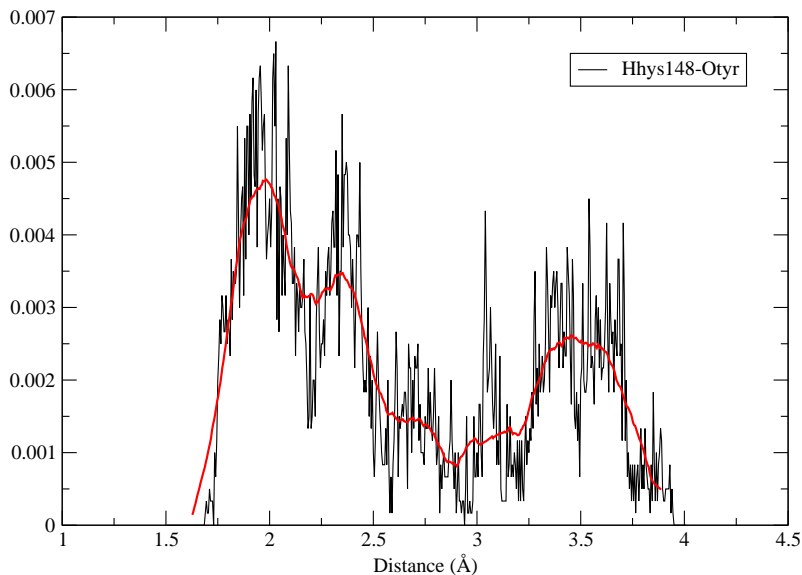
Fig. 2.3: Normalized distributions of His148(H)-Tyr(O) (Å) obtained from S_0 AIMD simulation at B3LYP/6-31+g(d,p) level of theory. The relative average values, made every 50 points, are shown by different colored curves.

ground state. This fact is really interesting because, as will be discussed later, a completely different scenario is found during the excited electronic state dynamics. Concerning the oxygens dihedral angle a spread distribution is observed with values almost focused around 2.5 degrees, even if other populated regions appear between -20 and -10 and 20 and 40 degrees. This evidence indicates a not regular or retained relative orientation of the hydrogen bond pocket, and of course a major ensamble of values is explored also thanks to the presence of the water molecule. On the other side, the main peak is observed at 2.2 degrees, suggesting that a planar orientation is on average favored for the multiple hydrogen bond interactions. A key residue, although not directly involved in the PT network is His148. The distribution between hydrogen atom linked to N_δ and tyrosine oxygen explores three populated regions:

Table 2.2: Average values, standard deviation and maximum values for the normalized distributions of the chromophore dihedral angle N-C-C-C, the inter-molecular oxygens dihedral angle Otyr-Owat-Oser205-Oglu222 (degrees), and for the Hhys-Otyr pair distance (Å) obtained from S_0 AIMD simulation at B3LYP/6-31+g(d,p) level of theory.

	degrees/Å	St.dev.	Max.val.
N-C-C-C	-1.55	5.76	
Otyr-Owat-Oser205-Oglu222	5.42	3.59	2.22
Hhys148-Otyr	2.62	0.65	1.99

around 1.995, 2.358 and 3.476 Å. Among these, the first one is the most important, suggesting that the interaction with the chromophore is quantitatively present during the simulation. However the not negligible presence of other populated regions at higher distance values suggests that the interaction is not constant during the dynamics, while we will see how it becomes crucial in the excited state dynamics.

The main parameters for the chromophore N-C-C-C dihedral angle, the inter-molecular Otyr-Owat-Oser205-Oglu222 dihedral angle and the Hhys-Otyr pair distance are shown in Table 2.2.

2.1.2 Excited State *Ab-Initio* Molecular Dynamics

The exploration of the ESPT was perfomed by employing excited state ab-initio dynamics in the Born-Oppenheimer approximation. In this way we tried to simulate the reaction event (always retaining the protein matrix) and give a molecular insight on the mechanism and on the main events promoting it. Because of the huge computational cost we could not perform a kinetics study, indeed we could not collect a satisfactory number of simulations to discuss the kinetics. On the other

side, we were able to discuss the reaction mechanism and structural rearrangements preliminar to the ESPT.

We proceeded by extracting random structures along with their velocities from the S_0 AIMD dynamics and started from these ones to run excited state dynamics. These structures can be thought as representative of the Franck Condon region of the PES in the ground state. Not all the analysed trajectories will be discussed because in some cases they lost the bright state after a small number of steps and so it was not possible to perform a meaningful trajectory analysis. However, we discuss three excited state dynamics.

In Figs. 2.4-2.9 all the main structural parameters extracted from the simulations are collected. The inter-molecular oxygen distances of the residues involved in the hydrogen bond network (Otyr-Owat, Owat-Oser205, Oser205-Oglu222), the inter-molecular hydrogen-oxygen distances (Htyr-Owat, Hwat-Oser205, Hser205-Oglu222), and the intra-molecular ones (O-Htyr, O-Hwat, O-Hser205). The chromophore dihedral angle N-C-C-C, the inter-molecular oxygens dihedral angle (Otyr-Owat-Oser205-Oglu222), the inter-molecular Hhis148-Otyr, are also shown.

By an ispection of 2.4 and 2.6, belonging to TrjI and TrjII, respectively, it is evident that the ESPT takes place. In particular around 350 fs in the first case, while it happens around 380 fs in the second case. This fact is clearly suggested by the sudden change of both intra and inter-molecular distance values, indeed an elongation of the intra-molecular hydrogen-oxygen distances until reaching values
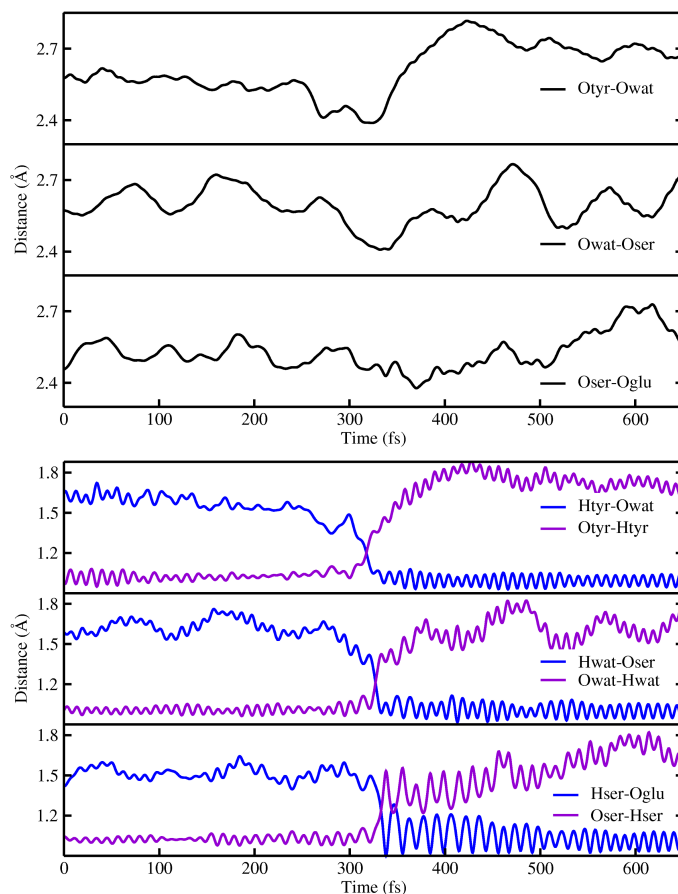
Fig. 2.4: Network distances (Å) evolution involved in the PT network obtained from TD-CAM-B3LYP/6-31+g(d,p) TrjI S_1 AIMD. Input coordinates and velocities randomly extracted from the CAM-B3LYP/6-31+g(d,p) S_0 AIMD. a)Oxygen-Oxygen distances:Otyr-Owat (top), Owat-Oser205 (middle), Oser-Oglu(bottom). b)Proton-Acceptor units distances: Htyr-Owat (top), Hwat-Oser205 (middle), Hser-Oglu (bottom). c)Proton-Donor units distances: Otyr-Htyr (top), Owat-Hwat (middle), Oser205-Hser205 (bottom).

typical of non-bonded atoms takes place. In the third trajectory (TrjIII) instead, the ESPT reaction is observed around 980 fs. Beyond the uncorrelated origin of the starting configurations, common behaviors of the analysed structural parameters can be clearly observed, suggesting that opportune rearrangements must be reached before the proton transfer beginning.

In all the cases a common concerted mechanism for the ESPT, although asyn-
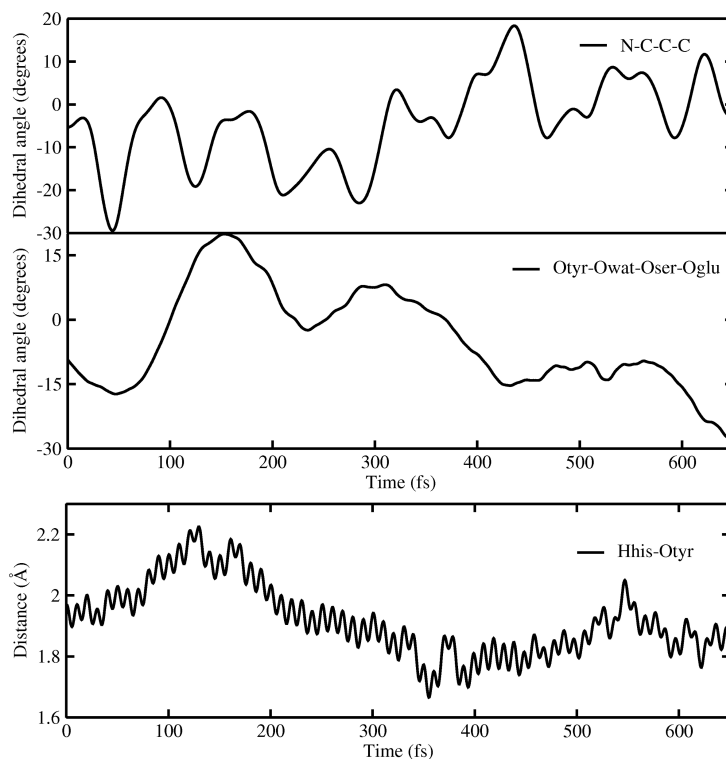
Fig. 2.5: Distances (Å) and dihedral (degree) angles dynamics, obtained from TD-CAM-B3LYP/6-31+g(d,p) TrjI S_1 AIMD. Input coordinates and velocities randomly extracted from the CAM-B3LYP/6-31+g(d,p) S_0 AIMD. Upper panels: the chromophore N-C-C-C dihedral angle (top) and the dihedral angle of oxygen atoms involved in the hydrogen bond network Otyr-Owat-Oser205-Oglu222 dynamics (bottom). Lower panel: the histidine148 Proton-OTyr pair distance dynamics.

chronous, is observed as is clearly seen by an ispection of the intra-molecular bonds break that happens at the same time. So no intermediate species are formed during the reaction. The oscillation ranges for the pair distances involving the water molecule generally explore a wider range of values, and this can be attributed to its major mobility compared to the residues bonded to the protein skeleton, indeed in the last pair (Ser205-Glu222), the inter-molecular distance oscillations are confined in a shorter range of values and are also characterized by a less oscillatory behav-
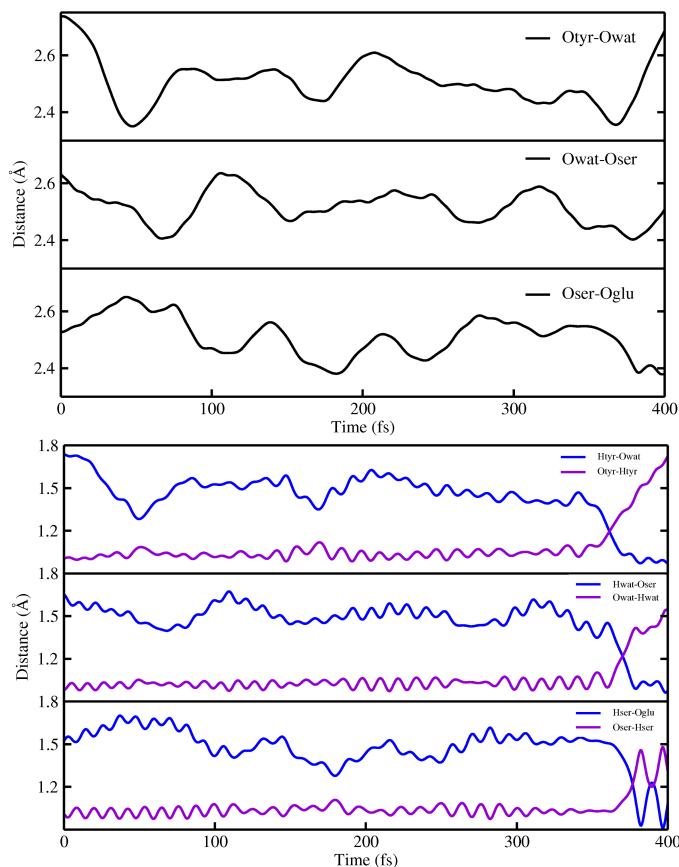
Fig. 2.6: Network distances (Å) evolution involved in the PT network obtained from TD-CAM-B3LYP/6-31+g(d,p) TrjII S_1 AIMD. Input coordinates and velocities randomly extracted from the CAM-B3LYP/6-31+g(d,p) S_0 AIMD. a)Oxygen-Oxygen distances:Otyr-Owat (top), Owat-Oser205 (middle), Oser-Oglu(bottom). b)Proton-Acceptor units distances: Htyr-Owat (top), Hwat-Oser205 (middle), Hser-Oglu (bottom). c)Proton-Donor units distances: Otyr-Htyr (top), Owat-Hwat (middle), Oser205-Hser205 (bottom).

ior. In all the trajectories no back proton transfer is observed, on the contrary it is evident that the new formed bond distance are so stable and do not suggest the possibility of a new break. In all the cases the hydrogen bond network is stiff because it is representative of configurations near the PES minimum, but this strong hydrogen bond nature characterizing the network is not enough to allow the ESPT to start (as we will also see in next discussions).
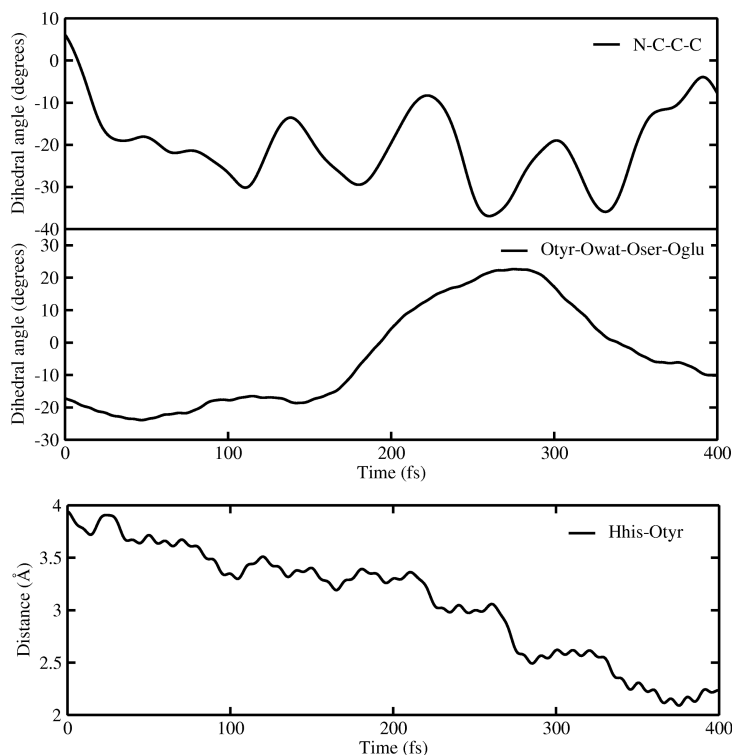
Fig. 2.7: Distances (Å) and dihedral (degree) angles dynamics, obtained from TD-CAM-B3LYP/6-31+g(d,p) TrjII S_1 AIMD. Input coordinates and velocities randomly extracted from the CAM-B3LYP/6-31+g(d,p) S_0 AIMD. Upper panels: the chromophore N-C-C-C dihedral angle (top) and the dihedral angle of oxygen atoms involved in the hydrogen bond network Otyr-Owat-Oser205-Oglu222 dynamics (bottom). Lower panel: the histidine148 Proton-OTyr pair distance dynamics.

It is very intersting the behavior of the chromophore N-C-C-C dihedral angle, indeed in all the trajectories it reaches values very far from planarity, and oscillates in a very irregular way. It explores values until -40 degrees, so causing an imporant out-of-plain of the two chromophore rings. This always verified distorsion seems to play a not trivial role in the understanding of the excited state events, indeed it is possible that this relative out-of-plain of the two rings promotes a better arrangement of the chromophore relative to the hydrogen bond network, and so facilitates
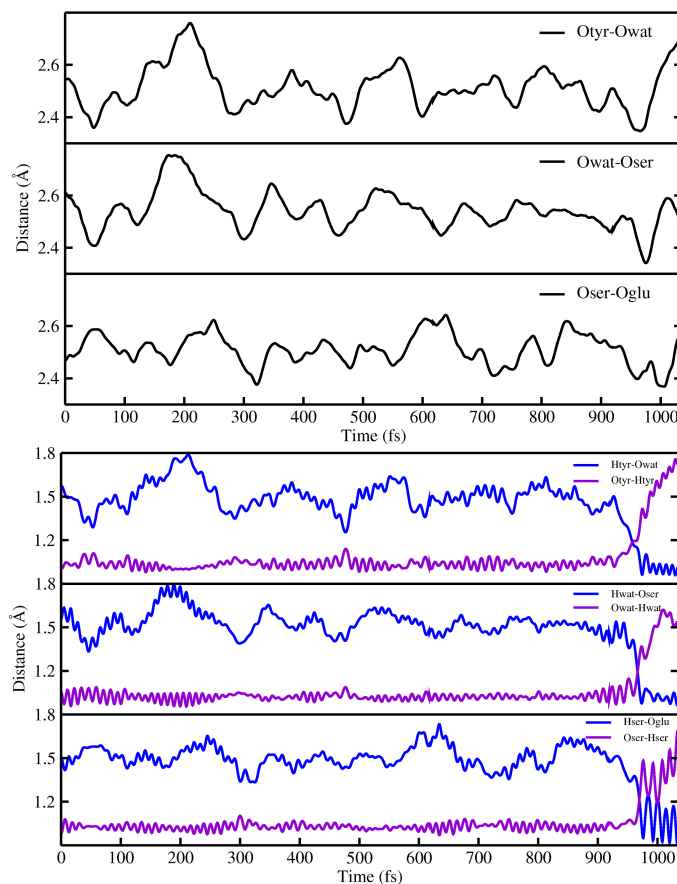
Fig. 2.8: Network distances (Å) evolution involved in the PT network obtained from TD-CAM-B3LYP/6-31+g(d,p) TrjIII S_1 AIMD. Input coordinates and velocities randomly extracted from the B3LYP/6-31+g(d,p) S_0 AIMD. a)Oxygen-Oxygen distances:Otyr-Owat (top), Owat-Oser205 (middle), Oser-Oglu(bottom). b)Proton-Acceptor units distances: Htyr-Owat (top), Hwat-Oser205 (middle), Hser-Oglu (bottom). c)Proton-Donor units distances: Otyr-Htyr (top), Owat-Hwat (middle), Oser205-Hser205 (bottom).

the ESPT. This fact is also suggested by the fact that this N-C-C-C behavior takes place before the reaction event, while it is evident that immediately before the proton transfer it returns to values more close to the planarity. This is particularly evident in TrjI: in this case the dihedral angle approaches to the planarity before the ESPT and, more interestingly, it retains this range of values after the formation of the anionic form. These results indicate an important fact: after the excitation
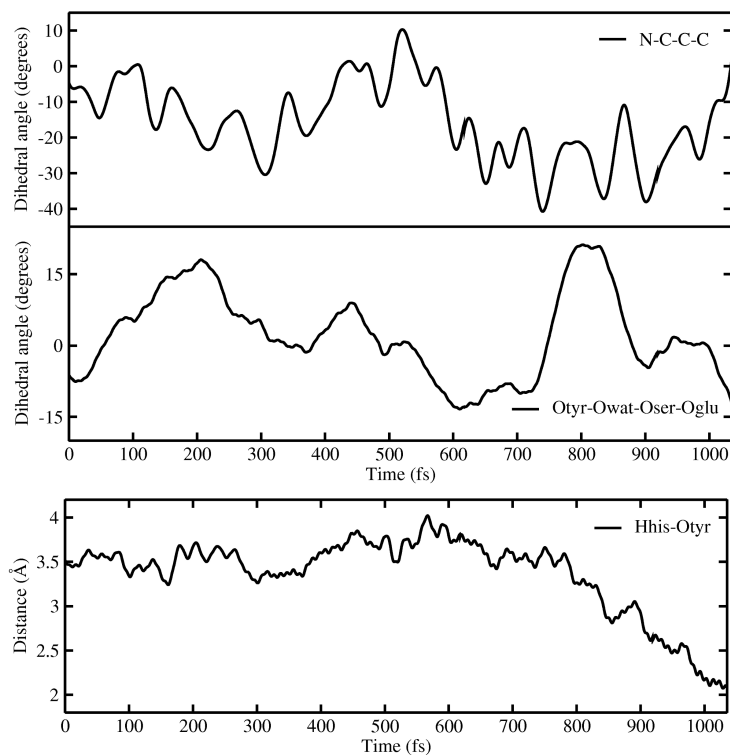
Fig. 2.9: Distances (Å) and dihedral (degree) angles dynamics, obtained from TD-CAM-B3LYP/6-31+g(d,p) TrjIII S_1 AIMD. Input coordinates and velocities randomly extracted from the B3LYP/6-31+g(d,p) S_0 AIMD. Upper panels: the chromophore N-C-C-C dihedral angle (top) and the dihedral angle of oxygen atoms involved in the hydrogen bond network Otyr-Owat-Oser205-Oglu222 dynamics (bottom). Lower panel: the histidine148 Proton-OTyr pair distance dynamics.

the chromophore rings are allowed to assume out-of-plain conformations and such conformation is preparatory to the ESPT because promotes the reaction by allowing a better reorganization of the hydrogen bond network. This conformation is not retained during the reaction and also after the formation of the product, confirming that it is just a preliminar crucial step. This innovative result is a first step to the understanding of the fact that the complex nature of the GFP photo-reactivity cannot be only reduced to photo-acidity, instead it is a very complicated event composed,

as we will discuss also in next sections, of many different promoting conditions. By a comparison of these trends with the ground state ones, it is evident how in the last case the coplanar chromophore rings conformation is favored, while after the excitation the electronic density reorganization causes a structural rearrangement of the chromophore that finally reaches a major conformational freedom.

By an ispection of the inter-molecular oxygens dihedral angle, values near the planarity are observed immediately before the reaction beginning. We can conclude that a common trend of this dihedral angle (Figs. 2.5, 2.7 and 2.9) can be recognized, showing values around -10 degrees in concurrence of the reaction. The planarity of the hydrogen network oxygens of course favors and enstablishes the optimal conditions for the multiple proton transfer, as confirmed by the fact that the planarity is reached in all the cases during the ESPT.

We also found particularly interesting the behavior of the residue His148. This residue is not directly involved in the reaction and is not part of the hydrogen bond network, instead, it is involved in an hydrogen bond with the chromophore phenolic ring. The role of His148 is recognized to be important in modulating the proton shuttle in the ground state [56], and also in stabilizing the anionic species I and B [58], while it is never been recognized that His148 could be important in the ESPT reaction.

The inter-molecular His148(hydrogen)-Phenolic(oxygen) distance is shown in Figs. 2.5, 2.7 and 2.9. In all the cases it is clear that until the histidine N-H

hydrogen interaction with the phenolic oxygen is not optimized the reaction does not take place. In TrjI since 200 fs the inter-molecular distance starts to decrease, and as it reaches a value around 1.8 Å , the proton transfer is observed. In TrjII, since the beginning there is an increasing approach of the two residues and, as the distance assumes values around 1.8 Å , the ESPT takes place. In TrjIII the His148-Tyr66 oscillates exploring distance values larger than 3.9 Å . After 800 fs this distance starts to decrease until reaching values around 2 Å in concurrence with the reaction event. These results open an important new scenario on the ESPT promoting events: it is evident that the role of His148 is crucial in promoting the proton transfer reaction in the excited state, and this fact is observed here for the first time. In Fig. 2.10 the Hhis148-Otyr hydrogen bond distances from all the excited state trajectories are shown all together.
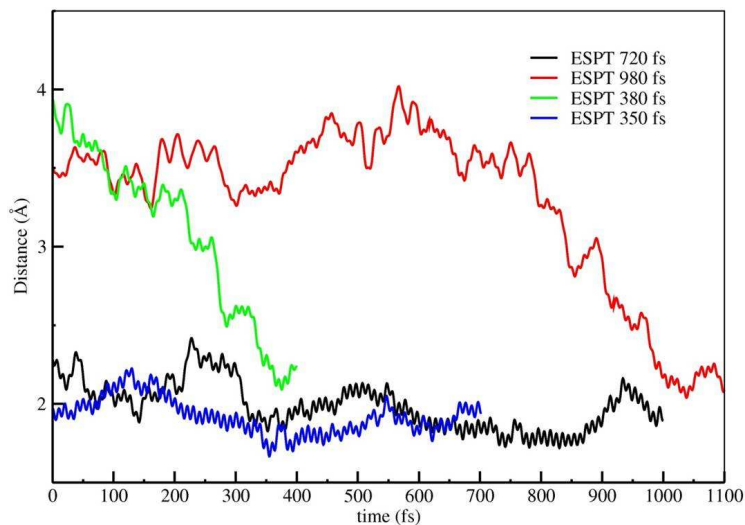
Fig. 2.10: The His148 Proton-OTyr pair distance dynamics (Å) obtained from TD-CAM-B3LYP/6-31+g(d,p) S_1 AIMDs. Input coordinates and velocities randomly extracted from the B3LYP/6-31+g(d,p) S_0 AIMD or from the optimized GFP structure.

Through this graphics it can be better appreciated how much is important the approach of this residue to the chromophore phenolic ring. Indeed the ESPT takes place always when the hydrogen bond distance is not longer than 2 Å. This condition suggests that it is not enough the chromophore distorsion through the N-C-C-C dihedral angle and an ad hoc arrangement of the residues directly taking part to the reaction, but also other favorable conditions are necessary to reach the best organization before the reaction event. In conclusion, it is the right combination of many factors to optimize the probability of the multiple proton transfer in the excited state. For example, in TrjI (Fig. 2.5), the N-C-C-C dihedral angle immediately deviates from values compatible with rings coplanarity, so allowing a better hydrogen bond network arrangement. On the other side, the phenolic ring interaction with His148 is not optimized, indeed the hydrogen bond assumes values longer than 2 Å. It is only when this interaction is stabilized that the reaction takes place. This evidence clearly demonstrates that these two quantities are cofactors and cannot be enough by themself. In TrjIII (Fig. 2.9) we observed a similar situation: although for the major part of the trajectory the two rings are not coplanar, until the His148 residue is far from the phenolic ring, the reaction does not take place. During the simulation there is a progressive approach of His148 to the chromophore, and only when the hydrogen bond is stronger (inter-molecular O-H distances around 2 Å), the reaction happens.

These evidences are of crucial importance because introduce another point of

view in the study of the GFP photo-reactivity, and in general in the right approach to the investigation of such complex phenomena. It is often not enough to take into account the *actors* of a chemical event, but all the environment and those elements that could indirectly take part to the reaction, as in the case of His148. So these kind of events cannot be reduced, for example, to a simple chromophore photo-acidity to explain the driving force of the reaction, but a more complex description based on a considerable number of cofactors has to be performed.

2.1.3 Ground vs. Excited Electronic State Structural Analysis

A direct comparison of the temporal evolution in the S_0 and S_1 electronic states of many structural parameters is discussed in this Paragraph. The starting configuation and velocities for both the simulations are chosen according the procedure described in the Computational Details Section. Interesting differences and rearrangements of the structural parameters are observed in the two trajectories, causing the proton transfer in the excited state with a concerted and almost synchronous mechanism as already discussed in the Previous Paragraph. We firstly analysed the S_1 MD results making a comparison with the first ps of the ground state simulation in order to appreciate the differences enforced by the change of the electronic state. We recall that the same initial coordinates and momenta characterize the two simulations.

In Fig. 2.11 the pair distances temporal evolution of all the atoms involved in the hydrogen bond network in the excited state simulation (red lines) in com-

parison with the ones from the first ps ground state trajectory (black lines) are presented. The inter-molecular oxygen pair distances (top: Otyr-Owat, Owat-Oser205, Oser205-Oglu222), inter-molecular hydrogen-oxygen (middle: Htyr-Owat, Hwat-Oser205, Hser205-Oglu222), intra-molecular hydrogen-oxygen (bottom: Otyr-Htyr, Owat-Hwat, Oser205-Hser205) are shown.

As first evident result it can be recognized that in the excited state simulation the proton transfer is observed around 720 fs. Although we are referring to the fastest process (3 ps, the conversion to the unrelaxed anionic form (I*)), the proton transfer rate is overstimated in our simulation. The two main reasons for this behavior are: a) density functional theory generally behaves understimating energy barriers, b) because of our protein modeling, our MD input structures are near the neutral (reactant) minimum where the hydrogen bond network involved in the PT reaction organization is more prepared to react. In spite of this peculiar observed time, we are still able to clearly observe a different structural dynamics in both the electronic states and so to investigate the PT mechanism and the role of the protein matrix on it.

Starting from the intra-molecular hydrogen-oxygen pair distance dynamics, it can be appreciated that in the excited state their oscillations nature is wider compared to the ground state ones, suggesting more unstable bonds. This fact is also supported by the inspection of inter-molecular hydrogen-oxygen pair distances dynamics in which a broad nature of oscillations is observed in all three cases also this time, and is
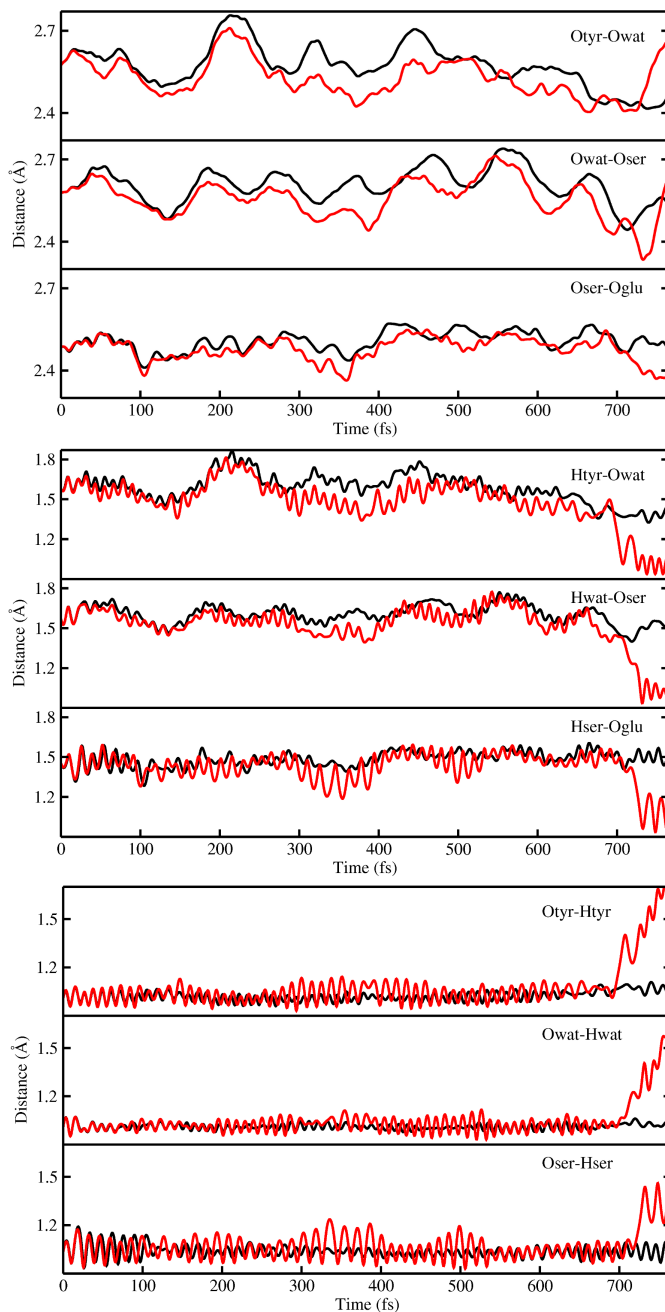
Fig. 2.11: Comparison of network distances (Å) evolution involved in the PT network obtained from B3LYP/6-31+g(d,p) S_0 AIMD (black) and TD-CAM-B3LYP/6-31+g(d,p) TrjIV S_1 AIMD (red). Top: Oxygen-Oxygen distances:Otyr-Owat (top), Owat-Oser205 (middle), Oser-Oglu(bottom). Middle: Proton-Acceptor units distances: Htyr-Owat (top), Hwat-Oser205 (middle), Hser-Oglu (bottom). Bottom: Proton-Donor units distances: Otyr-Htyr (top), Owat-Hwat (middle), Oser205-Hser205 (bottom).

especially evident for the Hser205-Oglu222 distance. By the inspection of the inter-molecular oxygen-oxygen distance dynamics a clear shrunk network characterizes the excited state. The excited state inter-molecular oscillations are confined to shorter values compared to the ground state ones during the whole trajectory, and this trend is observed in all the cases. This behavior is particularly evident in the pair distances involving the water molecule atoms (Otyr-Owat, Owat-Oser205), suggesting that the chromophore excitation is able to have an echo on the less rigid and tight part of the network. Regarding the Oser205-Oglu222 pair dynamics, in some parts of the trajectory the two oxygen atoms approach to closer distances (under 2.4 Å), in particular around 100 and 350 fs. These results suggest that forces between the inter-molecular oxygen pairs are different in the two electronic states, and this fact has an echo on the relative trends. So, the presence of shorter hydrogen bond network inter-molecular distances in the excited state suggests that the system can be more suitable for the ESPT reaction. These evidences again go in the direction of a complex picture of the reaction event because suggest that a structural rearrangement is taking place after the excitation and that it has a crucial role in determining the optimal conditions for the reaction.

From such analysis an insight on the ESPT mechanism can be also performed: the three protons move simultaneously without a partial formation of the product, and no back reaction takes place. It is also interesting to observe that immediately after the proton transfer the residues distances become again longer as can be

seen from the inter-molecular oxygens, suggesting that the tight network was just preparatory to the reaction.

The comparison of other structural parameters involving both the chromophore and the hydorgen bond network is performed. This further analysis supports our thesis that the electronic transition can affect the structural quantities, thus allowing the gain of the best conditions for the proton transfer. Hence the chromophore N-C-C-C dihedral angle, the dihedral angle involving the oxyen atoms in the hydrogen bond network (Otyr-Owat-Oser205-Oglu222), the Hhis148-Otyr distance dynamics for both the S_0 (black lines) and S_1 (red lines) MD are shown in Fig. 2.12.

Regarding the chromophore N-C-C-C dihedral angle a wider range of values is explored along the S_1 MD, it reaches values around -25 degrees while in the ground state it retains, on average, values centered around 0 degrees for the whole trajectory. This fact (already analysed in the Previous Paragraph), is clearly shown by this direct comparison, and is one of the clearest indications of how the excitation has important consequences on the nuclear dynamics. The two trajectories also differ in the oscillations nature that appears broader and less regular in the excited state. As already observed in the other excited state trajectories, also in this one the N-C-C-C dihedral angle returns to values representative of a rings coplanar conformation during the ESPT, that are more appropriate to the reaction event. So once the hydrogen bond network is optimized to favor the proton transfer through the chromophore rings out-of-plain allowed by the N-C-C-C dihedral angle opening,
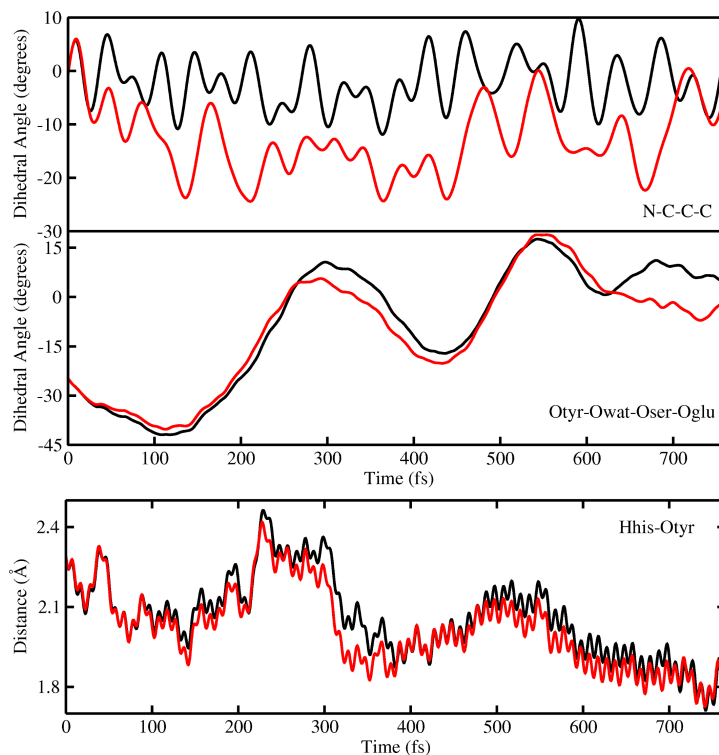
Fig. 2.12: Comparison of distances (Å) and dihedral (degree) angles dynamics, obtained from B3LYP/6-31+g(d,p) S_0 AIMD (black) simulation and TD-CAM-B3LYP/6-31+g(d,p) TrjIV S_1 AIMD (red). The chromophore N-C-C-C dihedral angle (top) and the dihedral angle of oxygen atoms involved in the hydrogen bond network Otyr-Owat-Oser205-Oglu222 dynamics (middle) are shown, respectively. The histidine148 Proton-OTyr pair distance dynamics is also shown (bottom).

this one returns to shorter values to permit the multiple proton transfer.

Hereafter in Fig. 2.12 (middle panel) we analyse the dihedral angle involving the oxygens of the hydrogen bond network (Otyr-Owat-Oser205-Oglu222). The trend is similar in both dynamics exploring values between -40 and 20 degrees. Discrepancies respect to the S_0 MD are observed since around 600 fs, indeed in the excited state values close to the planarity are retained until the ESPT event. This different behavior in the two electronic states suggests that a coplanar orientation of the

oxygens belonging to the residues involved in the reaction favors a better multiple proton transfer. This is a further proof supporting the hypothesis that the different electronic states can have an echo on the proton network modulated by the protein matrix. On the other side, as already underlined in the other three excited state trajectories, no general trends can be recognized for this dihedral angle, but just a common behavior during the reaction event.

In Fig. 2.12 the comparison of the distance between the histidine hydrogen atom linked to N_δ and chromkophore phenolic oxygen is shown. It cannot be recognized a different temporal evolution of this quantity in the two electronic states, although some differences can be underlined. In both cases the strength of the interaction is not costant during the time, alternating periods of stronger interaction (around 150 fs and 350 fs) to regions in which it is weaker (until 500 fs) while an increasing approach of His148 to the chromophore takes place and is retained until the end of the trajectories. However it can be recognized that since around 150 fs to 400 fs and since 500 fs until the end of the dynamics, the excited state oscillations explore shorter ranges of values, suggesting that although the temporal evolution is very similar, a difference in the interaction strength can be recognized. It is not possible to clarify the indirect role of histidine in the ESPT only on the basis of this analysis, but thanks to the support of the other trajectories, we can confirm that histidine148 promotes the formation and stabilises the just formed anion.

The results described in this Paragraph are of key importance in unveiling the

nuclear differences that take place after the excitation. By this direct comparison, the nuclear differences obtained after the excitation can be directly recognized and analysed. These differences are the direct proof of the effect that the electronic excitation has on nuclear dynamics. In this way it is so clear that the protein environment has a not trivial role in modulating the proton tranfer event.

2.2 Time-Resolved Frequency Analysis of GFP *Ab-Initio* Dynamics

For the first time the Continuous Wavelet Analysis is employed to investigate the photo-reactivity of a molecule. The analysis protocol is deeply discussed in the Methods Chapter, while in this one all the main results extracted from this analysis are discussed. The Wavelet Analysis was employed to extract the frequency-domain based information from the temporal evolution of several ad-hoc chosen structural parameters in order to disentangle the photo-reactivity in terms of the main activated motions ruling the ESPT. Thanks to the temporal information, intrinsic of such procedure, the couplings and the shifts among vibrational bands could be disentangled. Moreover the appearance and disappearance of vibrational bands during the time could also be catched. The potentiality of this protocol is absolutely underlined because a clear molecular picture of the event could be obtained in this way, and an understanding of the complex dynamics of the reaction was achieved. The complexity of the motions activated before and during the proton transfer describes a scenario that does not simply involve the groups of atoms taking part in

the reaction, but includes several motions of the whole hydrogen bond network. For the first time it is recognized that the collective and low frequency motions have a key role in driving the reaction instead of localized and high frequency ones such as, for example, intra-molecular O-H stretchings that are of course active during the reaction event, but do not represent the real promoting motions.

In this Chapter the Wavelet spectra of both structural quantities directly involved in the reaction (intra and inter-molecular O-H bonds), and parameters indirectly involved in the reaction are discussed.

2.2.1 The Excited State Proton Shuttle

We obtained and analysed all the pair distances involved in the proton wire, in terms of Wavelet power spectra, in order to investigate the frequencies temporal evolution affecting each signal.

In Fig. 2.13 we show the Wavelet power spectra of the intra-molecular (Otyr-Htyr, Owat-Hwat, Oser205-Hser205) and inter-molecular (Htyr-Owat,Hwat-Oser205, Hser205-Oglu222) hydrogen-oxygen network pair distances temporal evolution in both the ground and excited states (the ones discussed in the previous Paragraph).

From the inspection of the 2D Wavelet maps (S_0 and S_1) of the intra-molecular pair distances, spectra mainly composed by frequency bands around 3000 cm^{-1} are found. We simply associated these ones to the stretching modes of the intra-molecular O-H groups. Many differences between the ground and excited states could be recognized. First of all, a clear red shift of such bands in the excited state
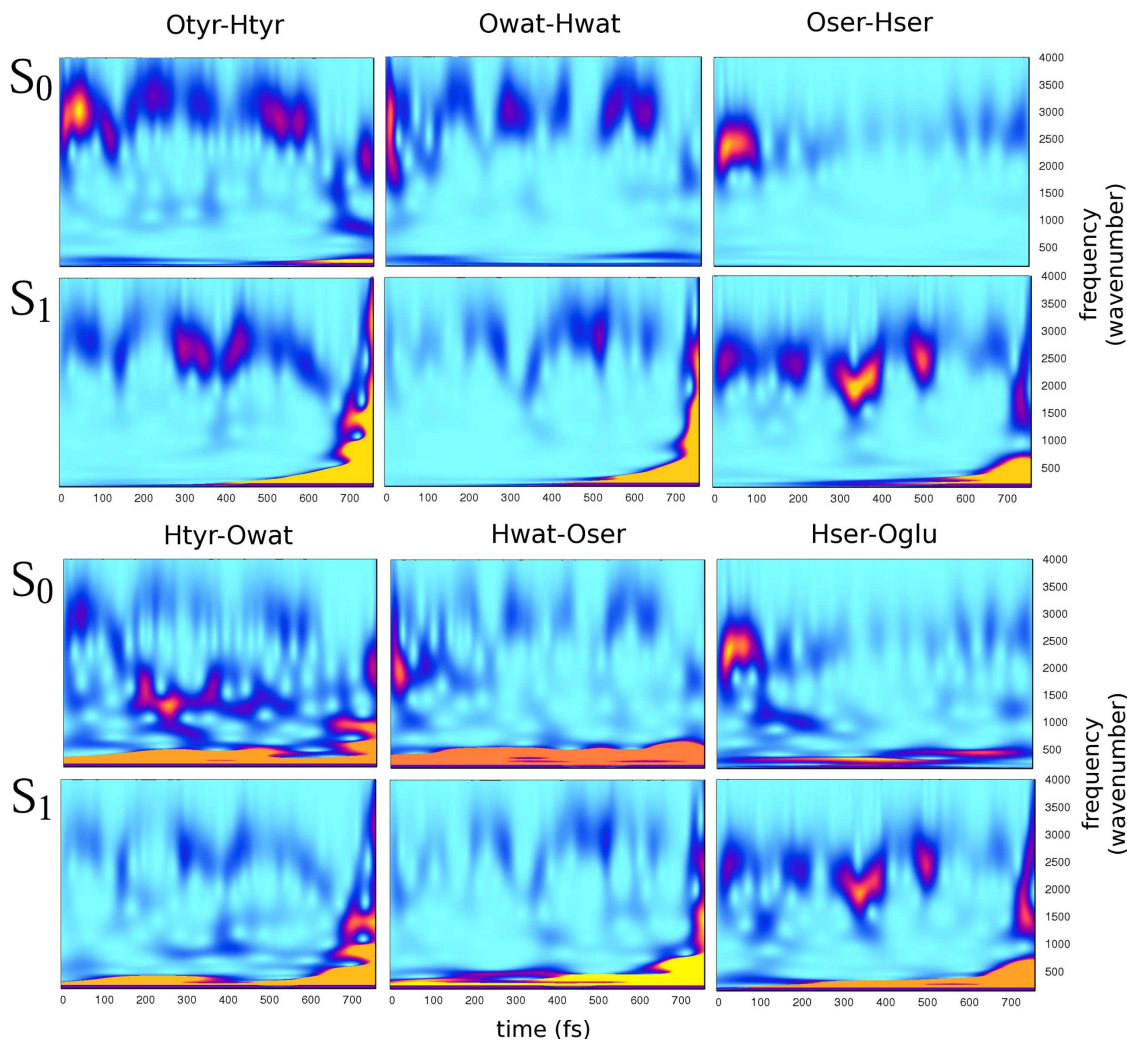
Fig. 2.13: 2D Wavelet maps of structural parameters extracted from TrjIV. Top panels: donors (O-Htyr, O-Hwat, O-Hser205). Bottom panels: acceptors (Htyr66-Owat, Hwat-Oser205, Hser205-Oglu222). The spectra are calculated for both the ground and excited states.

spectra is observed and this fact strongly supports the hypothesis of a weaker nature of the intra-molecular O-H bonds after the excitation, as found from the wider oscillations temporal evolution of O-H distances in the excited state trajectories. Moreover we found that this result is in excellent agreement with the frequency values obtained by the anharmonic analysis of the model (discussed later), where

stretching frequency values of 3329.55, 3098.99, 2533.24 cm^{-1} in S$_0$ and 3108.10, 2859.14, 2056.07 cm^{-1} in S$_1$ were found for Otyr-Htyr, Owat-Hwat and Oser205-Hser205, respectively. The energetic trend among the modes in which Otyr-Htyr is one appearing at higher frequencies, followed by by Owat-Hwat and Oser-Hser is also in excellent agreement with the static Hessian based analysis: this behavior is found also in the Wavelet Analysis. Another important difference is that a different temporal evolution characterizes such bands in the two electronic states. A more oscillatory behavior of the O-H vibrational bands in the excited state is observed during the time, compared to the ground state, and this is particularly evident in proximity of the proton transfer event. In fact in the excited state the first spectrum (Otyr-Htyr) shows a clear red shift after 500 fs that increases until the proton transfer event.

Concerning the inter-molecular hydrogen-oxygen 2D Wavelet maps, we can again find the bands associated to the intra-molecular O-H stretching modes, although these are less intense compared with the ones analysed before. Both the Otyr-Htyr and Htyr-Owat spectra in the excited state show frequency contributions around 1000 and 1500 cm^{-1}, attributed to a coupled Otyr-Htyr bending with a water libration and to the C-O streching of tyrosine ring, respectively, in agreement with the normal modes analysis. This coupling observed during the PT suggests that the activation of this normal mode is correlated to the reaction. Regarding the Hser205-Oglu222 pair, a band around 1500 cm^{-1} is clearly observed and is attributed to the

C-O asymmetric stretching mode of glutammic acid (in agreement with the normal modes analysis), and the same one, although less intense, is also present in the Oser205-Hser205. The strong activation of this band in the excited state highlights its active partecipation to the PT event, and this fact is not observed when the reaction does not take place in the ground state. In the Owat-Hwat and Hwat-Oser cases the region below 1000 cm^{-1} becomes deeply populated after the PT reaction. This area is correlated to collective motions of chromophore, network and water libration, according to the normal modes analysis discussed later. Also in this case a different temporal evolution of the bands is found, in agreement with the different dynamics characterizing the two electronic states.

A crucial difference between the vibrational bands in the two electronic states is represented by an increase in the population of low frequency vibrational bands in the excited state spectra. More in detail, in the three intra-molecular O-H spectra an important intensity increase of vibrational bands under and around 1000 cm^{-1} is found after 500 fs, and this feature is absent in the ground state. These bands can be easily associated to collective motions involving both the chromophore and the hydrogen bond network. It is an important result because it suggests that before the reaction it is necessary the activation of collective motions that are preparatory for the reaction event. So a collective rearrangement takes place and is well-catched by the Wavelet Analysis. In the ground state inter-molecular O-H spectra, the low frequency motions are activated during the whole trajectory, while in the excited

state it is observed an intensity increase after 500 fs of vibrational bands under $1000\ cm^{-1}$ that is not observed in the ground state. The population of these bands suggests again the activation of collective motions involving the whole proton wire and the chromophore as preparatory to the ESPT, in agreement with a discovered different structural dynamics at the two electronic states. Many parameters such as inter and intra-molecular hydrogen-oxygen pairs, N-C-C-C dihedral angle and inter-molecular oxygens dihedral angle present, indeed, different dynamics in the two electronic states.

In Figs. 2.14 and 2.15, the 2D Wavelet spectra of the intra-molecular O-H pair distances temporal evolution extracted from TrjI and TrjIII are presented.

Also in these cases vibrational bands associated to the intra-molecular O-H stretching modes can be recognized. Moreover, in Fig. 2.14 the events happening after the ESPT can be investigated. In the O-Htyr Wavelet spectrum after 350 fs (when the reaction happens), a vibrational band blue-shifted compared with the one present at the beginning, can be recognized. This band could be assigned to the just formed new intra-molecular O-H bond with the water molecule, moreover the fact that it is blue-shifted compared to the previous one not only suggests that the O-Htyr bond was weak compared to the new one, but also that the new one is stronger and so, indirectly, that a back proton transfer reaction is not favored at all. The same comments can be performed for the O-Hwat Wavelet spectrum: a clear red shift in correspondence of the ESPT is found while a blue shift characterizes the
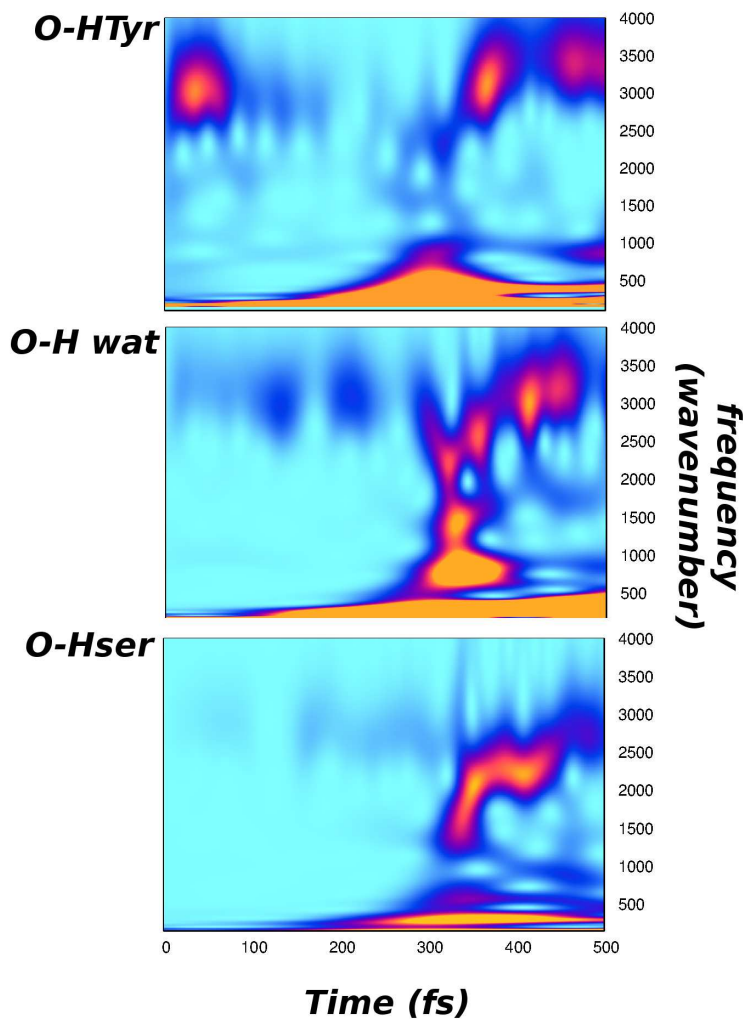
Fig. 2.14: 2D Wavelet maps of O-Htyr, O-Hwat, O-Hser205 pair distance temporal evolution in TrjI.

vibrational band appearing after the ESPT until the end of the trajectory. Also in

this case the vibrational band appearing after 350 fs can be easily attributed to the

just formed new O-H bond involving the water hydrogen and the Ser205 oxygen. In

the O-Hser case the vibrational band of the O-Hser bond stretching cannot be easily

recognized because it is not so intense. However after the reaction a very intense
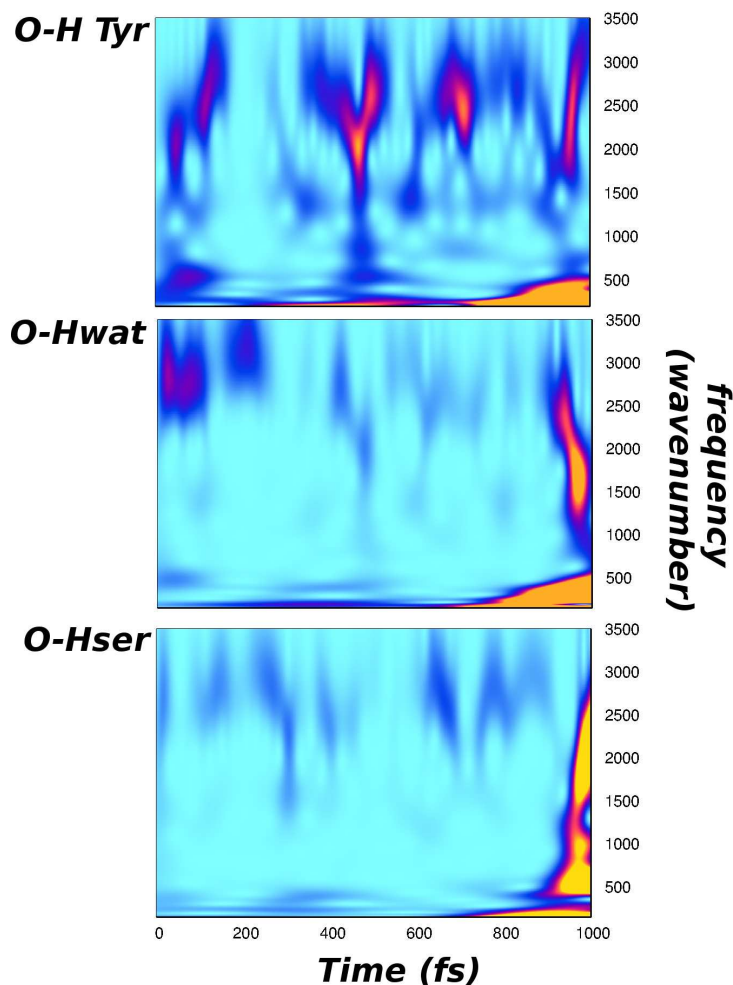
Fig. 2.15: 2D Wavelet maps of O-Htyr, O-Hwat, O-Hser205 pair distance temporal evolution in TrjIII.

band appears, again assigned to the new O-H bond.

In agreement with the previous dynamics, low frequency motions begin more intense suggesting an activation of the whole network during the ESPT. This fact is particularly enhanced in the O-Htyr spectrum, while in the O-Hwat one such modes remain intense also after the formation of the anionic form. In the O-Hwat spectrum vibrational bands around 1000 cm^{-1} and 1500 cm^{-1} are also intense. These ones

were assigned to the coupled O-Htyr bending and water libration (the first) and to the phenolic ring C-O stretching mode (the second). It is very interesting that they are activated substantially just during the period of time in which the ESPT reaction takes place. The vibrational band around 1500 cm^{-1} found in the O-Hser spectrum is related to the Glu222 asymmetric stretching. Also in this case it appears during the ESPT. The Wavelet Analysis allowed an *instantaneous* picture of the molecular event, and the capability to isolate vibrational bands confined both in the frequency and in the time domain is a point of crucial importance because we can recognize the main modes ruling the ESPT.

In Fig. 2.15 the Wavelet spectra of TrjIII O-H intra-molecular distances are shown. The same dynamics of the previous ones is observed, although in this case the intra-molecular vibrational bands are less intense. However the main evidence, that is the low frequency vibrational bands intensity increase, is found also in this case. So we had another confirmation of our hypotheses about the importance of low frequency motions activation before and during the ESPT.

These results represent a novel molecular insight in the GFP ESPT investigation, because it emerges for the first time the fact that the proton transfer is ruled by motions involving the whole network, and that it cannot be simply described by photo-acidity or just reduced to a multiple transfer involving only the O-H quantities through which the proton is transferred.

2.2.2 The Chromophore Rearrangement Dynamics

In agreement with the philosophy of our research, that was focused to build a complete picture of the GFP ESPT, we investigated structural quantities not directly involved in the reaction event, such as the chromophore dihedral angle N-C-C-C and the phenolic C-O and imidazolinone C-N bond distances temporal evolution. The Wavelet power spectrum for the chromophore dihedral angle N-C-C-C is shown in Fig. 2.16 for both the ground and excited states. The 3D Wavelet power spectra show the temporal evolution of the bands and their instantaneous positions clearly. In the ground state the main frequency band appears around 600 cm^{-1}, coupled with minor bands on both lower and higher frequencies.
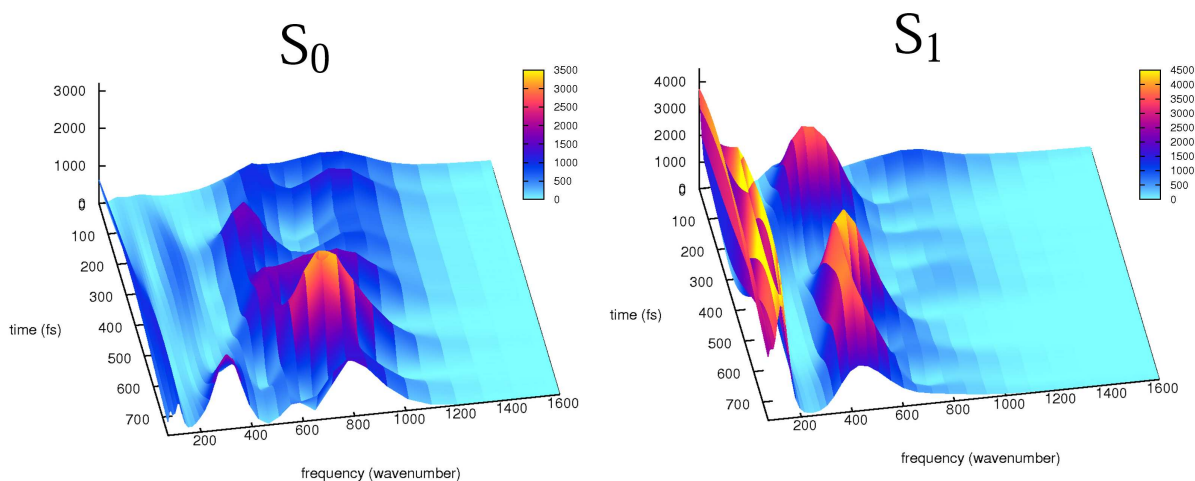
Fig. 2.16: Ground (left) and excited (right) state 3D Wavelet power spectra of N-C-C-C chromophore dihedral angle extracted from TrjIV.

The spectrum appears really different in the excited state, in fact it shows only one main band centered around 450 cm^{-1} without couplings with other bands dur-

ing the time. This absence of couplings is in agreement with the normal modes analysis in which a more coupled nature of the modes is generally observed in the ground state while a more separated nature of the modes is observed in the excited state. The temporal evolution of these frequencies reflects the different dynamics of this parameter in the two electronic states as shown before, so these frequency trends confirm the influence of the photo-excitation on the N-C-C-C dihedral angle dynamics. Its large oscillations allow out-of-plain conformations of the phenolic ring respect to the imidazolinone plane enforcing the interaction of the O-H phenolic group with the water molecule and so the following proton tranfer event. This is in agreement with the hypothesis of Prof. Mathies and co-workers [48] regarding the key role of the phenolic ring wagging motion ($120 \ cm^{-1}$) promoting a stronger interaction with the water molecule. In the normal modes analysis we actually found a normal mode around $100 \ cm^{-1}$ mainly composed by the wagging motion of the phenolic ring. Through the Wavelet transform we could give another important confirmation of the structural differences induced by the excitation and so the different evolution on the respective potential energy surfaces.

This analysis was also performed on other two trajectories, as shown in Figs. 2.17 and 2.18.

The spectrum shown in Fig. 2.17 (TrjI), presents only one vibrational band centered around $400 \ cm^{-1}$, in agreement with the red shift observed in the previous one. Moreover an additional red shift takes place after the ESPT, moving the band
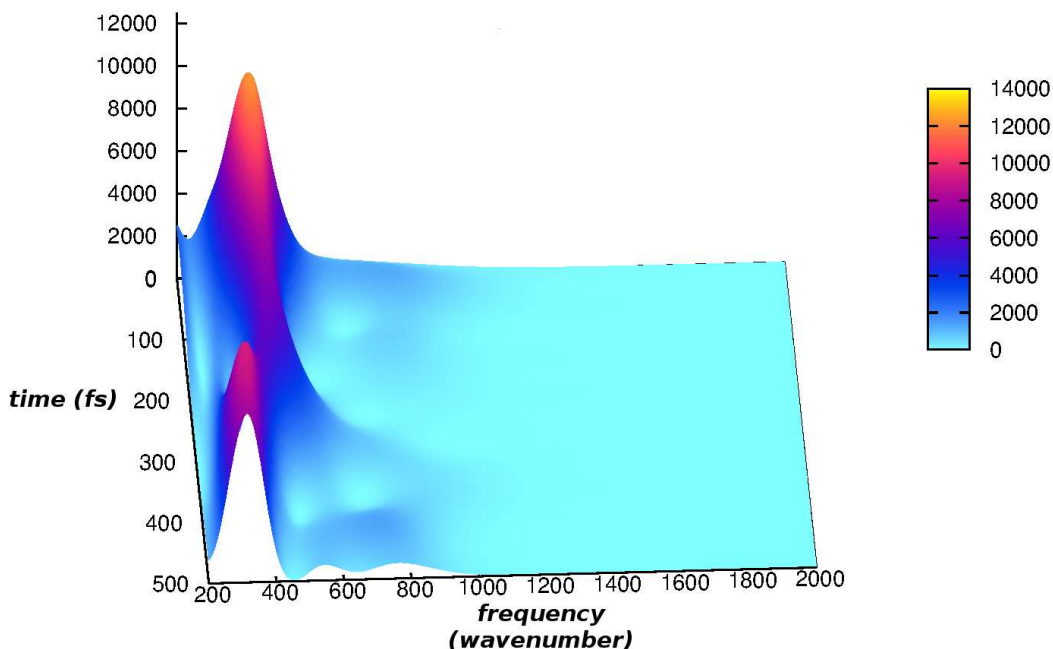
Fig. 2.17: Excited state 3D Wavelet power spectra of N-C-C-C chromophore dihedral angle extracted from TrjI.

around 300 cm^{-1}. The absence of coupling with other bands is again observed in agreement with the Hessian based vibrational analysis.

In Fig. 2.18 the N-C-C-C Wavelet power spectrum of the longer trajectory is presented (TrjIII). Only one main vibrational band can be recognized around 450 cm^{-1}. The convergence of such analyses is an important confirmation and support to our hypotheses concerning the complexity of the GFP photo-reactivity.

The time-resolved power spectra of the phenolic C-O and imidazolinone C-N distances belonging to TrjIV are shown as 2D maps in Fig. 2.19.

The investigation of such two parameters was enforced by the FSRS results of Prof. Mathies and coworkers, indeed they found that after the excitation out-
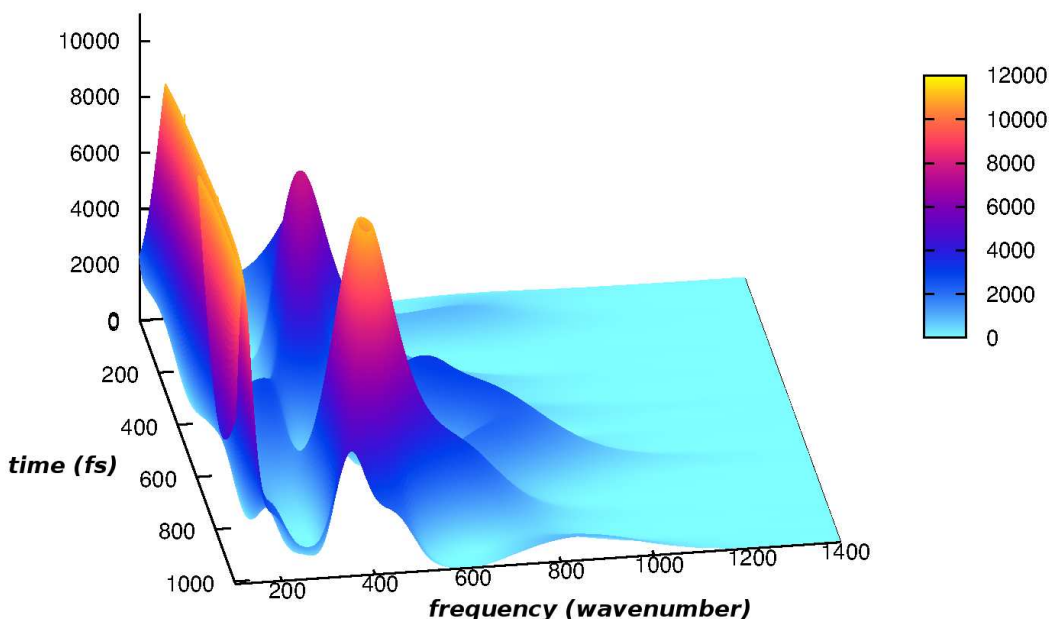
Fig. 2.18: Excited state 3D Wavelet power spectra of N-C-C-C chromophore dihedral angle extracted from TrjIII.

of-phase oscillations characterize such two quantities and also that the oscillation period was around 280 fs, corresponding to a phenolic ring wagging motion whose typical frequency is around 120 cm^{-1}. This motion should be responsible of a better relative orientation of the phenolic ring respect to the water molecule, in order to find the best orientation for the ESPT [48]. In our Wavelet spectra the main bands appear around 1500 and 1550 cm^{-1} and are attributed to the C-O and C-N stretching modes. A clear out-of-phase trend of these bands is observed during the time and it is in excellent agreement with Prof. Mathies results.

This analysis was repeated on other two excited state trajectories (TrjI and TrjIII), as shown in Figs. 2.20 and 2.21.
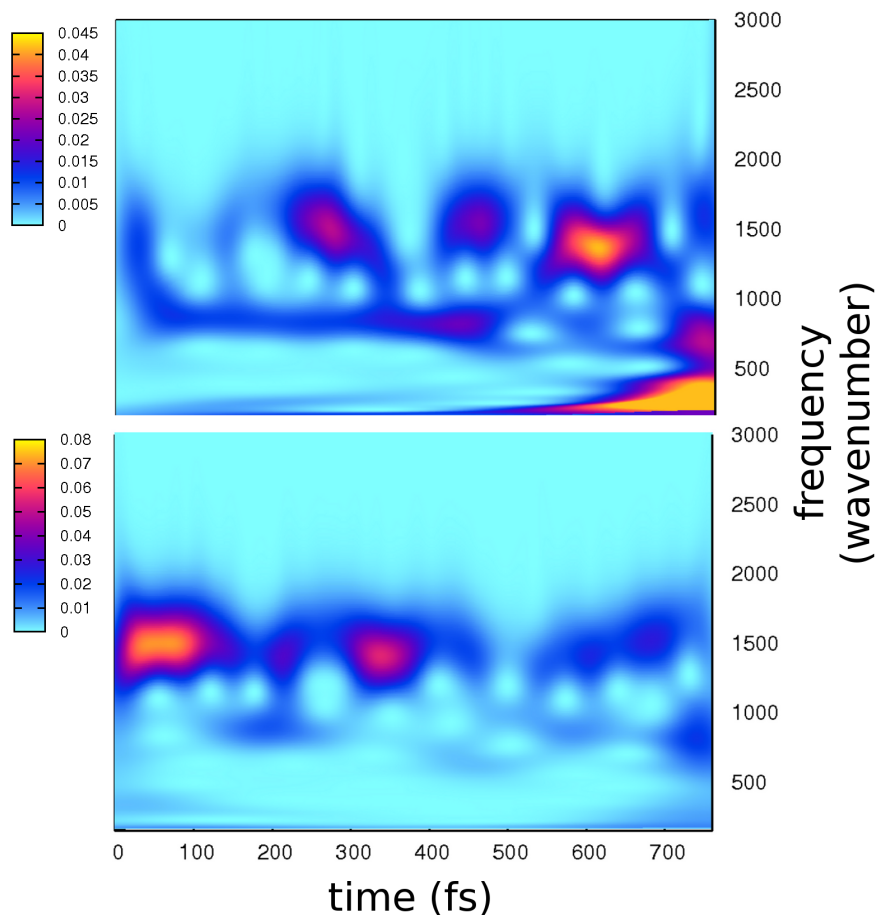
Fig. 2.19: 2D maps of phenolic C-O (top) and imidazole C-N (bottom) pair distance temporale evolution extracted from TrjIV.

First of all, the main vibrational bands are again found in the frequency range of the C-O and C-N stretching modes. In Fig. 2.20 an out-of-phase oscillation trend could again recognized for the two stretching bands, however it is observed just until 350 fs. Indeed, after the ESPT no particular trend is found.

On the contrary, the Wavelet spectrum in Fig. 2.21 is characterized by all out-of-phase oscillations, that propagate for about 1 ps. Of course in this case we could not have information after the ESPT, but the trend shown for the whole dynamics and
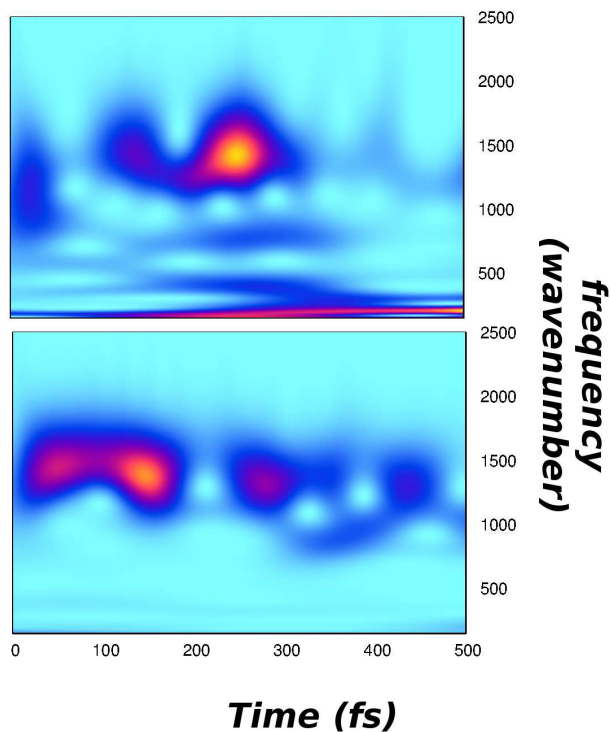
Fig. 2.20: 2D maps of phenolic C-O (top) and imidazole C-N (bottom) pair distance temporale evolution extracted from TrjI.

preceding the reaction is again in excellent agreement with Prof. Mathies results.

On the basis of our results and of this important agreement with experimental findings, we believe that the out-of-phase of the modes on the two different rings is a consequence of the elecronic density re-distribution after the photo-excitation, confirming again the strong correlation between electronic excitation and structural re-organization. Moreover this result has a major importance because is another confirmation of the great potentiality of the Wavelet Analysis as a powerful intrument for investigation of complex chemical problems.

The Wavelet Analysis of the hydrogen bond between His148 and the phenolic
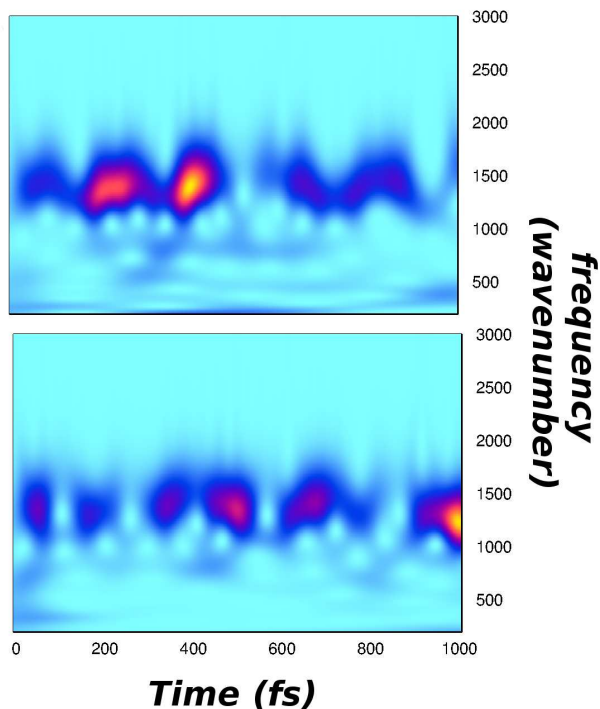
Fig. 2.21: 2D maps of phenolic C-O (top) and imidazole C-N (bottom) pair distance temporale evolution extracted from TrjIII.

ring is presented in Fig. 2.22 for TrjIV.

In this spectrum low frequencies vibrational bands around 600 and 1000 cm^{-1} that can be assigned to collective motions involving the chromophore ring, are observed. The most interesting thing is the increase of low frequency vibrational bands since around 600 fs until the end of the trajectory: this is the same trend found in the intra and inter-molecular O-H pair distances Wavelet spectra analysed before and clearly demonstrates that the His148 residue is influenced by the proton transfer event. So, this fact underlines and confirms the active role of His148 as one of the ESPT driving forces, as already found and discussed before in the time-domain
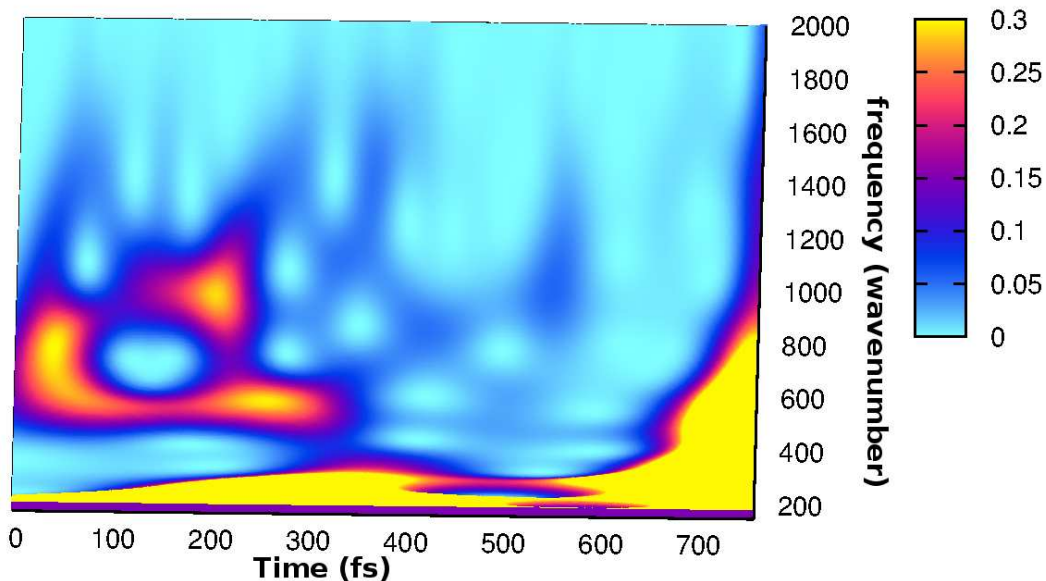
Fig. 2.22: 2D maps of pair distance temporal evolution extracted from TrjIV. The ESPT takes place at 720 fs.

based analysis.

2.2.3   GFP Reactant Model Anharmonic Analysis

Anharmonic frequency results in both the ground and excited state of the GFP neutral model, chosen following the procedure presented in the Methods Chapter, are discussed. It consists of the chromophore including the Ser65 side chain, the crystallografic water, Ser205 and Glu222. This analysis was performed in order to corroborate the results obtained from our simulations, and indeed from this normal modes analysis we obtained a strong confirmation of the structural analysis from molecular dynamics trajectories results. So, despite the absence of a statistical support coming from a reasonable number of molecular dynamics simulations in order to confirm the results obtained from these trajectories, we obtained a strong agree-

96

ment not only with the normal modes analysis but also with the energetic rigid scan of the chromophore dihedral angle (discussed later). The time-frequency analysis already supported a different behavior of the protein active site in terms of both normal modes and structural parameters extracted from dynamics simulations in the excited state, mainly suggesting advantageous conditions for the proton transfer reaction.

In particular, we found that some crucial modes involving the chromophore rings are red-shifted in the excited state and also show a different composition, as can be observed by an inspection of the displacement vectors depicting the modes shown in Fig. 2.23.

In the top panels the twisting of the two chromophore rings in the ground (left) and excited (right) states present a different composition. A wider amplitude of the displacement vectors and the red shift (56.71 cm^{-1} S_1 vs. 90.80 cm^{-1} S_0) in the excited state proves a larger conformational freedom of the bridge connecting the two rings, as a consequence of a redistribution of the electronic density upon the excitation on this part.

The out-of-plain of the two chromophore rings is shown in the middle panel of Fig. 2.23 for the ground (left) and excited (right) states. In the excited state it is red-shifted (100.98 cm^{-1} vs. 145.99 cm^{-1} S_0) and a minor contribution of the residues involved in the network is observed compared to the S_0 mode. This red shift goes in the same direction of the results obtained from dynamics simulation,
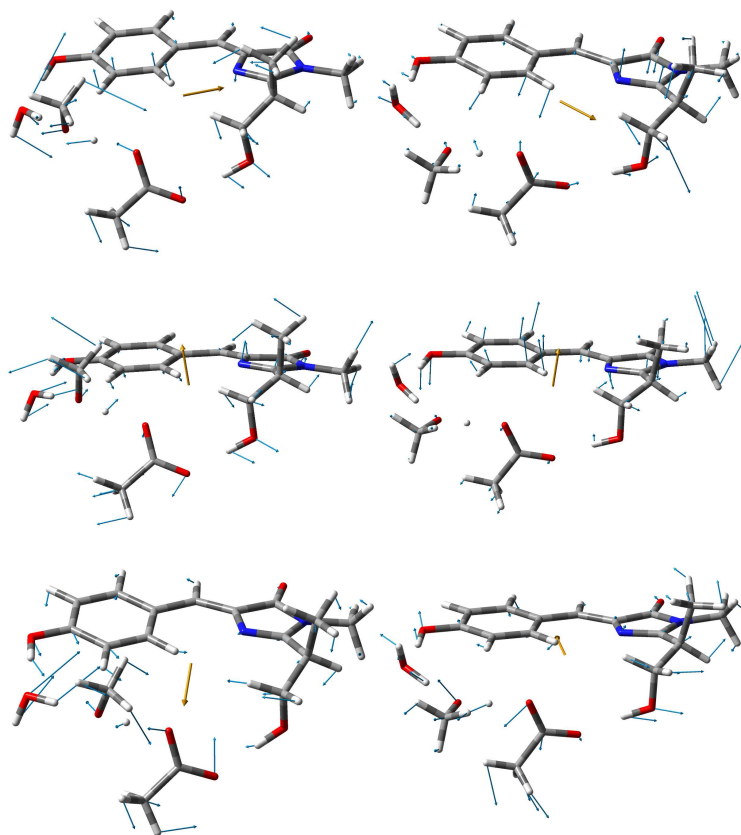
Fig. 2.23: Normal modes analysis of the GFP Model involving the chromophore and the residues involved in the hydrogen bond network performed at at B3LYP/6-31+g(d,p) level of theory.Upper panel: chromophore twisting mode in the ground (left) and excited (right) state. Middle panel: Chromophore rings out-of-plain in the ground (left) and excited state (right). Lower panel: Collective normal mode mainly involving the hydrogen bond network oxygens in the ground (left) and excited (right) states.

confirming the characteristic N-C-C-C dihedral angle behavior.

In the bottom panel of Fig. 2.23 we observed for both the ground (left) and the excited (right) states a mode involving a collective motion of all the atoms in the hydrogen bond network. Also this time a red shift is observed in the excited state (116.76 cm^{-1} vs. 171.78 cm^{-1} S_0). This red shift suggests that the collective motion of the network residues is energetically favored in the excited state, and this is in

agreement with lower inter-molecular distances between residues observed in the excited state trajectories, suggesting a more advantageous condition for the proton transfer reaction.

In Fig. 2.24 the intra-molecular O-H stretching modes are shown for both the ground (left panels) and excited (right panels) states.
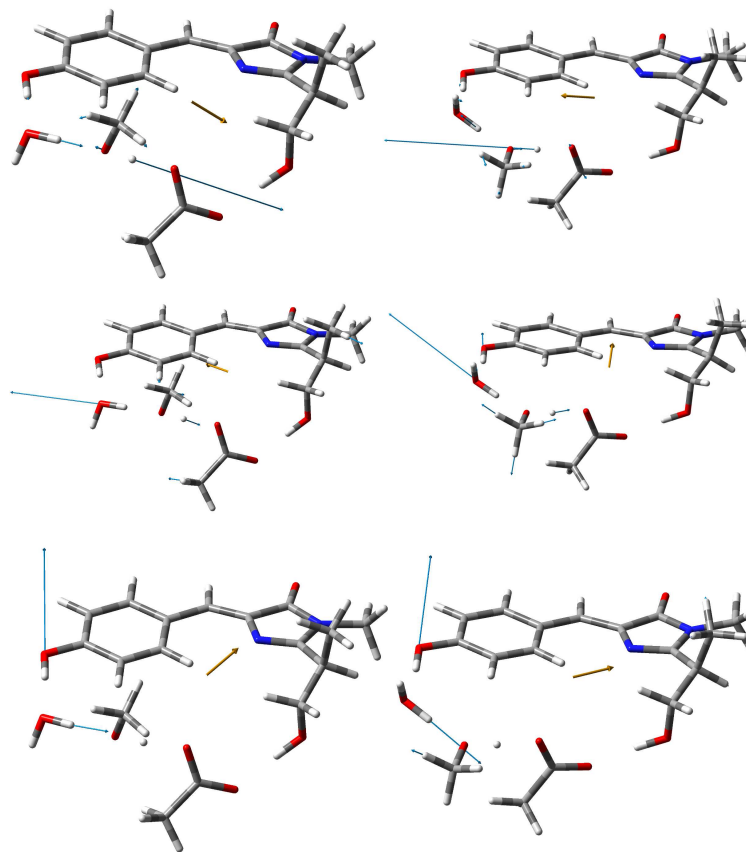
Fig. 2.24: Normal modes analysis of the GFP Model involving the chromophore and the residues involved in the hydrogen bond network performed at at B3LYP/6-31+g(d,p) level of theory.Top panel: Ser205 O-H stretching mode in the ground (left) and excited (right) states. Middle panel: Water O-H stretching mode in the ground (left) and excited (right) state. Bottom panel: Phenol ring O-H streching mode in the ground (left) and excited (right) states.

Red shift in the excited state is observed for all the O-H stretching modes and the Oser205-Hser205 one is the larger with a shift value of 477 cm^{-1}. Obviously the

frequency values of such modes reflect the different nature of the bonds: 3329.55, 3098.99, 2533.24 cm^{-1} in S_0 and 3108.10, 2859.14, 2056.07 cm^{-1} in S_1 for Otyr-Htyr, Owat-Hwat and Oser205-Hser205, respectively. The O-H stretching of Ser205 appears at 2533.24 cm^{-1} in the ground state and is accompanied by a water O-H stretching, as shown on the left side of the upper panel of Fig. 2.24. In the excited state it shows an important red shift with a frequency value of 2056.07 cm^{-1} and this time it is accopanied by a water bending (upper panel, right side) contribution. The water O-H stretching mode at 3098 cm^{-1} in the ground state is shown in the middle panel of Fig. 2.24 on the left side. It involves a minor contribution from tyrosine O-H and Ser205 O-H stretching. In the excited state (right side) the tyrosine O-H contribution is larger and a red shift around 239 cm^{-1} is observed. The tyrosine O-H stretching is shown in the lower panel of Fig. 2.24 for both the ground (left) and excited state (right) panel. In the first case it shows a frequency value of 3329.55 cm^{-1} and it is characterized by a water O-H stretching contribution. In the excited state it is red shifted of about 221 cm^{-1} and the water stretching contribution is enhanced.

The red shift affecting all the analysed modes in the excited state along with their different composition supports the different dynamics affecting the ground and excited states, in agreement with our results previously shown. This analysis supports the MD results overcoming a limited number of excited state trajectories due to their huge computational cost. The hypothesis of the existence of crucial struc-

tural differences in the ground and excited states is suggested by both the peculiar GFP neutral model frequency shifts and the oscillation distance trends of the donors obtained from the molecular dynamics simulation of the whole protein. The excellent agreement with Wavelet analysis results is also represented by the conserved relative energy of the intra-molecular O-H stretching bands, that is characterized by a more energetic O-Htyr stretching frequency, followed by the water O-H and Ser205 O-H stretching.

2.2.4   Energetic Analysis

In Fig. 2.25 we show rigid potential energy scans of the anionic form of HBDI chromophore obtained from single point energy calculation for both the ground and excited states at different values of the chromophore dihedral angle N-C-C-C.

The chosen range includes values between -30 and 30 degrees in order to cover the wide range of values explored in the excited state protein simulation. These calculations have been performed employing the same potential of the molecular dynamics simulations explained in the Methods Chapter.

Concerning the dihedral angle values from -5 to 5 degrees, the same energy values are found for both the electronic states. For values ranging from -14 to -7 and from 7 to 14 the energy difference grows from 0.18 to 0.78 Kcal/mol and from 0.18 to 0.76 Kcal/mol, respectively. This is more emphasized moving from -16 to -30 and from 16 to 30 degrees indeed in the first case the energy difference increases from 1.14 to 3.89 Kcal/mol and in the second case from 1.83 up to 3.87 Kcal/mol.
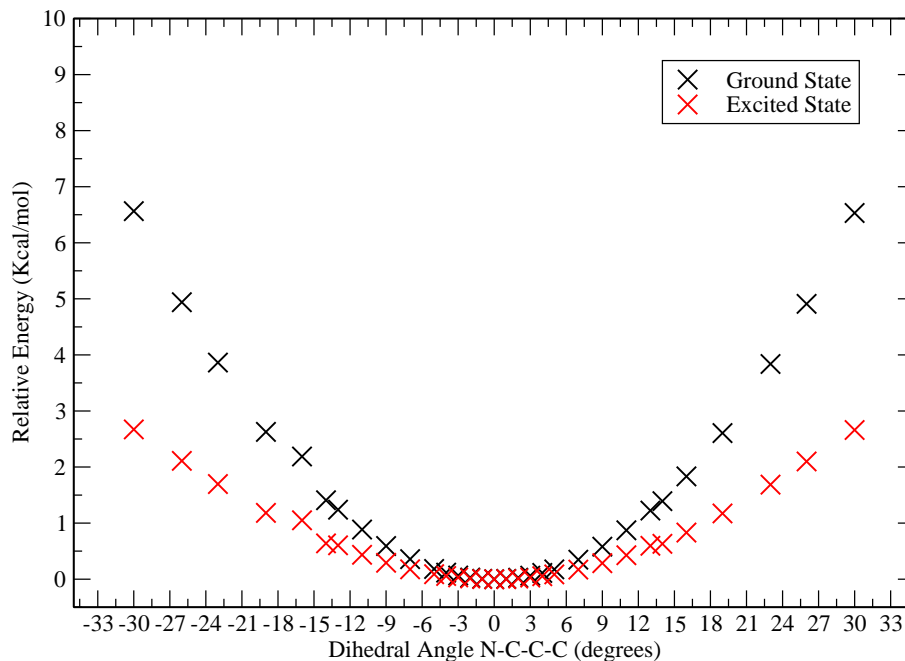
Fig. 2.25: Rigid energy scan of HBDI$^-$ gas phase model along the chromophore N-C-C-C dihedral angle at TD-CAM-B3LYP/6-31+g(d,p) S_1 (red) and B3LYP/6-31+g(d,p) S_0 (black) level of theory. The relative energy corresponding to the reference different minima for both the electronic states are reported in Kcal mol.

These results clearly suggest that in the excited state a wider range of dihedral angle values is energetically more accessible to the chromophore. It is also qualitatively expressed by the shapes of the curves. This result is in excellent agreement with the ones obtained from our molecular dynamics simulations and vibrational analysis, indeed the anionic form is favored by wider N-C-C-C dihedral angles in the excited state. During the simulation, as shown in the excited state trajectories, the dihedral angle N-C-C-C explores a range of values larger than the one explored in the ground state suggesting that a major conformational freedom is reached by the chromophore after the excitation.

Chapter 3

Polaron Pair Formation in Oligothiophene Models

In this Chapter the results obtained during my experience abroad, in Professor Xiaosong Li Research Group at the University of Washington, will be discussed. The discussed results were obtained thanks a combined approach based on techniques developed both in my Research Group and the one of Prof. Li. The Wavelet Analysis was employed for the first time to study the formation and dynamics of charged transient species such as the polaron pair formation on a oligothiophene model, moreover this technique was combined with the ab-initio non-adiabatic Ehrenfest dynamics for the first time. The capability to follow the electronic density propagation permitted by the Ehrenfest dynamics allowed to catch the instantaneously formed charge separation, while the temporal evolution of some crucial frequencies was of key importance to monitor the dynamics of such formed transient species, and it was done by employing the Wavelet Analysis. This study suggested an interesting protocol to treat such class of molecules and the non-equilibrium processes

characterizing these ones. A molecular insight can indeed be given in this way, and this is a crucial aspect in the field of photovoltaic because, although their huge number of applications, it is still lacking a detailed knowledge of how such devices work at a molecular level. So, on the basis of the promising results, we can believe that this protocol could be very useful in giving a molecular picture of excited transient species formation and evolution such as excitons or polarons.

3.1 Results and Discussion

3.1.1 The Polaron Pair Formation and Dynamics in the Time-Domain

Our study started with a preliminar characterization of the heptamer in terms of both frequencies and optical properties. Especially the last one was of key importance before starting the Ehrenfest simulation. First of all, the excited state of interest was prepared by promoting one electron from a selected occupied orbital to an unoccupied one in the ground state. Preliminar calculations, performed by employing LR-TDDFT theory level on the chosen heptamer structure obtained in agreement with the procedure described in the Methods Section, revealed that the electronic structure of the photo-excited 3-methylthiophene heptamer could be described by the dominant HOMO $\rightarrow$ LUMO transition. Once performed this transition, a non-stationary electron density that is representative of a coherent superposition of the ground and excited electronic states of interest is created. These frontier orbitals, as shown in Fig. 1.6, are delocalized, suggesting that photoexcita-

tion does not directly lead to instantaneous polaron formation. One has to probe the interplay between time evolutions of excited electronic wave function and molecular structure to understand the mechanistic driving force of polaron dynamics.

In order to investigate the polaron formation, it was firstly analysed the oligomer total dipole moment, that is shown in Fig. 3.1a.
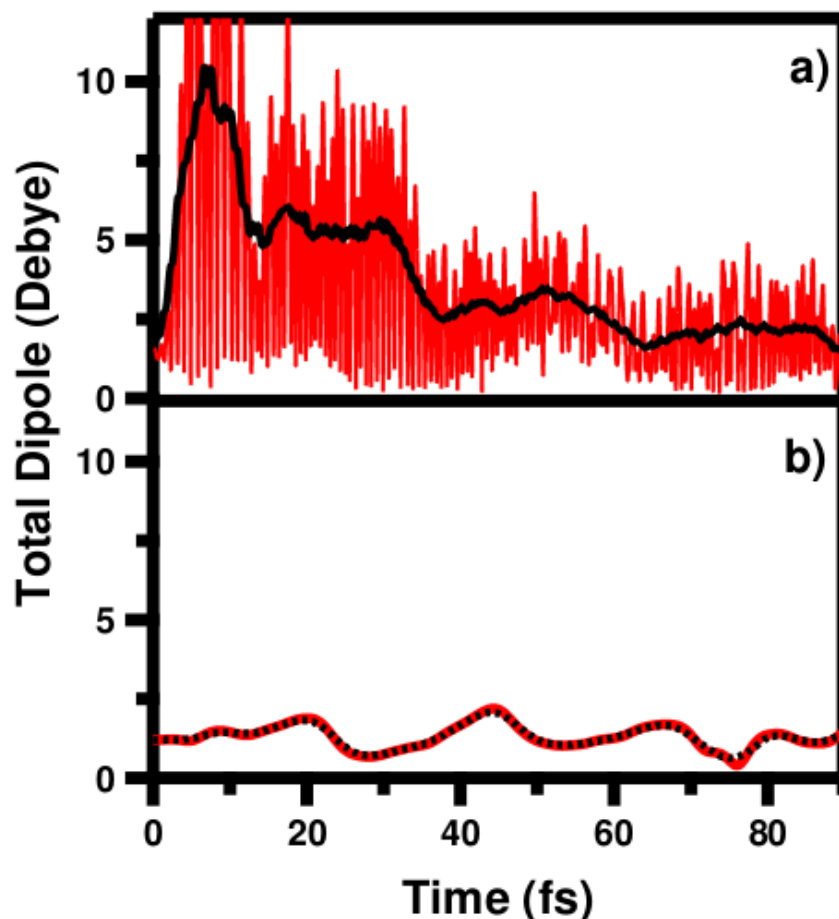
Fig. 3.1: (a) Total dipole moment temporal evolution of 3-methylthiophene heptamer during the Ehrenfest dynamics. (b) Total dipole moment temporal evolution of 3-methylthiophene heptamer during the ground state BOMD simulation. Red: instantaneous dipole moment for every $\Delta t_e = 0.001\,fs$. Black: time-averaged dipole moment over 5 fs.

We observed the temporal evolution of the total dipole moment of the photo-excited state during the Ehrenfest dynamics, collected every electronic time step (Δt_e) and time-averaged over every 5 fs. For a two-state system without dissipation or change in potential energy surface, the excited dipole moment will oscillate between values of the ground- and excited states with a simple frequency that corresponds to the excitation frequency. [111] However, convoluted with the oscillatory behavior of the dipole in Fig. 3.1a is an underlying trend clearly characterized by several regions in which the excited-state dipole moment exhibits different signatures. Within 10 fs of the excitation there appears to be an oscillatory behavior of the time-averaged dipole magnitude between ~1.8 D and ~10 D. This oscillatory behavior stops at ~12 fs, so concluding the first region of the dipole moment in which the larger oscillations are observed. At which point a constant dipole moment of ~5 D is observed and maintained until 30 fs, characterizing the second well-defined region. After 30 fs a quick decrease of the dipole takes place until around 38 fs. This event initiates the second long period of time in which the dipole retains, on average, constant values around 2.5−3 D until 50 fs and represents, at the same time, the third isolated dipole moment characteristic region. The fourth and final period is characterized by average oscillations around 2 D that persist until the end of the dynamics.

The analogous total dipole evolution is reported for the ground state Born-Oppenheimer molecular dynamics (BOMD) in Fig. 3.1b. In contrast to the char-

acteristics of the time-dependent dipole moment in Fig. 3.1b, the ground state dynamics only gave rise to dipole oscillations between 0.5 D and 2.5 D, simply due to molecular structural changes. So the analysis of the time-dependent dipole suggested that the excitation is responsible for a charge separated state in the system that is not observed in the ground state.

The observed periods of dipole plateaus in Fig. 3.1a suggested that electron-hole pair separation/recombination was temporarily trapped during the exciton-nuclear dynamics. In this trap state, the charge carriers' delocalization pathway was blocked, and the decay of time-dependent dipole was quenched. This could only arise from structural deformations induced by the charge carrier dynamics, creating short-lived exciton-vibrational trap states, or polarons. In other words, we have observed the signature of polaron formation in Fig. 3.1a. At this point the main question was to understand which one could be the driving force that underlies the formation of such short-lived polarons.

Fig. 3.2 plots the time-evolutions of dipole components from the exciton-nuclear dynamics (Fig. 3.2a) and the ground state dynamics (Fig. 3.2b). As shown in Fig. 3.2b, all three dipole components from the ground state dynamics do not show significant changes. In contrast, in the exciton-nuclear dynamics (Fig. 3.2a), a dominant contribution from the dipole component along the polymer chain (x direction) was found, compared to the other two components (dipole along the shortest axis in the polymer plane, y, and the out-of-plane axis, z). As the main contribution
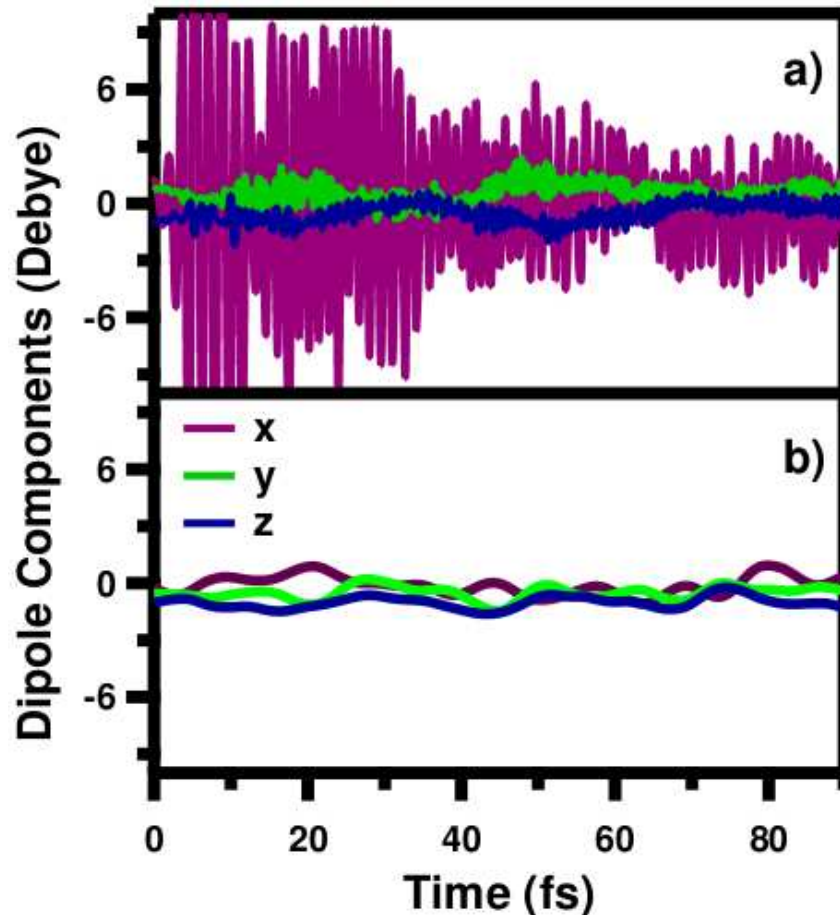
Fig. 3.2: (a) Time evolution of dipole moment components of 3-methylthiophene heptamer during the Ehrenfest dynamics. (b) Time evolution of dipole moment components of 3-methylthiophene heptamer during the BOMD simulation.

to the total dipole moment, the time-dependent characteristics of the x component followed the trend observed in Fig. 3.1a, i.e. periods of dipole plateaus. However a careful comparison of the time-dependent x, y and z components revealed that changes in x component were synchronized with the slow profile oscillations of the y and z components. This fact suggested that the polaron formation may be a result of structural changes along the y and z directions, i.e. the polymer backbone

out-of-plane motion.

The dipole analyses suggested that polaronic states could be formed after the excitation, as we just demonstrated. However, especially through the dipole components analysis, it seemed clear that we could obtain a more detailed molecular description of the polaron dynamics by a structural analysis. The interesting trends of the y and z dipole components clearly indicated that the different zones in which the charge is trapped were correlated to a different contribution of such two components. In other words it seemed that when there is some structural rearrangement, for example in terms of out-of-plain motions, the polaron dynamics changes, and this is a very important result because not only directly connects the polaron formation and dynamics with the nuclear dynamics, but also opens a another perspective for the investigation of such species in terms of nuclear dynamics, despite the very short time scale that characterizes such species.

3.1.2   Different Length Oligomers Excited State Investigation

The excited states of other oligomers were investigated by the Ehrenfest dynamics. In particular the trimer and pentamer models, presented in Fig. 3.3 and Fig. 3.4, were analysed.

It was very interesting to find substantial differences in both these models and also compared to the heptamer. Like the heptamer, also these systems were modeled with methyls side chains instead of hexyl chains, in order to reduce the computational
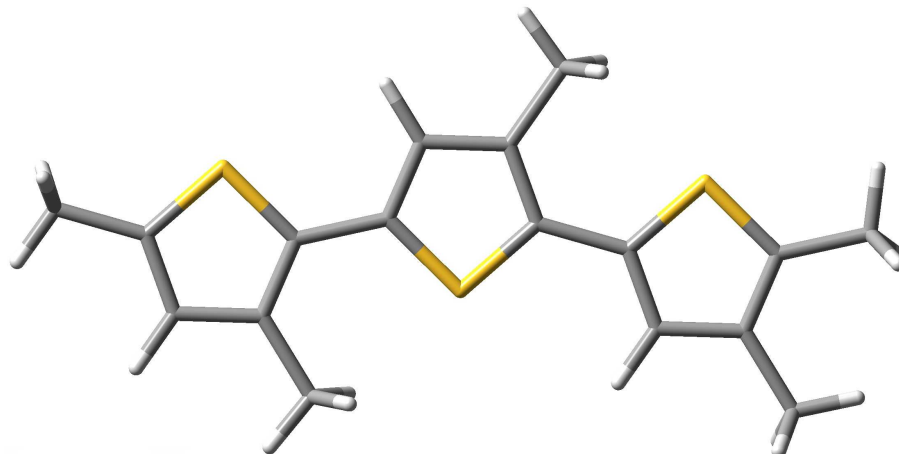
Fig. 3.3: The 3-methylthiophene trimer model.
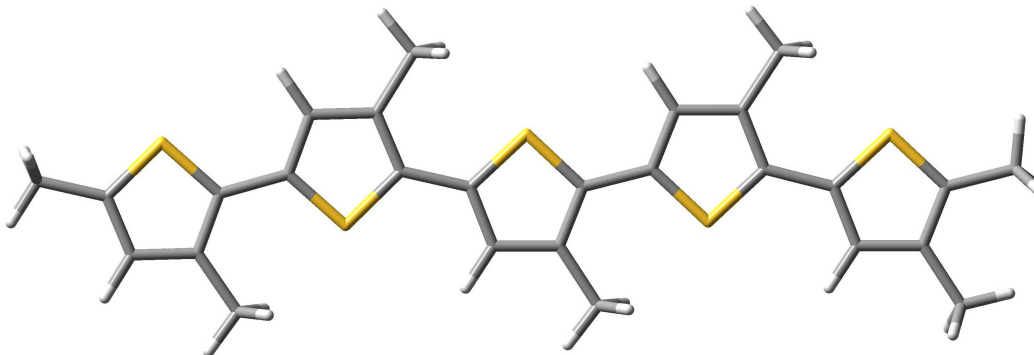
Fig. 3.4: The 3-methylthiophene pentamer model.

cost. From the performed Ehrenfest dynamics we extracted the temporal evolution of the total dipole moment and its components for both the systems.

In Fig. 3.5 the trimer total dipole moment averaged every 5 fs and collected for 555 fs, is presented. A clear difference of the dipole dynamics compared to the heptamer, is found. An important sudden increase until reaching values of 7 D, starting from initial values araund 2 D, is observed in less than 10 fs after the excitation. In agreement with the heptamer dynamics, also in this case the hypothesis of a charged
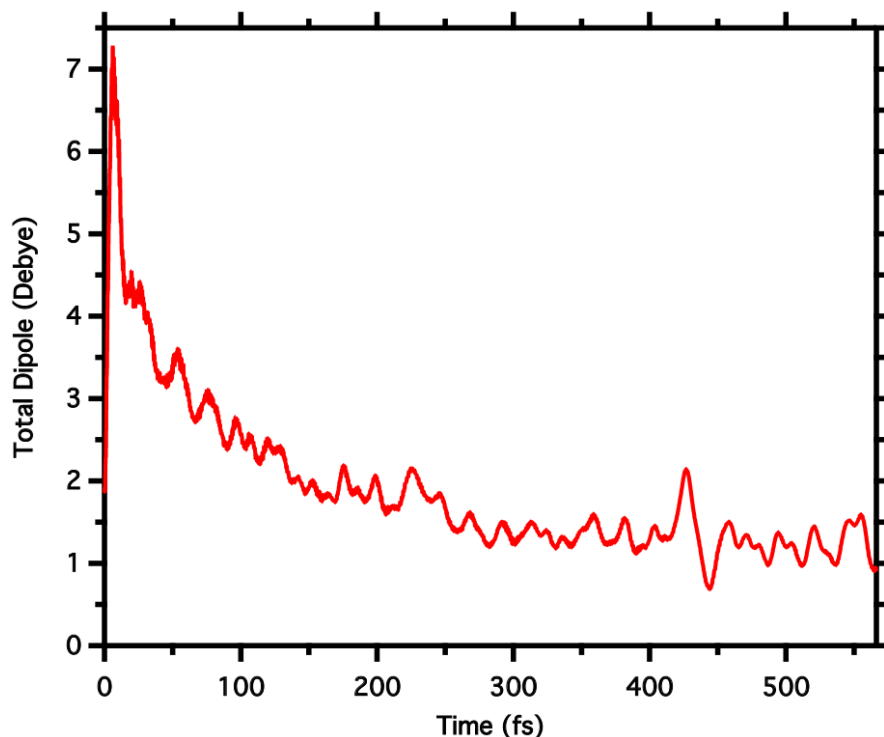
Fig. 3.5: Total dipole moment temporal evolution of 3-methylthiophene trimer during the Ehrenfest dynamics time-averaged over 5 fs.

transient species formation is confirmed, however crucial differences with the heptamer are found. An ultrafast decrease of the dipole magnitude is observed. More in detail, after the sudden increase, after about 20 fs the first decrease takes place, causing the dipole to oscillate around 4.5 D. This value is retained for about 20 fs, indeed since around 40 fs it started decreasing again, reaching values around 3.5 D. Then, a continuous decrease takes place until 250 fs when, apart a localized increase around 450 fs, it retains values around 1.5 D until the end of the trajectory. The dipole behavior found in the trimer suggests that although the polaron formation takes place, as proved by the huge total dipole magnitude increase, it is not able to

survive, indeed a constant decrease takes place after 20 fs. This trend can be easily

assigned to the small size of the oligomer because the charge sepatation that takes

place after the excitation cannot spead along the chain because of its small length,

so it quickly recombines causing a fast decrease of the dipole moment and of course

determining an ultrafast life of the polaron.
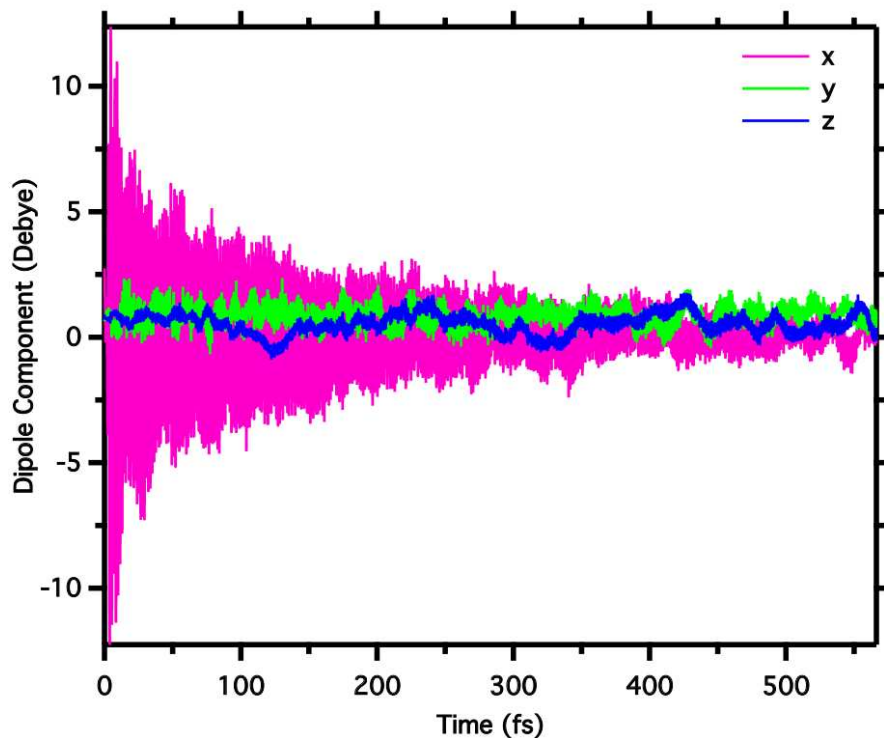
Fig. 3.6: Time evolution of dipole moment components of 3-methylthiophene trimer during the Ehrenfest dynamics.

Taking a look on the dipole components (Fig. 3.6), as already happened in the

heptamer model, also in this case the component mostly increased after the excita-

tion is the one running along the oligomer chain (i.e. the x component). A very

fast increase, reaching values larger than +10 and -10 D characterizes its tempo-

ral evolution, and the very fast decrease, starting after 20 fs like the total dipole moment, takes place. Concerning the y component (the one along the shorter side of the molecule), its oscillations are almost centered around constant values spanning around 1 D and so particular trends or changes in this kind of oscillations can be recognized. However it is more interesting the z component behavior: although it shows oscillations centered around constant values, it also exhibits some small regions during the time in which it deviates from the average values, such as around 120 fs and 340-350 fs. It is interesting to notice that around 120 fs there is a change in the slope of the total dipole moment decrease, while around 340 fs it stops decreasing and starts oscillating around almost constant values. This results is really interesting because is an important proof of the important role of the nuclear dynamics on the polaron dynamics destiny: the z axis represents indeed the molecule out-of-plain, so indicating that changes in the rings conjugation can importantly affect the electronic dynamics. Moreover, comparing these results with the ones obtained from the heptamer, another important finding is that the chain length strongly influences the polaron evolution. So in terms of optimization of such systems for practical applications it must be taken into account how much is important their length in changing and improving the device performances. At the same time the rings conjugation is also crucial in determining the polarons recombination velocity.

In Fig. 3.7 the pentamer total dipole moment averaged every 5 fs and collected
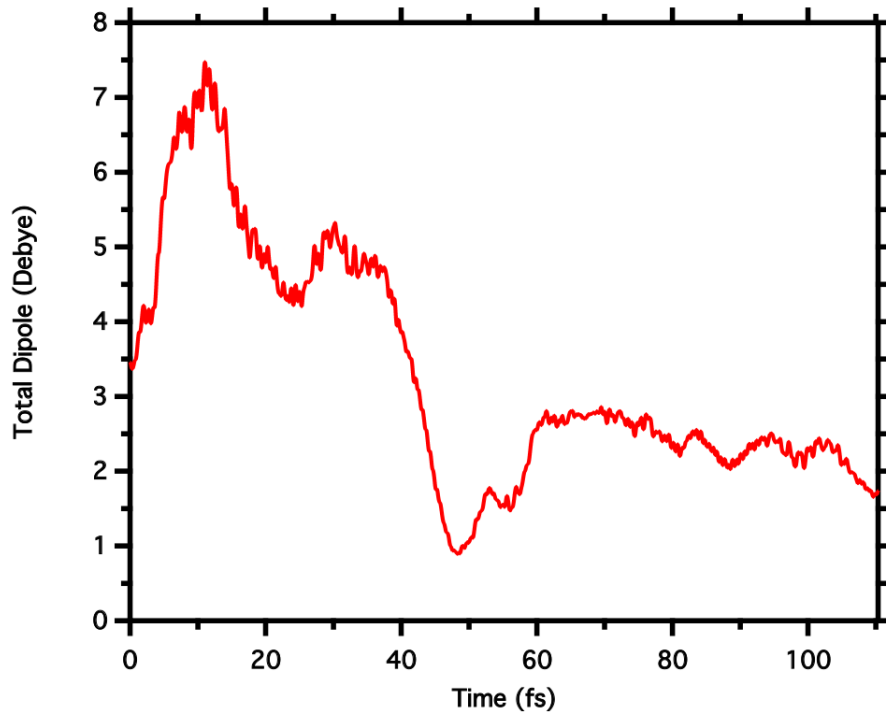
Fig. 3.7: Total dipole moment temporal evolution of 3-methylthiophene pentamer during the Ehrenfest dynamics time-averaged over 5 fs.

for 108 fs, is shown. The formation of a charge separated state is observed also in the pentamer model, however a very different behavior compared to the trimer model is found: characteristic regions can be easily recognized during the time unlike the trimer dipole ultrafast decay. In this case the dipole increase is not instantaneously observed after the excitation, on the contrary, starting from values around 3.5 D it retains a very short plateau around 4 D, then it starts increasing until reaching values of 7.5 D around 18 fs. From this first region the dipole starts decreasing since about 18 fs, and around 25 fs its decrease stops at 4.5 D. The second region is opened with another small increase of the dipole, reaching values around 5 D, retained until

40 fs when a most important decrease takes place driving the dipole to values of 1 D at 50 fs. Then it increases again, opening the third region, since 50 until 60 fs, when the dipole reaches and almost retains until the end of the trajectory, values around 2.5 D. These evidences suggest and confirm the influence of the chain length on the polarons dynamics as already found by the comparison of the trimer results with the heptamer ones. An increase in the oligomer length of just two monomeric units, drastically changed the polaron dynamics.
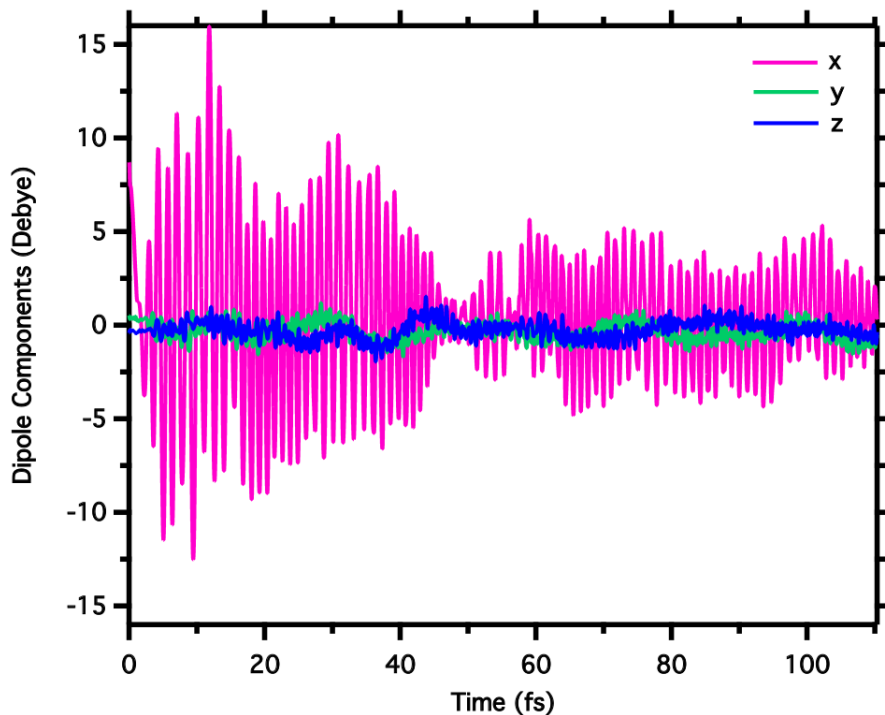
Fig. 3.8: Time evolution of dipole moment components of 3-methylthiophene pentamer during the Ehrenfest dynamics.

The dipole components temporal evolutions are shown in Fig. 3.8. The dipole component mostly contributing to the total dipole increase in the x one, for which

almost the same oscillations of the total dipole are found. Concerning the other two components, it is interesting to observe that around 25 fs, in concurrence with the total dipole decrease, there is a deviation of the z component from its average values, a similar trend is found around 40 fs when it again deviates from the previously assumed values in corrispondence of the total dipole moment important decrease. More interestingly, such deviations are always related to an out-of-phase oscillation of such component with the y one, indeed apart these ones, the two component almost oscillate together until 60 fs. After 60 fs there is a regular and almost retained out-of-phase oscillation trend until the end of the trajectory and this happens when, on the other side, the total dipole moment retains constant values since 60 fs.

The crucial role of the nuclear dynamics is again confirmed, as clearly shown in the dipole moment components behavior, suggesting that the out-of-plain motions of the molecule during the time strongly affect the polaron dynamics. In the pentamer case, like in the heptamer, clear periods of time can be recognized in which the dipole decreases in a stepwise way. This fact represents the evidence of the necessity to employ longer chains to allow the polaron formation and an its longer life, moreover in this contest, the modulation of the inter-rings conformation must be taken into account.

3.1.3 Excited State Nuclear Dynamics Investigation

So the polaron formation can be observed by monitoring both the charge carrier and structural parameters' evolution during the excited state dynamics. On the basis

of such results, it was interesting to understand in detail the molecular properties that determine the driving force that creates these polaron states. First of all, we decided to monitor a key parameter in determining the rings coplanarity in order to search for a correlation between excitonic dynamics observed in Fig. 3.1a and the molecular structural dynamics.
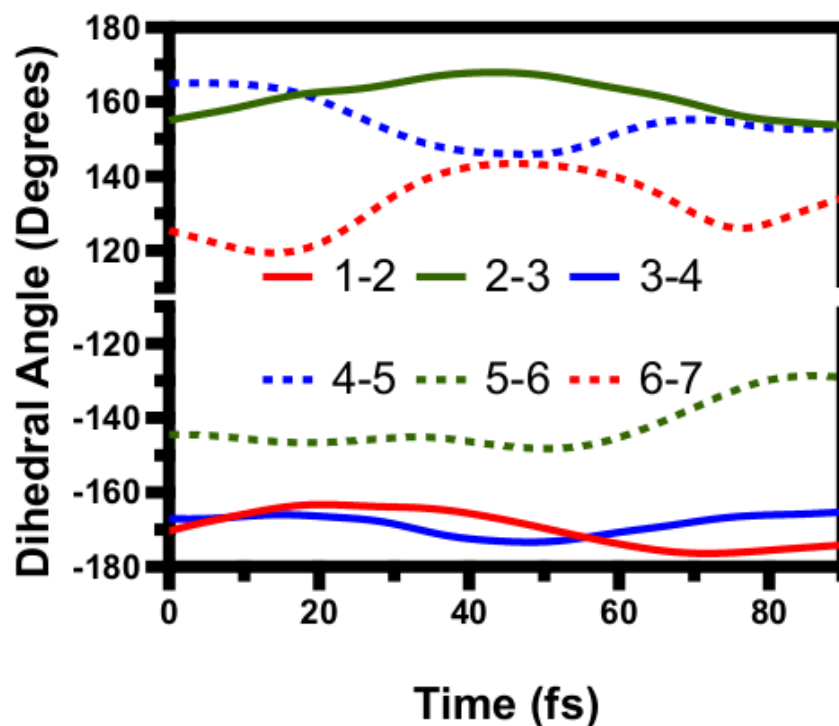
Fig. 3.9: Time evolution of S-C-C-S dihedral angles of 3-methylthiophene heptamer during the Ehrenfest dynamics.

The stepped decay in the extent of charge separation following the photoexcitation could be interpreted in light of structural reorganizations when both analyses are performed in the time domain. Fig. 3.9 shows the time-evolution of the oligomer intermolecular dihedral angles S−C−C−S, which measure the degree of planarity

of the system, in the excited state Ehrenfest dynamics. The temporal evolution of all the six dihedral angles is shown in Fig. 3.9b. Close examination of Fig. 3.9b reveals a strong correlation of motion between the dihedral dynamics and that of dipole moment observed in Fig. 3.1a.

In greater detail, the dihedral angle 6−7 after the first 20 fs approaches planarity. Starting from values around 125 degrees, it reaches values of 140 degrees that are retained for a period of about 30 fs. Later it gradually returns to its initial value. This structural trend is correlated to the 4−5 dihedral angle, but in this case the behavior is the opposite. The 4−5 dihedral starts from values more close to planarity of the two rings (165 degrees), and begins to deviate from planarity after 20 fs approaching to values around 140 degrees. It exhibits the same dynamics of the 6−7 dihedral angle, in this case retaining the same value for about 30 fs. Such a concurrence of dihedral angle motions created step-wise localization of charges as the out-of-plane vibrations broke the conjugation between adjacent monomer rings. The dynamics of these two dihedral angles also closely correlates with the step-wise trend found for the dipole moment behavior. The regions isolated in this analysis are in agreement with the stepwise behavior of the dipole moment, and go in the direction of a direct connection between polarons and nuclear dynamics. One can also observe correlations between the step-wise dipole dynamics and other dihedral angle motion. For example, the 5−6 dihedral angle shows almost constant values around -145 degrees, but after 50 fs it starts deviating from planarity until reaching

values around -130 degrees. This motion correlates to the generation of the last step-wise dipole moment in Fig. 3.1a.

The direct connection between the charge separation and structural rearrangements suggested that the formation of a polaron pair is associated with the out-of-plane motion of the polymer backbone dynamics. This is understandable because the conjugation and electron delocalization strongly depend on the planarity of the structure. The out-of-plane motions can trap the exciton and prevent it from freely recombining/diffusing. When the planarity of adjacent monomers deviates from ideal conjugated structure, time-evolving electron density can be trapped in a few monomer rings, and polarons are formed and quickly decay with a lifetime of $\sim$10 fs.

3.1.4   The Polaron Formation in the Frequency Domain

Apart the role of structural rearrangements as driving force of polaron formation in organic polymer, their dynamics can be investigated also by the analysis of intramolecular parameters such as the the C-C bonds. The Wavelet Analysis is the precious instrument that allows to follow the temporal evolution of the vibrational bands associated to such quantities in order to investigate possible shifts during the time. Through this analysis we showed that the polaron dynamics can be monitored also through the peculiar trends of vibrational bands evolution during the time and the capability to obtain this information is of key importance in the study of such excited state processes. The Wavelet spectra reveal if shifts of such bands take

place because of the polaron pair formation. In Fig. 3.10 the Wavelet spectra of the C_1-C_2 and C_3-C_4 bonds belonging to ring 7 are shown (the labels used for the $C-C$ bonds are those shown in Fig. 1.5). The Wavelet spectrum is presented in a two-dimensional plot, where the temporal evolution of the vibrational band is retained as can be seen from the temporal axis that allows resolution of both the main frequency bands and their shifts in time.

In Fig. 3.10a the main vibrational band is the one centered around 1500 cm^{-1} and can be simply assigned to the $C-C$ stretching motion. At around 50 fs this band undergoes a blue shift, suggesting that additional electron density localizes on this bond around that time. It is also probable that this vibrational band contains also other contributions arising from other molecular motions, but it is so difficult to catch and to isolate each contribution because of the very short time of sampling that causes such a very broad vibrational band. Anyway, an important result is otained: despite the short trajectory, we are able to observe the effect of the polaron formation in the frequency domain, indeed we catch the ultrafast blue shift on a time scale lower than 100 fs, revealing the absolute power of the Wavelet Analysis as a precious instrument in the investigation of ultrafast processes.

Comparing this spectrum with that of Fig. 3.10b a different trend is found. In this case the $C-C$ bond motions are strongly influenced by another vibrational band centered around 1000 cm^{-1}, which can be assigned to collective motions of the rings. A less intense band around 1500 cm^{-1} is found and could be assigned to
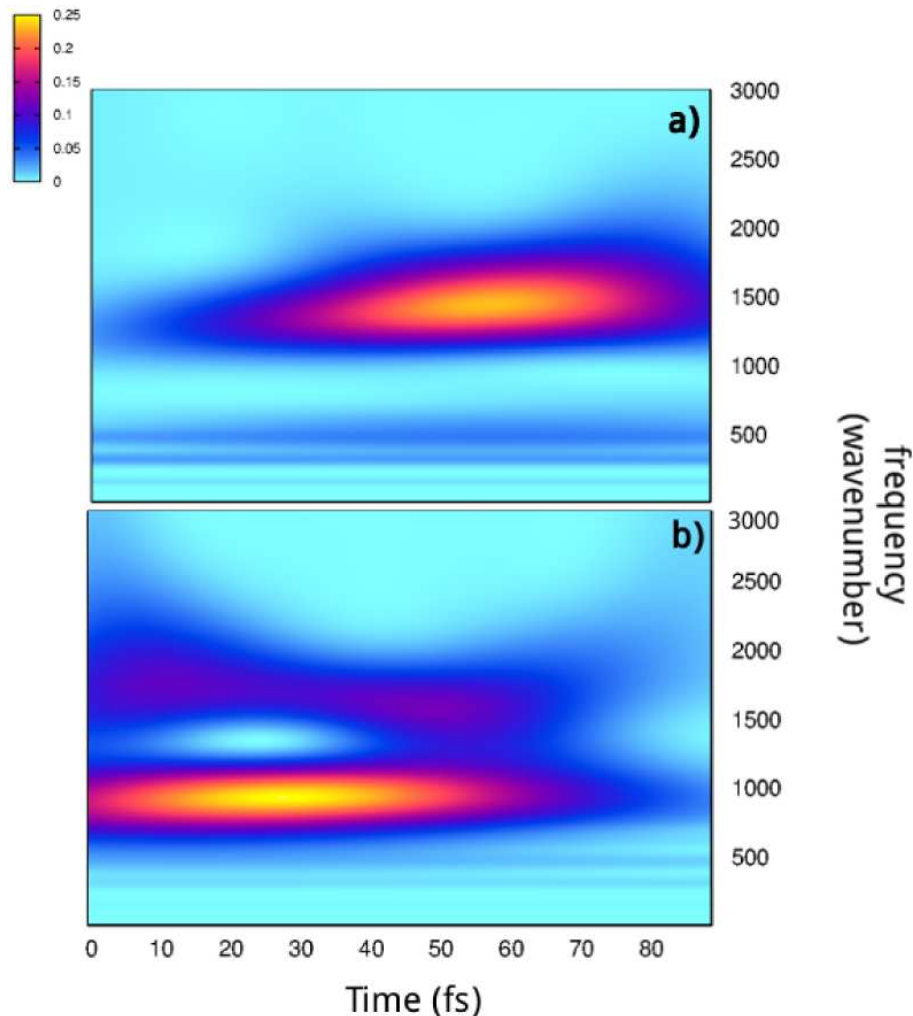
Fig. 3.10: (a) Wavelet power spectra of the C_1-C_2 bond distance temporal evolution during the Ehrenfest dynamics. (b) Wavelet power spectra of the C_3-C_4 bond distance temporal evolution during the Ehrenfest dynamics.

the intramolecular C-C stretching. In this case a red shift is observed during the time, so suggesting a depletion of electronic density. Also in this case the simple assignment of the band centered around 1500 cm^{-1} just to the C-C bond stretching seems an approximation, other frequencies contribution could reasonably be present in this band, such as the stretching of other C-C bonds that, unfortunately, cannot

be easily disentangled.

These results suggest that during the time regions in the molecule in which the electronic density is locally and instantaneously localized can be recognized. So this investigation represents another possible way to follow the polaron dynamics, because it can be easily followed in the frequency domain and the polaron can be directly monitored.

Our results are in agreement with time-resolved Raman spectra in which shifts of the C−C vibrational bands are associated to the presence of polaron pairs in the polymer, [83] making the vibrational analysis of such bands an important instrument to investigate the polaron pair formation and dynamics and, more importantly, make the Wavelet Analysis crucial to make connections with experimental results.

Conclusions and Perspectives

This Ph.D. Project introduced and validated an innovative and powerful protocol to analyse a huge number of chemical processes at non-equilibrum conditions: the Wavelet Analysis, demonstrating the possibility to make a generalization of this approach for several different systems. The Wavelet Analysis is a precious instrument to disentangle the complex dynamics of the GFP ESPT or the formation of polaron pairs in an oligothiophene model. The molecular insight given by us on the studied processes was allowed by the knowledge of the temporal evolution of the molecular motions ruling the investigated dynamics: the atomistic time scale has been followed with a *real time* resolution. This was the main goal reached by us: the knowledge, with a microscopic detail, of the complexity that, of course, characterizes complex molecular events.

Regarding the GFP study, it was based on a deep structural investigation mainly focused on the ESPT reaction mechanism and, more importantly, its driving forces. Here different rearrangements in the ground and excited states were found when we analysed crucial parameters related to the chromophore and to the most important residues. These results suggested an almost structural-controlled ESPT more than

a chromophore photoacidity driven process. Despite the system complexity and the huge computational cost we were able to perform a study almost focused on the mechanism more than on the kinetics, we were able to observe structural changes of the chromophore,the residues involved in the reaction and also of His148 in the excited state dynamics compared to the ground state, and we were also able to identify crucial parameters favoring the ESPT. The role of the protein matrix, investigated with such a fine analysis, and the importance of *spectators* residues, is affirmed here for the first time.

We also investigated the ESPT mechanism, that we found to be concerted and asynchronous, in good agreement with the theoretical-computational work of Vendrell and co-workers based on an EVB approach [57] performed on a model system composed of the chromophore (without the Ser65 side chain) and the residues directly involved in the reaction. However in our case it was more difficult to assert that the first proton transfer was the one between the Ser205 and Glu222 residues, as they suggest, because of the complex dynamics of the proton donors and acceptors distance trends in proximity of the PT event. Zhang and co-workers [56] also proposed a theoretical study but this time focused on the PT reaction mechanism in the ground state, proposing a concerted mechanism instead of a stepwise one. They worked on a model system in which a deep theoretical investigation of the main chromophore forms involved in the reaction was performed.

In our results structural rearrangements of the chromophore and of the main

residues involved in the reaction to accomodate the PT are observed. The crucial role of structural re-organization brings into serious question the hypothesis of a substantially photoacidity driven proton transfer.

Our study aimed to investigate the whole system, that we believe to be necessary to understand the molecule behavior, through a high level theoretical-computational point of view based on ab-initio molecular dynamics simulations for the first time perfrmed on the whole GFP to unveil the ESPT mechanism and coupled with the Wavelet Analysis to deeply investigate the main interesting physical quantities obtained from the trajectories. This promising analysis allowed us to reatain the temporal information of the signals and to investigate the istantaneous frequency contributions involved in the ESPT.

The obtained results on GFP were also in excellent agreement with Prof. Mathies hypothesis of a necessary strctural re-organization before the reaction. Also rearrangements involving the residues belonging to the hydrogen bond network were observed suggesting, as also Van Tohr hypothesized, that the different strength of the hydrogen bonds is crucial for the PT reaction.

Regarding the study on the formation of polaron pairs and their dynamical evolution in the heptamer model, for the first time a combined approach of first-principles exciton-nuclear dynamics and Wavelet Analysis was employed to track the real-time formation of a polaron pair with excellent performances of the WT. The dynamical evolution of the polaron pair was monitored, characterizing both in a qualitative

and quantitative way the charge changes upon the excitation.

Further evidence for the polaron formation were provided by the closely correlated charge carrier and structural dynamics. In particular, the correlation between the step-wise decay of time-dependent dipole and the dynamics of $S-C-C-S$ dihedral angles suggested that the formation of a polaron pair was modulated by the out-of-plane motion of the polymer backbone dynamics. When the planarity of adjacent monomers deviates from ideal conjugated structure, time-evolving electron density can be trapped in a few monomer rings, forming a polaron.

Utilizing the Wavelet analysis method allowed to give a spectroscopic point of view on the phenomena taking place during the polaron dynamics. The exciton-nuclear dynamics was indeed also studied through the time-resolved vibrational spectra of some of the $C-C$ bonds of the system using the multiresolution Wavelet Analysis to resolve their non-equilibrium temporal signals. We followed the polaron dynamics through the blue or red shifts characterizing the $C-C$ bonds vibrational bands temporal evolution, giving this insight for the first time. The Wavelet Analysis results strongly suggested that the polaron pair dynamics can be monitored by structural parameters and also by spectroscopic investigations that are sensitive to the temporal evolution of these geometric deformations. Both the shifts of these vibrational bands and the inter-ring rearrangements were correlated to the polaron pair dynamics as also suggested by experimental results. [77, 81, 83]

Finally, we can affirm that the Wavelet Analysis is a promising method to anal-

yse stationary and non stationary time series of chemical interest. The capability to localize frequencies in time, the versatility toward different kind of signals are among the main advantages of the Wavelet protocol, that showed to be a powerful instrument for both the equilibrium and especially for non equilibrium analysis. In conclusion, the protocols proposed in this work show very low barriers in terms of potentialities and applications.

The main goals were reached, demonstrating, at the end, that it is the *time*, the *dynamics* of an event to tell us the molecule story more than the molecule its self. Maybe, something similar could be deduced by the Salvador Dalí   *The Persistence of Memory*.
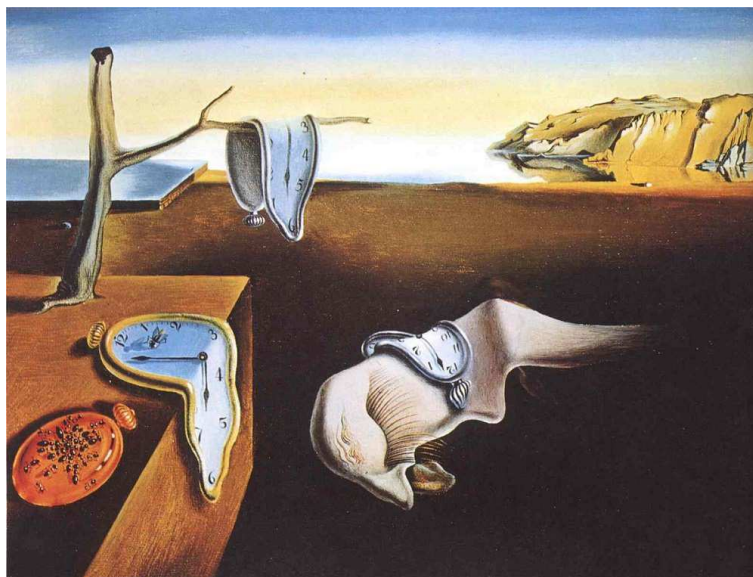
Fig. 3.11: *The Persistence of Memory* Salvador Dalí(1931).

List of Figures

List of Tables

Bibliography

[1] S. Iuchi, A. Morita, and S. Kato, J. Phys. Chem. B **106**, 3466 (2002).

[2] G. D. Reid and K. Wynne, *Handbook of Laser Technology and Applications* (Taylor and Francis 2003, 2003).

[3] A. H. Zewail, J. Phys. Chem. A **104**, 5660 (2000).

[4] R. R. Frontiera and R. A. Mathies, Laser Photonics Rev. **1**, 102 (2011).

[5] P. Kukura, D. W. McCamant, S. Yoon, D. B. Wandschneider, and R. A. Mathies, Science **310**, 1006 (2005).

[6] D. W. McCamant, P. Kukura, S. Yoon, and R. A. Mathies, Rev. Sci. Instrum. **75**, 4971 (2004).

[7] P. Kukura, D. W. McCamant, and R. A. Mathies, Annu. Rev. Phys. Chem. **58**, 461 (2007).

[8] S. Shim and R. A. Mathies, J. Phys. Chem. B **112**, 4826 (2008).

[9] S. Laimgruber, H. Schachenmayer, B. Schmidt, W. Zinth, and P. Gilch, Appl. Phys. B, Laser Opt. **85**, 557 (2006).

[10] M. Yoshizawa, H. Aoki, and H. Hashimoto, Bull. Chem. Soc. Jpn. **75**, 949 (2002).

[11] G.Beddard, Rep. Prog. Phys. **56**, 63 (1993).

[12] H. B. Schlegel, J. M. Millam, S. S. Iyengar, G. A. Voth, A. D. Daniels, G. E. Scuseria, and M. J. Frisch, J. Chem. Phys. **114**, 9758 (2001).

[13] S. S. Iyengar, H. B. Schlegel, J. M. Millam, G. A. Voth, G. E. Scuseria, and M. J. Frisch, J. Chem. Phys. **115**, 10291 (2001).

[14] H. B. Schlegel, S. S. Iyengar, X. Li, J. M. Millam, G. A. Voth, G. E. Scuseria, and M. J. Frisch, J. Chem. Phys. **117**, 8694 (2002).

[15] D. L. Bunker, Meth. Comp. Phys. **10**, 287 (1971).

[16] L. M. Raff and D. L. Thompson, *Theory of Chemical Reaction Dynamics* (CRC, Boca Raton,FL, 1985).

[17] E. W. L. Hase, ed., *Advances in Classical Trajectory Methods* (JAI, Stamford,CT, 1991).

[18] T. Helgaker, E. Uggerud, and H. J. A. Jensen, Chem. Phys. Lett. **173**, 145 (1990).

[19] D. F. Walnut, *An introduction to Wavelet Analysis* (Birkhäuser Boston, Department of Mathematical Sciences George MAson University Fairfax, VA 22030 USA, 2002).

[20] I. Daubechies, IEEE Transactions on Information Theory **36**, 961 (1990).

[21] O. Rioul and M. Vetterli, IEEE Signal Processing Magazine **8**, 14 (1991).

[22] C. Torrence and C. P. Compo, Bulletin of the American Meteorological Society **79**, 61 (1998).

[23] G. Beddard, Rep. Prog. Phys. **56**, 63 (1993).

[24] D. A. McQuarrie, *Statistical Mechanics* (University Science Books, University Science Books Sausalito, California, 2000).

[25] V. Barone, R. Improta, and N. Rega, Acc. Chem. Res. **41**, 605 (2008).

[26] A. Strachan, J. Chem. Phys. **120**, 1 (2004).

[27] I. N. Levine, *Quantum Chemistry* (Prentice Hall, Brooklyn College, City University of New York, 2009).

[28] E. Wilson, J. Decius, and P. Cross, *Molecular vibrations: the theory of infrared and Raman vibrational spectra* (Dover Pubns, 1980).

[29] N. Rega, Theor. Chem. Acc. **116**, 347 (2006).

[30] D. A. McQuarrie, *Statistical Mechanics* (Harper an Row, New York, 1976).

[31] Z. Li, A. Borrmann, and C. C. Martens, Chem. Phys. Lett. **214**, 362 (1993).

[32] N. Charbkaew, T. Suwanasri, T. Bunyagul, and A. Schnettler, IEEE Transactions on Electrical and Electronic Engineering **7**, 13 (2012).

[33] Ş. Saraydemir, N. Taşpınar, O. Eroğul, H. Kayserili, and N. Dinçkan, J. Med. Syst. **36**, 3205 (2012).

[34] G. P. Bello, L. Daudet, S. Abdallah, C. Duxbury, M. Davies, and M. B. Sandler, IEEE Transactions on Speech and Audio Processing **13**, 1305 (2005).

[35] A. A. Bharath and J. Ng, IEEE Transactions on Image Processing **14**, 948 (2005).

[36] M. Svensson and N. A. Krüger, J. Popul. Econ. **25**, 1215 (2012).

[37] M. Maroncelli, J. Mol. Liq. **57**, 1 (1993).

[38] J. L. P. Lustres, S. A. Kovalenko, M. Mosquera, T. Senyushkina, W. Flasche, and N. P. Ernsting, Angew. Chem. Int. Ed. **44**, 5635 (2005).

[39] A. Petrone, G. Donati, P. Caruso, and N. Rega, J. Am. Chem. Soc. **136** (42), 14866 (2014).

[40] M. Chalfie, Y. Tu, G. Euskirchen, W. Ward, and D. Prasher, Biochem. Biophys. Res. Commun. **263**, 802 (1994).

[41] M. Zimmer, Chem. Rev. **102**, 759 (2002).

[42] T. Kogure, S. Karasawa, T. Araki, K. Saito, M. Kinjo, and A. Miyawaki, Nature Biotechnology **24**, 577 (2006).

[43] M. Matz, A. Fradkov, Y. Labas, A. Savitsky, A. Zaraisky, and M. Markelov, Nature Biotechnology **17**, 969 (2002).

[44] J. Kennis, I. van Stokkum, D. Peterson, A. Pandit, and R. Wachter, J. Phys. Chem. B **117**, 11134 (2013).

[45] M. Chattoraj, B. King, G. Bublitz, and S. Boxer, Proc. Natl. Acad. Sci. **93**, 8362 (1996).

[46] M. Kondo, I. Heisler, D. Stoner-Ma, P. Tonge, and S. Meech, J. Photochem. Photobiol. A **234**, 21 (2012).

[47] K. Brejc, T. Sixma, P. Kitts, S. Kain, R. Tsien, M. Ormo, and S. Remington, Proc. Natl. Acad. Sci. **94**, 2306 (1997).

[48] C. Fang, R. Frontiera, R. Tran, and R. Mathies, Nature **462**, 200 (2009).

[49] D. Stoner-Ma, A. Jaye, P. Matousek, M. Towrie, and S. Meech, J. Am. Chem. Soc. **127**, 2864 (2005).

[50] J. V. Thor, G. Zanetti, K. Ronayne, and M. Towrie, J. Phys. Chem. B **109**, 16099 (2005).

[51] D. Stoner-Ma, E. Melief, J. Nappa, K. Ronayne, P. Tonge, and S. Meech, J. Phys. Chem. B **110**, 22009 (2006).

[52] J. V. Thor, C. Lincoln, B. Kellner, K. Bourdakos, L. Thompson, M. Bearpark, P. Champion, and J. Sage, Vib. Spectrosc. **62**, 1 (2012).

[53] M. D. Donato, L. van Wilderen, I. V. Stokkum, T. Stuart, J. Kennis, K. Hellingwerf, R. van Grondelle, and M. Groot, Phys. Chem. Chem. Phys. **13**, 16295 (2011).

[54] T. Fujisawa, H. Kuramochi, H. Hosoi, S. Takeuchi, and T. Tahara, JACS **138**, 3942 (2016).

[55] M. Lill and V. Helms, Proc. Natl. Acad. Sci. **99**, 2778 (2002).

[56] M. Zhang, M. Nguyen, and A. Ceulemans, Chem. Phys. Lett. **404**, 250 (2005).

[57] O. Vendrell, R. Gelabert, M. Moreno, and J. Llunch, J. Chem. Theory Comput. **4**, 1138 (2008).

[58] B. Grigorenko, A. Nemukhin, I. Polyakov, D. Morozov, and A. Krylov, J. Am. Chem. Soc. **135**, 11541 (2013).

[59] M. Nadal-Ferret, R. Gelabert, M. Moreno, and J. M. Lluch, PCCP **17**, 30876 (2015).

[60] C. W. Tang, Appl. Phys. Lett. **48** (2), 183 (1986).

[61] A. W. Hains, Z. Liang, M. A. Woodhouse, and B. A. Gregg, Chem. Rev. **110** (11), 6689 (2010).

[62] M. Scharber and N. Sariciftci, Progress in Polymer Science **38** (12), 1929 (2013).

[63] N. Kaur, M. Singh, D. Pathak, T. Wagner, and J. Nunzi, Synthetic Metals **190**, 20 (2014).

[64] J. Casado, R. P. Ortiz, and J. T. L. Navarrete, Chem. Soc. Rev. **41**, 5672 (2012).

[65] G. Wellein and H. Fehske, Phys. Rev. B **58** (10), 6208 (1998).

[66] N. Oldani, S. Tretiak, G. Bazan, and S. Fernandez-Alberti, Energ. Environ. Sci. **7**, 1175 (2014).

[67] J. Clark, T. Nelson, S. Tretiak, G. Cirmi, and G. Lanziani, Nat. Phys. **8**, 225 (2012).

[68] J. D. Servaites, M. A. Ratner, and T. J. Marks, Energ. Environ. Sci. **4**, 4410 (2011).

[69] L. J. A. Koster, Phys. Rev. B **81**, 205318 (2010).

[70] A. Zhugayevych and S. Tretiak, Annu. Rev. Phys. Chem. **66**, 305 (2015).

[71] M. Yan, L. J. Rothberg, F. Papadimitrakopoulos, M. E. Galvin, and T. M. Miller, Phys. Rev. Lett. **72**, 1104 (1994).

[72] E. L. Frankevich, Phys. Rev. B **46**, 9320 (1992).

[73] B. Schweitzer, V. I. Arkhipov, and H. Bässler, Chem. Phys. Lett. **304**, 365 (1999).

[74] P. Parkinson, C. Müller, N. Stingelin, M. B. Johnston, and L. M. Herz, J. Phys. Chem. Lett. **1**, 2788 (2010).

[75] J. F. Chang, J. Clark, N. Zhao, H. Sirringhaus, D. W. Breiby, J. W. Andreasen, M. M. Nielsen, M. Giles, M. Heeney, and I. McCulloch, Phys. Rev. B **74**, 115318 (2006).

[76] D. Emin, *Polarons* (Cambridge University Press, New York, USA, 2013).

[77] R. Tautz, E. D. Como, T. Limmer, J. Feldmann, H.-J. Egelhaaf, E. von Hauff, V. Lemaur, D. Beljonne, S. Yilmaz, I. Dumsch, S. Allard, and U. Scherf, Nat. Commun. **3**, 1 (2012).

[78] S. Karabunarliev and E. R. Bittner, The Journal of chemical physics **118** (9), 4291 (2003).

[79] E. R. Bittner and M. N. Kobrak, Synthetic Metals **121** (1-3), 1635 (2001).

[80] J. Guo, H. Ohkita, H. Benten, and S. Ito, J. Am. Chem. Soc. **131**, 16869 (2009).

[81] W. Yu, P. J. Donohoo-Vallett, J. Zhou, and A. E. Bragg, J. Chem. Phys. **141**, 044201 (2014).

[82] W. Yu, J. Zhou, and A. E. Bragg, J. Phys. Chem. Lett. **3**, 1321 (2012).

[83] T. J. Magnanelli and A. E. Bragg, Chem. Phys. Lett. **304**, 438 (2015).

[84] J. Nelson, J. J. Kwiatkowski, J. Kirkpatrick, and J. M. Frost, Acc. Chem. Res. **42** (11), 1768 (2009).

[85] X. Li, J. C. Tully, H. B. Schlegel, and M. J. Frisch, J. Chem. Phys. **123** (8), 084106 (2005).

[86] C. M. Isborn, X. Li, and J. C. Tully, J. Chem. Phys. **126**, 134307 (2007).

[87] A. Petrone, D. B. Lingerfelt, N. Rega, and X. Li, Phys. Chem. Chem. Phys. **16** (44), 24457 (2014).

[88] F. Ding, J. J. Goings, H. Liu, D. B. Lingerfelt, and X. Li, J. Chem. Phys. **143**, 114105 (2015).

[89] A. Rahaman and R. A. Wheeler, J. Chem. Theory Comput. **1**, 769 (2005).

[90] M. Pagliai, F. Muniz-Miranda, G. Cardini, R. Righini, and V. Schettino, J. Phys. Chem. Lett. **1**, 2951 (2010).

[91] C. Dorize and L. F. Villemoes, IEEE p. 2029 (1991).

[92] A. Askar, A. E. Cetin, and H. Rabitz, J. Phys. Chem. **100**, 19165 (1996).

[93] T. Otsuka and H. Nakai, J. Comput. Chem. **28**, 1138 (2007).

[94] B. S. Mallik and A. Chandra, J. Mol. Liq. **143**, 31 (2008).

[95] M. Pagliai, F. Muniz-Miranda, G. Cardini, R. Righini, and V. Schettino, J. Mol. Struct. **993**, 438 (2011).

[96] S. D. Meyers, B. G. Kelly, and J. J. O'Brien, Mon. Weather Rev. **121**, 2858 (1993).

[97] F. Yang, L. G. Moss, and J. G. N. Phillips, Nat. Biotechnol. **14**, 1246 (1996).

[98] S. Dapprich, I. Komaromi, K. S. Byun, K. Morokuma, and M. J. Frisch, J. Mol. Struct. (Theochem) **462**, 1 (1999).

[99] T. Vreven, K. S. Byun, I. Komaromi, S. Dapprich, J. A. M. Jr., K. Morokuma, and M. J. Frisch, J. Chem. Theory and Comput. **2**, 815 (2006).

[100] T. Vreven and K. Morokuma, *Annual Reports in Computational Chemistry* (Vol. 2, pp. 35-51, Ed. D. C. Spellmeyer, 2006, 2006).

[101] F. Clemente, T. Vreven, and M. J. Frisch, *Quantum Biochemistry* (Ed. C. Matta (Wiley VCH), 2008).

[102] A. Petrone, P. Caruso, S. Tenuta, and N. Rega, Phys. Chem. Chem. Phys. **15**, 20536 (2013).

[103] K. Bolton, W. L. Hase, and G. H. Peslherbe, *Modern Methods for Multidimentional Dynamics Computation in Chemstry* (Edited by D. L. Thompson., World Scientific, Singapore, 1998; Vol. 95, pp 143-189, 1998).

[104] J. M. Millam, V. Bakken, W. Chen, W. L. Hase, and H. B. Schlegel, J. Chem. Phys **111**, 3800 (1999).

[105] A. D. Becke, J. Chem. Phys. **98**, 5648 (1993).

[106] M. E. Casida, C. Jamorski, K. C. Casida, and D. R. Salahub, J. Chem. Phys **108**, 4439 (1998).

[107] R. E. Stratmann, G. E. Scuseria, and M. J. Frisch, J. Chem. Phys **109**, 8218 (1998).

[108] C. V. Caillie and R. D. Amos, Chem. Phys. Lett. **308**, 249 (1999).

[109] K. Burke and E. K. U. Gross, *Density functionals: theory and applications* (pp. 116-146, Springer Berlin, 1998, 1998).

[110] T. Yanai, D. Tew, and N. Handy, Chem. Phys. Lett. **393**, 51 (2004).

[111] X. Li, S. M. Smith, A. N. Markevitch, D. A. Romanov, R. J. Levis, and H. B. Schlegel, Phys. Chem. Chem. Phys. **7**, 233 (2005).

[112] L. Verlet, Phys. Rev. **159** (1), 98 (1967).

[113] W. Liang, C. T. Chapman, and X. Li, J. Chem. Phys. **134** (18), 184102 (2011).

[114] C. et al., Acta Crystallographica. **D66**, 12 (2010).

[115] W. D. Cornell, P. Cieplak, C. I. Bayly, and P. A. Kollman, J. Am. Chem. Soc. **117**, 5179 (1995).

[116] N. Reuter, H. Lin, and W. Thiel, J. Phys. Chem. B **106**, 6310 (2002).

[117] T. Vreven, K. Morokuma, O. Farkas, H. B. Schlegel, and M. J. Frisch, J. Comput. Chem. **24**, 760 (2003).

[118] T. Vreven, B. Mennucci, C. O. da Silva, K. Morokuma, and J. Tomasi, J. Chem. Phys. **115**, 62 (2001).

[119] S. J. Mo, T. Vreven, B. Mennucci, K. Morokuma, and J. Tomasi, Theor. Chem. Acc. **111**, 154 (2003).

[120] T. Yanai, D. P. Tew, and N. C. Handy, Chem. Phys. Lett. **393**, 51 (2004).

[121] U. Salzner and A. Aydin, J. Chem. Theor. Comput. **7**, 2568 (2011).

[122] H. Li, R. Nieman, A. J. A. Aquino, H. Lischka, and S. Tretiak, J. Chem. Theor. Comput. **10**, 3280 (2014).

[123] M. J. Frisch, G. W. Trucks, H. B. Schlegel, G. E. Scuseria, M. A. Robb, J. R. Cheeseman, G. Scalmani, V. Barone, B. Mennucci, G. A. Petersson, H. Nakatsuji, M. Caricato, X. Li, H. P. Hratchian, A. F. Izmaylov, J. Bloino, G. Zheng, J. L. Sonnenberg, W. Liang, M. Hada, M. Ehara, K. Toyota, R. Fukuda, J. Hasegawa, M. Ishida, T. Nakajima, Y. Honda, O. Kitao, H. Nakai, T. Vreven, J. J. A. Montgomery, J. E. Peralta, F. Ogliaro, M. Bearpark, J. J. Heyd, E. Brothers, K. N. Kudin, V. N. Staroverov, T. Keith, R. Kobayashi, J. Normand, K. Raghavachari, A. Rendell, J. C. Burant, S. S. Iyengar, J. Tomasi, M. Cossi, N. Rega, J. M. Millam, M. Klene, J. E. Knox, J. B. Cross, V. Bakken, C. Adamo, J. Jaramillo, R. Gomperts, R. E. Stratmann, O. Yazyev, A. J. Austin, R. Cammi, C. Pomelli, J. W. Ochterski, R. L. Martin, K. Morokuma, V. G. Zakrzewski, G. A. Voth, P. Salvador, J. J.

Dannenberg, S. Dapprich, P. V. Parandekar, N. J. Mayhall, A. D. Daniels, O. Farkas, J. B. Foresman, J. V. Ortiz, J. Cioslowski, and D. J. Fox, *Gaussian Development Version Revision H.12+*. Gaussian Inc., Wallingford CT 2011.

[124] G. Dennler, M. C. Scharber, and C. Brabec, Adv. Mater. **21**, 1323 (2009).

[125] A. Facchetti, Chem. Mater. **23**, 733 (2011).

[126] G. Li, R. Zhu, and Y. Yang, Nat. Photonics **6**, 153 (2012).

[127] G. H. Peslherbe, H. Wang, and W. L. Hase, *Monte Carlo Sampling for Classical Trajectory Simulations* (John Wiley & Sons, Inc., Hoboken, NJ, USA, 2007), pp. 171–201.

[128] W. L. Hase, R. J. Duchovic, X. Hu, A. Komornicki, K. F. Lim, D.-H. Lu, G. H. Peslherbe, K. N. Swamy, S. R. V. Linde, A. Varandas, H. Wang, and R. J. Wolf, Quant. Chem. Prog. Exch. **16**, 671 (1996).

[129] X. Li, J. M. Millam, and H. B. Schlegel, J. Chem. Phys. **113**, 10062 (2000).